Thomas Steiner, BSc

Development of a Molecular Sampling Algorithm in Wolfram Mathematica

MASTERARBEIT

zur Erlangung des akademischen Grades

Diplom-Ingenieur

Masterstudium Verfahrenstechnik

eingereicht an der

Technischen Universität Graz

Betreuer

Assoc.Prof. Dipl.-Ing. Dr.techn. Thomas Wallek

Institut für Chemische Verfahrenstechnik und Umwelttechnik

Fakultät für Technische Chemie, Verfahrenstechnik und Biotechnologie

Graz, Oktober 2019

EIDESSTATTLICHE ERKLÄRUNG

Ich erkläre an Eides statt, dass ich die vorliegende Arbeit selbstständig verfasst, andere als die angegebenen Quellen/Hilfsmittel nicht benutzt, und die den benutzten Quellen wörtlich und inhaltlich entnommenen Stellen als solche kenntlich gemacht habe. Das in TUGRAZonline hochgeladene Textdokument ist mit der vorliegenden Masterarbeit identisch.

Datum

Unterschrift

Danksagung

Ich möchte jenen Personen, die mich auf meinem Weg zum Abschluss des Masterstudiums Verfahrenstechnik an der Technischen Universität Graz begleitet haben, meinen Dank aussprechen.

Bei Professor Thomas Wallek bedanke ich mich für die intensive Betreuung dieser Arbeit, die mittlerweile jahrelange Wegbegleitung und für den Freiraum, den er mir stets zur Entfaltung eigener Ideen und zur selbstständigen Arbeit gelassen hat. Christoph Mayer danke ich für seinen wesentlichen Beitrag zur Betreuung dieser Masterarbeit und seinen persönlichen Einsatz. Dem Institutsleiter Professor Matthäus Siebenhofer danke ich für die Sicherstellung der Rahmenbedingungen dieses Projektes, die Unterstützung während meines Studiums und sein offenes Ohr für Anliegen jeglicher Art.

Allen voran bedanke ich mich bei meiner Familie. Meine liebe Mutter und mein kürzlich verstorbener Vater haben mir erst ermöglicht, diesen Weg zu gehen und mich über all die Jahre unterstützt. Meinem Bruder Christoph danke ich für die zahlreichen Gespräche und für seine Hilfe in den verschiedensten Angelegenheiten während meines Studiums. Meinen Freunden und Kollegen, die zur Entstehung der vorliegenden Arbeit durch wertvolle Diskussionen und ihre Expertise beigetragen haben, möchte ich ebenfalls meine Wertschätzung aussprechen.

Abstract

A molecular sampling algorithm has been developed in Wolfram Mathematica to evaluate interaction energies in clusters of molecules. In the simplest case, pairs of molecules are rotated either randomly or according to the 24 rotations within the cube-symmetry-group and are constrained to satisfy a physical interaction distance. Consecutively, translations and rotations of the molecules are performed and the intermolecular potential energies are computed using the OPLS-AA force field. The influence of relative orientations of the partners is investigated with respect to the molecule types.

These intermolecular energies are taken as energetic input parameters for Monte Carlo simulations in a rigid, cubic lattice. This is achieved via coupling of cube-symmetry-group rotations of molecules during the sampling and a molecular, six-sided dice model. The resulting excess enthalpies and the excess free enthalpies of the binary mixtures acetone - n-heptane, n-heptane - 1-butanol, acetone - methanol and acetone - n-dodecane are compared to experimental data. Excess free enthalpies can be predicted very well for several configurations, while excess enthalpies can oftentimes not be predicted correctly. Within the scope of these results, the influences of molecular orientations, intermolecular distances, polarity, chain length and the transition from molecular sampling to cubic lattice models are discussed.

Kurzfassung

Ein Molecular Sampling Algorithmus wurde in Wolfram Mathematica entwickelt, um Wechselwirkungsenergien in Molekülclustern zu berechnen. Im einfachsten Fall werden Paare von Molekülen entweder zufällig oder entsprechend der 24 Elemente der Würfel-Symmetriegruppe rotiert, während sie physikalische Wechselwirkungsdistanzen einhalten müssen. Translationen und Rotationen werden nacheinander durchgeführt und die intermolekularen, potenziellen Energien mittels OPLS-AA Kraftfeld berechnet. Der Einfluss relativer Orientierung der Partnermoleküle wird hinsichtlich ihrer Sorten untersucht.
Die erhaltenen intermolekularen Energien dienen als Eingangsparameter für Monte Carlo Simulationen im starren, kubisch-primitiven Gitter. Dies wird erreicht, indem die Rotationen der Würfel-Symmetriegruppe mit einem sechsseitigen Würfelmodell der Moleküle gekoppelt werden. Als Ergebnisse werden die Exzessenthalpien und die freie Exzessenthalpien der binären Mischungen Aceton - n-Heptan, n-Heptan - 1-Butanol, Aceton - Methanol und Aceton - n-Dodekan erhalten und mit Messdaten verglichen. Die freie Exzessenthalpie kann durch mehrere Konfigurationen sehr gut beschrieben werden, die Exzessenthalpie hingegen oftmals nicht. Im Rahmen dieser Ergebnisse werden die Einflüsse der Molekülorientierung, des intermolekularen Abstands, der Polarität, der Kettenlänge und der Übergang von Molecular Sampling zum kubischen Gittermodell diskutiert.

Contents

List of Figures

List of Tables

1. Introduction

Over the past decades, especially in the light of the rapid development of computer technologies, molecular simulations have become important tools in various scientific fields. Their applications range from fundamental research, where they help understand the behavior of microscopic systems and associated phenomena [1], to effective and practical usage for prediction of chemophysical properties on a macroscopic scale [2]. Nowadays, there is a number of well-established branches within the area of these simulations, such as Molecular Dynamics and Monte Carlo simulations [3] or Molecular Mechanics [4]: In Molecular Dynamics the transient equations of motion are solved for a defined system of molecules which interact. With Monte Carlo simulations a system starting from a (usually) random state undergoes successive changes with a certain - thermodynamically meaningful - probability until a configuration of minimum energy is reached. Molecular Mechanics deals with internal and external interactions of molecules; the aim is to properly describe those interactions using mechanical models, also known as force fields.

Especially the force-field-based method of Molecular Mechanics plays an important role within the scope of this work. When it is possible to characterize the atomic and molecular behavior of targeted substances, this information can be used to quantify the energies of clusters. A cluster is an arrangement

of a number of individual molecules which are close enough to each other to interact. In specific, the number of molecules in a cluster can range from two (i.e. pairs) to basically any desired upper limit, depending on the coordination number and the intermolecular distance at which energetic contributions from interactions become negligible. Furthermore, the maximum number of participants is also limited by computational time, since the numerical cost of force field evaluations rises dramatically with increasing system size.

When clusters of molecules are built, the corresponding intramolecular and intermolecular energies can be computed. Repeating this process for different configurations results in a molecular sampling method. In this work, the size of clusters is limited from two to eight (without being restricted to only this range), with clusters of two molecules being used the most often. A recently published thermodynamic model [5] uses variables describing clusters of molecules, which are abstracted as six-sided dice with possibly differing energetic properties on each face. The model input requires knowledge of these properties for contacting faces specifically. It is, therefore, important to develop methods for obtaining energies of contacting faces for different systems of interest. Moreover, the distance between molecules within clusters as well as their relative orientations influence the computed results.

The aim of this work is to use the molecular force field "Optimized Potential for Liquid Simulations - All Atom" (OPLS-AA) by Jorgensen et al. [6] with rigid molecules to investigate the energetic interactions within clusters. A molecular sampling algorithm, capable of generating data which can be used for calculations in thermodynamic models like [5], is developed. The code used for numeric evaluation was written in *Wolfram Mathematica*®. Furthermore, the influence of orientations of different molecules within certain configurations as well as the transition from molecular sampling to lattice systems are

addressed.

In the following chapters, a brief overview of molecular force fields and particularly the OPLS-AA force field is given. The new molecular sampling algorithm is explained and multiple case studies are discussed in order to assess the characteristics and the capabilities of the routine presented. Since it is important to validate computational results against real experimental data, several Monte Carlo (MC) simulations are conducted, using the results of various molecular sampling runs as input parameters. The excess enthalpy h^E and the excess free enthalpy g^E of the four binary mixtures acetone - n-heptane, n-heptane - 1-butanol, acetone - methanol and acetone - n-dodecane are obtained through these simulations and compared to measurements.

2. Molecular Force Fields

Before molecular sampling methods are discussed, the concept of force fields is briefly summarized. Starting from a simple example of two neighboring atoms, the complexity shall be increased gradually by combining atoms to molecules via bonding and subsequent introduction of additional degrees of freedom within molecules.

2.1. General Concepts

In order to elaborate on the concept of molecular force fields, consider an exemplary system consisting of two atoms. Whenever an atom is positioned somewhere around another atom, they either want to attract or repel each other, unless they are at an equilibrium distance. So-called van der Waals interactions are caused by the shift of electron distributions around the nucleus, leading to temporary dipoles [7]. A simple, well-known model to describe this phenomenon is given by the Lennard-Jones-12-6-potential E_{LJ}.

$$E_{\mathrm{LJ}} = 4\epsilon \left(\left(\frac{\sigma}{r} \right)^{12} - \left(\frac{\sigma}{r} \right)^{6} \right) \tag{2.1}$$

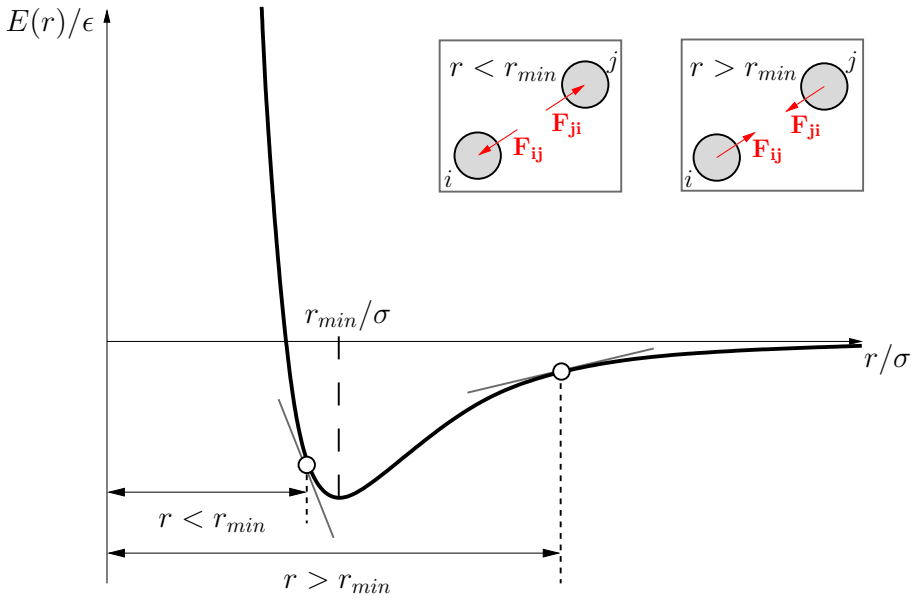

Figure 2.1.: Dimensionless Lennard-Jones potential and resulting forces $F_{\mathrm{ij}} = F_{\mathrm{ji}}$ acting on particles i and j. For $r > r_{min}$ there is attraction, for $r < r_{min}$ repulsion takes place

For any given pure substance, the well-depth ϵ and distance σ of zero potential are set. The potential thus only depends on the interatomic distance r. The force acting on a particle i due to the influence of particle j is the negative derivative of the potential function

$$F_{ij} = -\frac{\mathrm{d}E_{\mathrm{LJ}}}{\mathrm{d}r} \ . \tag{2.2}$$

Figure 2.1 illustrates the dimensionless Lennard-Jones potential function and shows the forces acting on particles i and j resulting from their interaction. At close distance r, the steep increase of the potential with decreasing r results in strong repulsion. At $r = r_{\mathrm{min}}$, a minimum of the potential function indicates that no forces are acting; the two particles are at the equilibrium distance. If the interatomic distance r further increases, attraction takes place. Once particles i and j are far from each other, attractive forces become negligible.

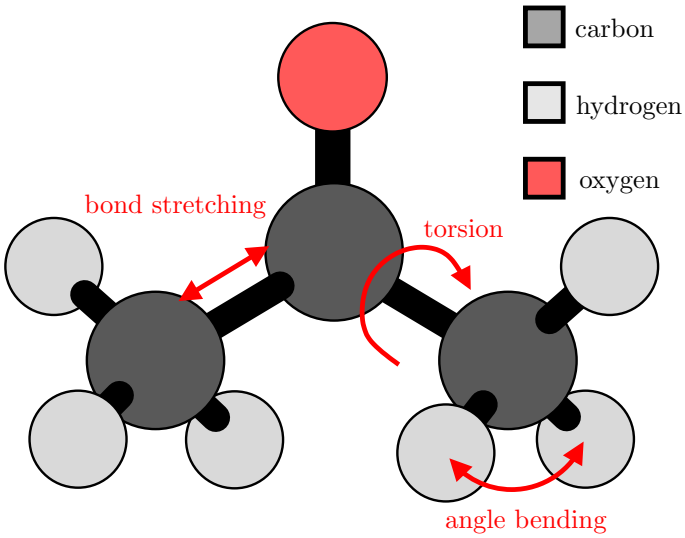

Figure 2.2.: Bond stretching, angle bending and torsion as contributors to intramolecular energy, using acetone as an example

When several atoms are combined to form a molecule, the same principles apply. However, the situation becomes more complicated, because the atoms of a molecule are not only attracted or repelled by external neighbors, but also intramolecular interactions take place. Atoms which are covalently bonded want to keep a certain distance from each other while also experiencing forces acting due to neighboring species. In order to describe such behavior, the simple Lennard-Jones potential function E_{LJ} in equation (2.1) is not sufficient.

To understand the components necessary for a more versatile potential function, the degrees of freedom within a single molecule can be investigated [8]. As an example, the possible phenomena typically covered by more detailed force fields are shown in Figure 2.2 for acetone. The terms bond stretching, angle bending and torsion shall be explained.

Atoms which are directly connected through a single or multiple bond experience a strong constraint regarding their relative distance. A basic approach

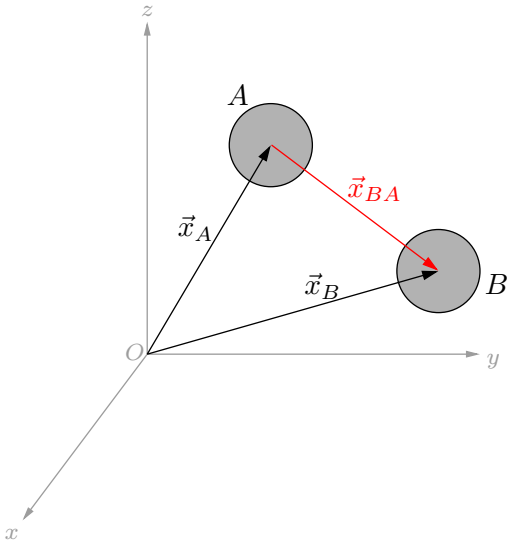

Figure 2.3.: Determination of the distance between two atoms A and B

is to only attribute the energetic contribution E_{bond} to the difference Δr of the actual bond distance to the equilibrium distance. Let two atoms A and B have the position vectors $\vec{x}_A$ and $\vec{x}_B$, respectively. Figure 2.3 illustrates an example. The actual distance r_{AB} between A and B is then simply

$$r_{AB} = \|\vec{x}_A - \vec{x}_B\| \ . \tag{2.3}$$

Similar to atomic bonds, there are also angular degrees of freedom. Based on the hybridization of atoms, certain angles between three particles A, B and C are energetically more favorable than others, as atoms want to keep their distance from each other. Let atom B be the central particle, with A and C both being connected to B. The angle α_{ABC} between them can be computed as

$$\alpha_{ABC} = \arccos\left(\frac{(\vec{x}_A - \vec{x}_B)\cdot(\vec{x}_C - \vec{x}_B)}{\|\vec{x}_A - \vec{x}_B\| \cdot \|\vec{x}_C - \vec{x}_B\|}\right) \tag{2.4}$$

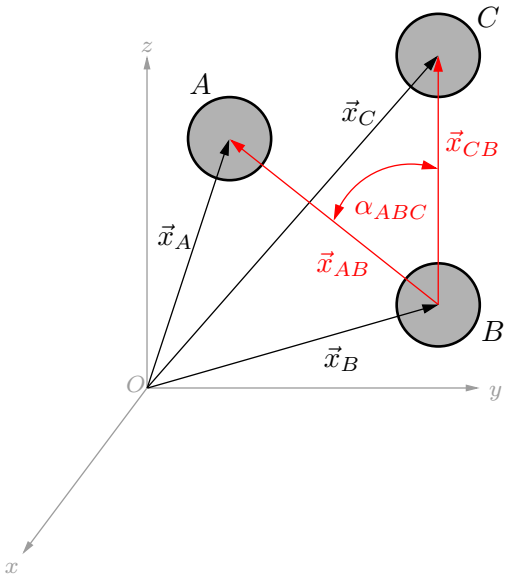

Figure 2.4.: Determination of the angle α_{ABC} between three atoms A, B and C

with $\vec{x}_C$ being, in accordance with the definition for A and B, the position vector of particle C. Figure 2.4 showcases the procedure and provides the relevant vectors for calculating this angle α_{ABC}. For every possible angle of three atoms within a molecule, an equilibrium angle is the most favorable in terms of energy. As with atomic bonds, the energetic contribution E_{angle} of an angle α_{ABC} depends on the difference between the actual angle and the equilibrium angle.

Another type of angle can be defined when four-particle-configurations are considered. A graphical example for such a situation is illustrated in Figure 2.5. Particle A is bonded to B, B is bonded to C and C is bonded to D, which has the position vector $\vec{x}_D$. The dihedral angle α_{ABCD} is defined as the angle between $\vec{x}_{AB} = \vec{x}_A - \vec{x}_B$ and $\vec{x}_{DC} = \vec{x}_D - \vec{x}_C$, after both these vectors have been projected onto the normal plane n_{BC} of the bond B-C. To calculate the

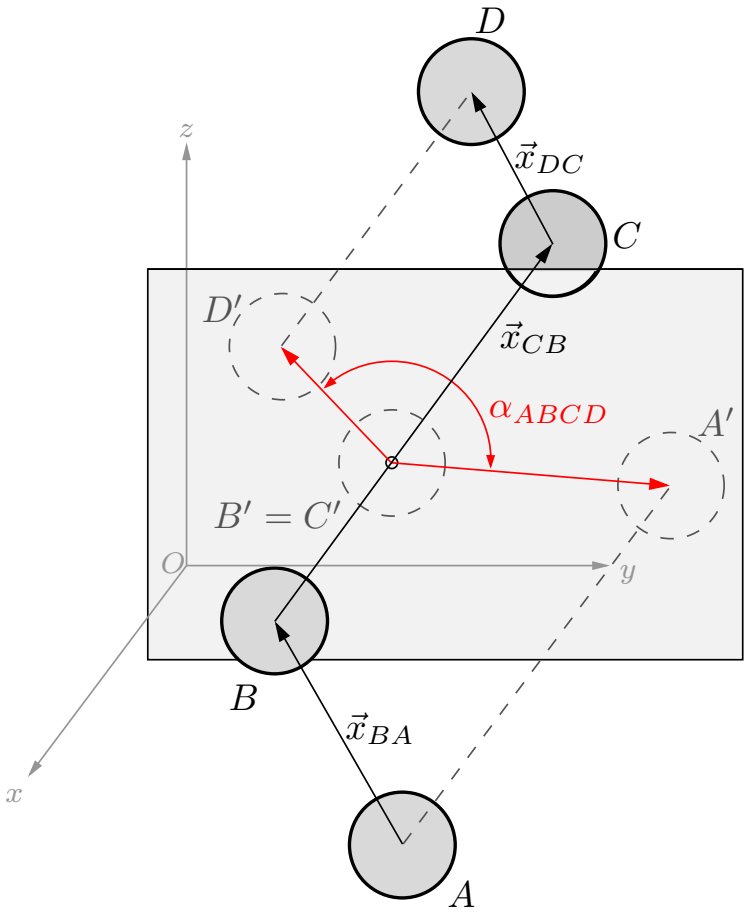

Figure 2.5.: Determination of the dihedral angle α_{ABCD} between four atoms A, B, C and D

dihedral angle α_{ABCD}, the normal vectors $\vec{n}_{ABC}$ and $\vec{n}_{BCD}$

$$\vec{n}_{ABC} = \vec{x}_{BC} \times \vec{x}_{AB} \tag{2.5}$$

$$\vec{n}_{BCD} = \vec{x}_{BC} \times \vec{x}_{CD} \tag{2.6}$$

can be computed as vectorial cross products. Similar to equation (2.4), the dihedral angle is

$$\alpha_{ABCD} = \arccos\left(\frac{|\vec{n}_{ABC} \cdot \vec{n}_{BCD}|}{\|\vec{n}_{ABC}\| \cdot \|\vec{n}_{BCD}\|}\right). \tag{2.7}$$

Based on this angle the energetic contribution E_{torsion} can be calculated.

It is worth mentioning that there is also so-called out-of-plane-bending [8]. When an atom (e.g. carbon in sp^2 hybridization) wants to maintain a planar configuration with its neighbors, any deviations from planarity will come with notable energetic penalties. In other words, planar setups pose a form of energy barriers for these degrees of freedom. Practically, they can be modeled like torsion (which makes the respective angles so-called "improper dihedrals") [8] with special parameters and angles.

Another important concept regarding molecular force fields is the resolution of molecules and single atoms. Ideally, microscopic phenomena and the physics governing intrinsic behavior can be completely resolved. With the ongoing increase in computational power during the past decades, the necessity of choosing lower resolutions in order to obtain results within realistic time scales became smaller. Nonetheless, it is important to understand the impact of resolution and the trade-off between precision and computational costs, especially when a force field model and the corresponding parameters have to be chosen. In Molecular Mechanics, typically three types/depths/degrees of resolution are

distinguished: There are all-atom (AA), united-atom (UA) and coarse-grained approaches [4].

Starting with the lowest molecular resolution, coarse-grained models combine multiple atoms to whole groups, very similar to functional groups and group contribution methods in chemical engineering thermodynamics. A molecule thus consists of several groups of atoms, which are also parameterized as such. The advantage of these kinds of methods is the decrease in time needed for computation of interactions due to the smaller number of participants during evaluation loops. However, it is then obvious that microscopic behavior can only be properly described as long as the coarse-grained model is capable of characterizing all of the molecular interactions and effects that are necessary.

United-atom approaches constitute a group of models which try to resolve the whole molecule, except for nonpolar hydrogen atoms [4]. In specific, hydrogen atoms bonded to carbon atoms in hydrocarbons like alkanes or alcohols are neglected. Due to the greatly reduced number of sites during numerical evaluations, computation time is saved. The atoms carrying hydrogen (mostly carbon) are handled as united atoms, resulting in sets of parameters which do not only represent the single constituent, but also account for the hydrogen-parts dropped.

All-atom representations of molecules resolve every single atom, also leading to sets of parameters for every single one of them. At the cost of higher simulation time, the results are more accurate.

Now that the basic principles and components of force fields have been explained, the force field used throughout this work is presented in the following section. Jorgensen et al. [6] published their model “Optimized Potentials for Liquid Simulations - All Atom”, an all-atom force field for condensed phase

fluids. Their potential functions were adopted for the development of the molecular sampling algorithm, as explained in chapter 3.

2.2. OPLS-AA Force Field

During the sampling of a certain configuration (e.g. a pair) of molecules, the intra- and intermolecular potential energies need to be calculated. Therefore, potential functions are required in order to describe the interactions of targeted species. In the literature, numerous different models are proposed and the choice should certainly be based on the application and the substances in use. Still, it shall be noted that many of them only differ in details, while the general form of the potential function terms is often the same. To give a few examples, Weiner et al. [9, 10] have published their *AMBER* force field for nucleic acids and proteins. An interesting feature is the explicit consideration of hydrogen bonds in their energy expression, represented by a 12-10-potential. Other prominent force fields are *CHARMMS* [11] and *GROMOS* (in several of its adaptations) [12].

The force field chosen for this work was published by Jorgensen et al. [6]. Their "Optimized Potentials for Liquid Simulations" in its all-atom form (OPLS-AA) is a further development of a previous united-atom representation. In specific, united-atom models were published as optimized potentials for liquid hydrocarbons [13] and liquid alcohols [14], followed by potential functions for proteins [15]. Their all-atom force field OPLS-AA is capable of describing the interactions of organic constituents in the condensed fluid phase. The parameters in use were designed to properly reproduce common liquid properties like densities ρ and heats of vaporization Δh^{v}. On the occasion that there

is special interest in the exact procedure of obtaining the sets of parameters, the reader is referenced to the publications given here. It shall be stated that, in the past, the OPLS-AA force field has received broad acceptance within the field of molecular simulations and, thus, has undergone extensive testing, benchmarking and reparameterization through the originators [6] and other publications [16, 17, 18, 19].

In order to calculate the intra- and intermolecular energies of a molecular system under investigation, the OPLS-AA force field comprises several terms, most of which are already explained in the previous section. The total potential energy function for two molecules A and B reads [6]

$$E = E_{\text{OPLS-AA}} = E_{\text{bond}} + E_{\text{angle}} + E_{\text{torsion}} + E_{\text{AB}} \tag{2.8}$$

$$\text{with } E_{\text{bond}} = \sum_{\text{bonds}} K_r \left(r - r_{\text{eq}}\right)^2 \tag{2.9}$$

$$E_{\text{angle}} = \sum_{\text{angles}} K_\theta \left(\theta - \theta_{\text{eq}}\right)^2 \tag{2.10}$$

$$\begin{aligned} E_{\text{torsion}} = \sum_{i}^{\text{dihedrals}} & \frac{V_1^i}{2}\left[1 + \cos\left(\phi_i + f_1^i\right)\right] + \\ & + \frac{V_2^i}{2}\left[1 - \cos\left(2\phi_i + f_2^i\right)\right] + \\ & + \frac{V_3^i}{2}\left[1 + \cos\left(3\phi_i + f_3^i\right)\right] \end{aligned} \tag{2.11}$$

$$E_{\text{AB}} = \sum_{i}^{\text{on A}} \sum_{j}^{\text{on B}} \left[\frac{q_i q_j e^2}{r_{ij}} + 4\epsilon\left(\frac{\sigma_{ij}^{12}}{r_{ij}^{12}} - \frac{\sigma_{ij}^{6}}{r_{ij}^{6}}\right)\right] f_{ij} \tag{2.12}$$

As discussed earlier, the intramolecular energy consists of contributions for bonds, angles and torsion. Bond stretching energies E_{bond} and angle bending energies E_{angle} are described as sums of quadratic, spring-like functions, with a spring-constant K_r and K_θ and a displacement $\Delta r = r - r_{\text{eq}}$ and $\Delta\theta = \theta - \theta_{\text{eq}}$ from equilibrium, respectively. For a given molecule, one has to sum up every

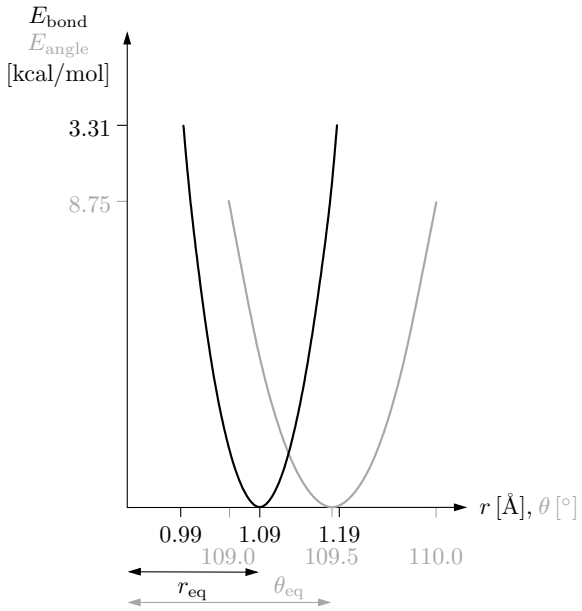

Figure 2.6.: Example for bond energy E_{bond} (of a CT-HC bond) as a function of interatomic distance r and angular energy E_{angle} (of an HC-CT-HC angle) as a function of angle θ

single bond and angle contribution to obtain their total energy value. Torsion is modeled as a Fourier series for the dihedral angles ϕ_i, with constants V_1^i, V_2^i, V_3^i and phase angles f_1^i, f_2^i, f_3^i. The summation over i has to incorporate every dihedral angle ϕ_i.

Examples for bond energy E_{bond} given by equation (2.9) and angle energy E_{angle} given by equation (2.10) are shown in Figure 2.6. The parameters chosen represent a CT-HC bond, meaning sp^3 hybridization of carbon and a hydrogen atom bonded to it, and the angle between two hydrogen atoms bonded to such a carbon (HC-CT-HC) in alkyl groups. As can be seen, the quadratic functions account for displacement from equilibrium through higher energy contributions. Very notably, an angular displacement of only $0.5\,^\circ$ already leads to $E_{\text{angle}} = 8.75\,\text{kcal/mol}$. Obviously, to avoid this huge gain in potential such bonds and angles will mostly be very stiff, meaning close to their equilibrium

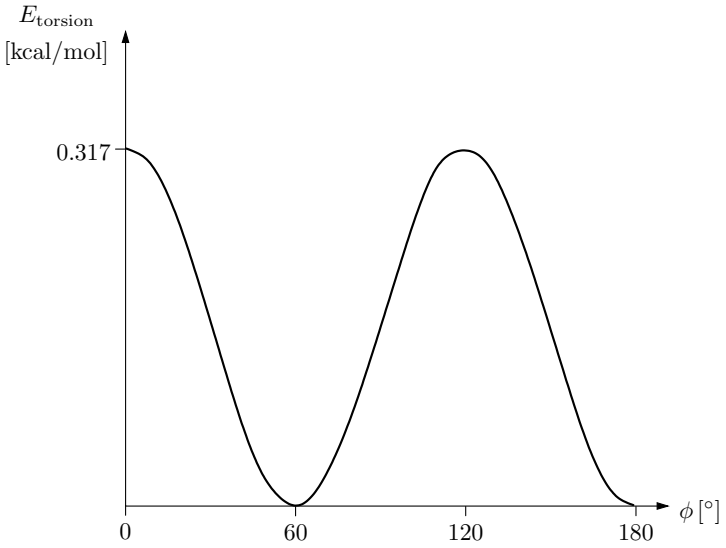

Figure 2.7.: Example for torsional energy E_{torsion} (of HC-CT-CT-HC) as a function of dihedral angle ϕ

value. Another important fact is that for $r = r_{\text{eq}}$ and $\theta = \theta_{\text{eq}}$, respectively, no energy arises from those specific interactions.

In addition to bonds and angles, an example for common torsional energy E_{torsion} in alkanes, according to equation (2.11), is depicted in Figure 2.7. When two sp^3-hybridized carbon atoms are interconnected and both of them carry hydrogen atoms, a HC-CT-CT-HC torsion can occur. As can be seen, two maxima are reached at dihedral angles $\phi = 0\,^\circ$ and $\phi = 120\,^\circ$. For $\phi = 60\,^\circ$ and $\phi = 180\,^\circ$ there is no energetic contribution. Such HC-hydrogen-atoms usually come in pairs of three, typically on CH_3 alkyl groups; this means, that the consideration of torsion for all of these participants will most likely lead to a total potential gain.

The intermolecular energy consists of two parts: The Lennard-Jones potential in equation (2.12) was already explained in the previous section and given in equation (2.1) for pure substances (i.e. only particles of the same kind). Now,

since a molecule might comprise different types of atoms, the well-depth ϵ_{ij} and the distance σ_{ij} of zero potential are functions of those atom-types i and j. They can be computed from pure substance parameters using the mixing rules [6]

$$\sigma_{ij} = (\sigma_{ii}\sigma_{jj})^{0.5} \tag{2.13}$$

$$\epsilon_{ij} = (\epsilon_{ii}\epsilon_{jj})^{0.5} \quad . \tag{2.14}$$

Atoms also carry electrostatic charges q_i and q_j, which lead to either a strong increase or a strong decrease in potential energy at close proximity. The so-called Coulomb potential energy

$$E_{\text{Coulomb}} = \frac{q_i q_j e^2}{r_{ij}} \tag{2.15}$$

is inversely proportional to the interatomic distance r_{ij}. The factor e^2 is a conversion factor which includes the components of the general Coulomb potential energy equation

$$E_{\text{Coulomb,gen}} = \frac{q_i q_j}{4\pi\epsilon_0}\frac{1}{r_{ij}} \tag{2.16}$$

and accounts for the insertion of non SI units. If equations (2.15) and (2.16) are equalized, the conversion factor e^2 amounts to

$$e^2 = \frac{(1.602 \cdot 10^{-19}\,\text{C/e}^-)^2 \cdot 10^{10}\,\text{Å/m}}{4\pi\epsilon_0 \cdot 4184\,\text{J/kcal} \cdot 6.022 \cdot 10^{23}\,1/\text{mol}} = 332.0\,\frac{\text{kcal Å}}{(\text{e}^-)^2\,\text{mol}}$$

with an elementary charge of $1.602 \cdot 10^{-19}\,\text{C/e}^-$, two unit conversion factors of $4184\,\text{J/kcal}$ and $10^{10}\,\text{Å/m}$, Avogadro's number $N_A = 6.022 \cdot 10^{23}\,\text{mol}^{-1}$ and the vacuum electric permittivity $\epsilon_0 = 8.854 \cdot 10^{-12}\,\text{C}^2(\text{J·m})^{-1}$. Thus, the Coulomb energy E_{Coulomb} is obtained in kcal/mol (like all energies in the OPLS-AA

model, using standard parameters), the interatomic distance r_{ij} is inserted in Å and the charges q_i and q_j are inserted in elementary charges e^-.

Moreover, it is important to point out another detail in equation (2.12). The expression f_{ij} equals 1, if the interactions computed are shared between the atoms of two different molecules. However, this term also accounts for van der Waals and electrostatic interactions within a single molecule. In reality, atoms of the same molecule will feel attraction and repulsion due to the proximity to the other constituents. Equation (2.12) thus not only summarizes the intermolecular energy arising from molecules within the neighborhood, but also accounts for these long-ranged potentials influencing the molecule's own atoms. By convention, $f_{ij} = 0.5$ when two atoms of the same molecule are separated by exactly three bonds, making it a "1-4" interaction between them. Atoms with more than three bonds (i. e. 1-5, 1-6, 1-7,... interactions) between them contribute with the full magnitude of the Lennard-Jones and Coulomb potential energies, meaning $f_{ij} = 1$. It is also worthwhile to note that the potential energy function (2.8) does not include individual terms to describe hydrogen bonds, unlike models like *AMBER* [9]. The authors [6] mention that hydrogen bonds can already be described properly by the current equations (2.8)-(2.12) and their set of parameters derived.

To sum up, the potential given by the OPLS-AA force field can be split up into intramolecular and intermolecular parts.

$$E = E_{\text{intra}} + E_{\text{inter}} \tag{2.17}$$

$$\text{with } E_{\text{intra}} = E_{\text{bond}} + E_{\text{angle}} + E_{\text{torsion}} + (E_{\text{Coulomb}} + E_{\text{LJ}})_{\text{intra}} \tag{2.18}$$

$$\text{and } E_{\text{inter}} = (E_{\text{Coulomb}} + E_{\text{LJ}})_{\text{inter}} \tag{2.19}$$

When a system consists of several molecules and the total potential energy

has to be computed, every molecule contributes intramolecular energy given by equation (2.18). After defining which molecules shall interact, E_{inter} can be computed for every single pair. A summation according to equation (2.17) yields the desired energy magnitude.

Before a molecular sampling algorithm for clusters is presented in the next chapter, it shall also be noted that there is a vast number of parameters available for different force fields in the literature [6, 9, 10, 13, 14, 15]. However, prior to applying these parameters to the model of choice, the selection has to occur with caution [4]. When parameter sets are derived, error/energy minimization procedures are conducted already with respect to the model used. Thus, it is usually not appropriate to adopt parameters coming from a different set of equations. The OPLS-AA force field comes with a broad array of parameters and other authors [20, 21] might contribute to this database over time.

3. Molecular Sampling Algorithm

The method presented in this work uses small clusters of molecules and quantifies the respective contributions of pairs to the energy of the system. As mentioned previously, a cluster can in general consist of two or more molecules and is characterized by its energetic interactions. For smaller clusters, typically a molecule is placed at a central position with several neighbors coordinated to it [22]. Where, how and how many of these molecules are positioned usually depends on the model requirements. In a more simplistic case, one molecule is placed at the origin of coordinates and a second molecule is placed in its proximity, so that the constructed pair of molecules (i.e. the configuration) is subject to a specific interaction. The nature and the energetic scale of this interaction is determined by the force field used, as explained in chapter 2.

3.1. Interatomic and Intermolecular Distances

Independent of cluster size, an initial question to be answered is how exactly molecules can be positioned relatively to each other. The chosen relative distances have to be able to replicate realistic, physical behavior. In addition to that, orientations of molecules have an influence, since atoms are unevenly sized and molecules might be asymmetric in shape. As can be figured, overlap

must be avoided at any time. On one hand, the intermolecular potential energies given by equation (2.19) dictate minimum distances, because repulsive forces between partners become huge with decreasing distances. In dynamic simulations, atoms and molecules cannot stay arbitrarily close to each other, as these resulting repulsive forces (and unfavorable, high potentials) will push them apart. On the other hand, intermolecular interactions tend to level off at far distances, yielding energies indifferent to certain atom types or molecular orientations. It is thus evident, that very specific spacing between molecules is required to avoid both these effects and properly describe microscopic interactions.

Two different definitions for interaction distances D have been identified in the literature. In their recent publication Sweere and Fraaije [23] presented their "Pair Configurations to Molecular Activity Coefficients (PAC-MAC) method", which is an excess Gibbs energy (g^{E}) model based on molecular pair sampling. Pair configurations of molecules with randomized orientations are sampled and intermolecular energies are evaluated using the OPLS-AA force field. The distance D used between these pairs of molecules can be derived directly from the Lennard-Jones potential equation (2.1). Firstly, the distance $r = r_{\min}$ of minimum potential is obtained through derivation

$$\begin{aligned} \frac{\mathrm{d}\, E_{\mathrm{LJ}}}{\mathrm{d}\, r} &= 4\epsilon \left(-12 \cdot \frac{\sigma^{12}}{r^{13}} + 6 \cdot \frac{\sigma^{6}}{r^{7}} \right) \stackrel{!}{=} 0 \\ r_{\min} &= \left(2\sigma^6\right)^{\frac{1}{6}} = 2^{\frac{1}{6}}\sigma \ . \end{aligned} \tag{3.1}$$

Using an arithmetic mixing rule [23] for σ_{ij} for heteroatoms, the Lennard-Jones potential is minimized by the interatomic distance

$$r_{ij} = 2^{\frac{1}{6}}\sigma_{ij} = 2^{\frac{1}{6}} \cdot \frac{\sigma_{ii} + \sigma_{jj}}{2} = 0.561 \cdot (\sigma_{ii} + \sigma_{jj}) \ . \tag{3.2}$$

In PAC-MAC, however, this potential-minimizing distance r_{ij} is not used directly. Molecular dynamics simulations have shown fluctuations around this equilibrium value, and thus, to incorporate these uncertainties, an optimized factor of $s = 0.62$ is chosen instead of 0.561 [24].

$$D_{\text{PAC-MAC},ij} = 0.62 \cdot (\sigma_{ii} + \sigma_{jj}) \ . \tag{3.3}$$

The second possibility identified to adjust the spacing between atoms and molecules is the approach of touching van der Waals surfaces. Van der Waals radii r_{vdW} are given in different sources, most notably [25]. They describe the "interaction-size" of atoms regarding dispersive forces/potentials and are defined as half the distances between the nuclei of two neighboring, but not bonded atoms [7]. Spherical van der Waals surfaces are calculated as

$$S_{\text{vdW}} = 4\pi r_{\text{vdW}}^2 \ . \tag{3.4}$$

Therefore, applying the condition of two surfaces touching each other, the distance $D_{\text{vdW},ij}$ is simply the sum of the van der Waals radii $r_{\text{vdW},i}$ and $r_{\text{vdW},j}$ of the two atoms i and j interacting.

$$D_{\text{vdW},ij} = r_{\text{vdW},i} + r_{\text{vdW},j} \tag{3.5}$$

With these two possibilities for physical interaction distances, it is now straightforward to decide whether neighboring molecules have been placed properly or not. If every single interaction distance D_{ij} between all atoms i of molecule A and all atoms j of molecule B is calculated, the actual distances r_{ij} between them have to be at least equal to or greater than the minima D_{ij}. Having this

condition

$$r_{ij} \geq D_{ij} \quad \forall i, j \tag{3.6}$$

not satisfied will indicate overlap and the configuration must be dropped. Furthermore, by convention at least one atom i of molecule A has to be in contact with at least one atom j of molecule B, meaning that their actual distance r_{ij} is equal to D_{ij}. Only then are the surrounding molecules coordinated to a central one.

Choosing either one of the definitions of interaction distances D_{ij} given before, molecular clusters can be organized in a way that condition (3.6) is always satisfied. Blanco [26] as well as Fan et al. [2], together with their pair sampling method, suggest an algorithm to determine the minimum positive and negative shift distances $r_{\pm}$ in the vectorial direction $\vec{n}$ after two molecules have been placed at the origin of coordinates with random orientations. For every atom i of molecule A and every atom j of molecule B, which shall have the coordinates $\vec{x}_i$ and $\vec{x}_j$, respectively, the solution of

$$r_{\pm} = -(\vec{x}_{ij} \cdot \vec{n}) \pm \left((\vec{x}_{ij} \cdot \vec{n})^2 - \|\vec{x}_{ij}\|^2 + D_{ij}^2\right)^{0.5} \tag{3.7}$$

gives the necessary positive and negative shift along axis $\vec{n}$ using $\vec{x}_{ij} = \vec{x}_i - \vec{x}_j$. Repeated evaluation of equation (3.7) until every possible pair ij received such a shift distance $r_{\pm}$ yields an array of different, postulated shift distances to satisfy condition (3.6). Neglecting the negative solution of the square root in equation (3.7), the maximum value in the array for $r_{\pm}$ is chosen. Therewith, overlaps are excluded, at least one pair of atoms ij of the two molecules just touch each other and the remaining ones are separated as postulated by condition (3.6).

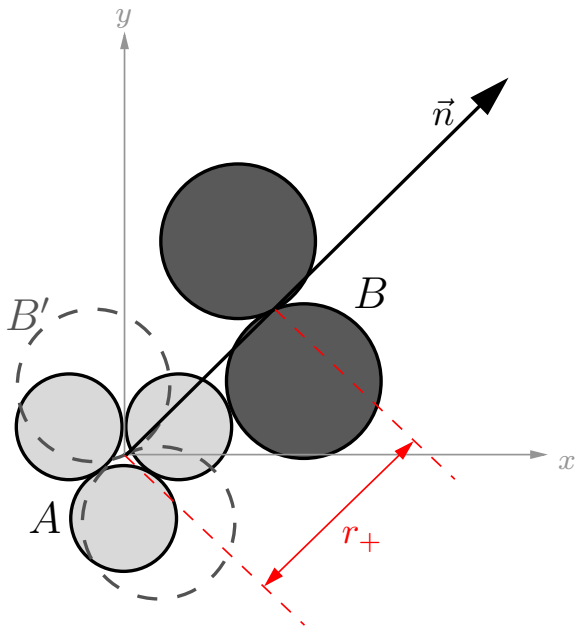

Figure 3.1.: Two-dimensional example for shift distance r_+ along axis $\vec{n}$ in a configuration of two molecules A and B consisting of three and two atoms, respectively.

Figure 3.1 illustrates a simple example in two dimensions. Molecule A consists of three atoms and molecule B consists of two atoms. Both shall be randomly orientated and placed at the origin of coordinates, with B being at the initial position B'. With the algorithm explained above, the maximum value according to equation (3.7) for each possible pair of atoms between them is chosen. This maximum value is the desired shift distance r_+. If molecule B is now moved along $\vec{n}$ with shift distance r_+, none of the atoms overlap and one pair of atoms just touches while preserving both molecular orientations.

3.2. Building Clusters for Sampling

With the possibility of regulating the spacing between molecules as given in section 3.1, clusters can now be generated in a more or less arbitrary way. Initially, three-dimensional coordinates of molecules and all the atoms contained have to be set up. There is a huge selection of (free) structure and coordinate files in the internet, with many of them being offered in a minimum energy configuration. Differences between various types of structure files are often subtle and many of them can be easily converted into others. To give a few examples, a common molecular three-dimensional coordinate file is ".sdf" (or ".mol"). The most important pieces of information contained are three-dimensional Cartesian coordinates of all the constituent atoms and which of them are bonded to each other, along with the respective atom types (i. e. the elements). Protein molecular simulations often use the ".pdb" file format. While being similar to the ".sdf" or ".mol" file format, it also gives insight into atomic charges and so called residue groups (which are sorts of functional units of atoms). Molecular simulation tools like GROMACS [27], which is a widely used software in the field of Molecular Dynamics, can use these ".pdb" files, or may have their own input formats (".gro").

When the molecular structures of the species of interest have been acquired, a certain number of molecules is placed at the origin of coordinates. This enables the user to rotate them freely around arbitrary axes, without the need of considering translation or translation-correction. The simplest cluster used in this work consists of two molecules. For simplicity, it is convenient to use the Cartesian x-axis for shifting one molecule from the original position according to section 3.1. Between two molecules, the cluster energy is indifferent to the chosen direction of shifting, given that both partners have random orienta-

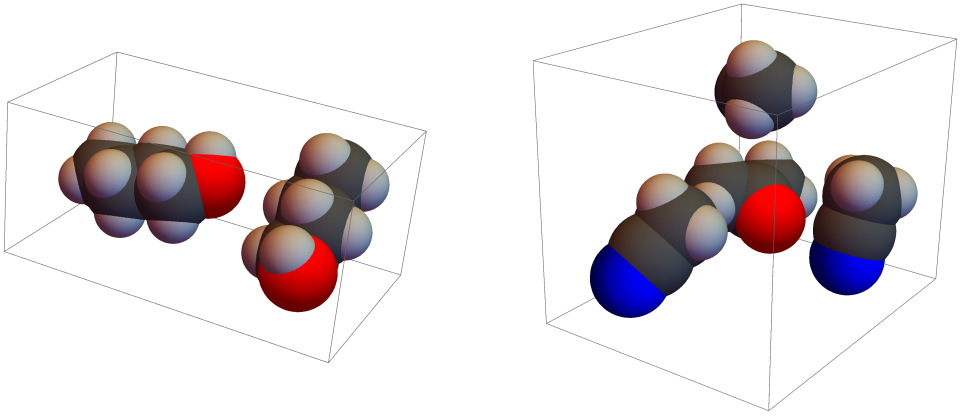

(a) 1-Butanol - 1-Butanol (b) Acetone - Acetonitrile

Figure 3.2.: Examples for clusters of (a) two and (b) four molecules using random orientations

tions.

The same principles apply to four-molecule-clusters. A certain molecule is chosen to be in a central position, while three other molecules are coordinated to this center in positive x-, y- and z-directions, respectively. At the beginning, all molecules are placed at the origin of coordinates, rotated and successively shifted along the chosen directional vectors with distances corresponding to those given in section 3.1. Figures 3.2(a) and (b) show examples of such clusters for the two arbitrary substance systems 1-butanol - 1-butanol and acetone - acetonitrile with random rotations.

These random rotations of molecules are not the only ones considered during this work. A second possibility for orientational permutations, which stems from the concept of rigid, cubic lattices in condensed phase thermodynamics, is introduced. The symmetry group of a cube with its edges parallel to the x-, y- and z-axes includes all the possible rotations which do not change the cube itself, but change the directions its faces are showing. There are, including

Table 3.1.: Symmetry group of a cube

Symmetry element	Angle of rotation [rad]	Rotational axis
1	identity	identity
2	$\pi/2$	$(0, 0, 1)$
3	$3\pi/2$	$(0, 0, 1)$
4	π	$(0, 0, 1)$
5	π	$(1/\sqrt{2}, 0, 1/\sqrt{2})$
6	$2\pi/3$	$(1/\sqrt{3}, -1/\sqrt{3}, 1/\sqrt{3})$
7	$4\pi/3$	$(1/\sqrt{3}, 1/\sqrt{3}, 1/\sqrt{3})$
8	$3\pi/2$	$(0, 1, 0)$
9	$4\pi/3$	$(1/\sqrt{3}, -1/\sqrt{3}, 1/\sqrt{3})$
10	$3\pi/2$	$(1, 0, 0)$
11	π	$(0, -1/\sqrt{2}, 1/\sqrt{2})$
12	$2\pi/3$	$(-1/\sqrt{3}, -1/\sqrt{3}, 1/\sqrt{3})$
13	$2\pi/3$	$(1/\sqrt{3}, 1/\sqrt{3}, 1/\sqrt{3})$
14	$\pi/2$	$(1, 0, 0)$
15	π	$(0, 1/\sqrt{2}, 1/\sqrt{2})$
16	$4\pi/3$	$(-1/\sqrt{3}, 1/\sqrt{3}, 1/\sqrt{3})$
17	$\pi/2$	$(0, 1, 0)$
18	$2\pi/3$	$(-1/\sqrt{3}, 1/\sqrt{3}, 1/\sqrt{3})$
19	$4\pi/3$	$(-1/\sqrt{3}, -1/\sqrt{3}, 1/\sqrt{3})$
20	π	$(-1/\sqrt{2}, 0, 1/\sqrt{2})$
21	π	$(1, 0, 0)$
22	π	$(-1/\sqrt{2}, 1/\sqrt{2}, 0)$
23	π	$(1/\sqrt{2}, 1/\sqrt{2}, 0)$
24	π	$(0, 1, 0)$

the identity element, 24 elements in this symmetry group [28]. In summary, molecules can either be rotated randomly before shifting them apart, or, when they are abstracted as cubes (or dice), they can be rotated to match one pattern within a cube's symmetry group. Table 3.1 shows every element of the symmetry group of a cube, given by the rotational axis in unit vectors and the angle of rotation.

3.3. Sampling Methodology

With the previous chapters and sections explaining force fields and cluster setups, molecular sampling algorithms can now be discussed in detail. As the word "sampling" already indicates, it means a statistical process of creating possible configurations out of a population of possibilities, at least when speaking about random sampling. When only cube-symmetry-group rotations are considered, all of the possible setups (namely 24 per molecule) in the population can be sampled within reasonable time-scales, as long as clusters are small enough. In general, in order to sample molecular configurations, there are several steps required, most of which have already been covered.

1. Decide on the species of interest, acquire three-dimensional structural data on these species, choose the cluster size and a force field (OPLS-AA).

2. Place every molecule at the origin of coordinates. Perform a random rotation or a cube-symmetry-group rotation per molecule.

3. Determine the shift distances from the designated central molecule, which stays at the origin of coordinates, along the desired axes according to section 3.1 for every other molecule. For two molecules the x-axis is chosen, for four molecules the x-, y- and z-axes are chosen.

4. Move every molecule (except for the central one) along the respective axis. The cluster created might look like those given in Figure 3.2.

5. Evaluate all the pair interactions of the outer molecules with the central one. In general, every molecule carries intramolecular energy E_{intra}

according to equation (2.18) and every pair interaction gives an intermolecular energy E_{inter} according to equation (2.19).

6. In the case of random rotations, repeat steps 2-5 for a defined number of samples. In the case of cube-symmetry-group rotations, repeat steps 2-5 until every single constituent has taken every single orientation given by Table 3.1.

The number of samples needed for random rotations has to be big enough to be statistically representative of the population. As a result, every sampling step yields a total potential energy $E = E_{\text{intra}} + E_{\text{inter}}$ given by the force field. In order to characterize the system and its interactions, a distribution of energetic states can be constructed.

An important point to make is that for the remainder of this work, only the intermolecular energies E_{inter} are considered. The intramolecular energies E_{intra} do not provide any information on the interaction of partnering molecules. When systems with constant concentrations of constituents are sampled, every rigid molecule always contributes its same intramolecular energy. In total, this leads to an offset in the distribution of possible energetic states. However, no additional information on the shape of this distribution is acquired. Moreover, other publications like [2] or [22], but most notably the recently published PACMAC model [23], have shown that intermolecular energies E_{inter} are sufficient to describe energetic interactions in clusters. It is thus convenient to only look at the distribution of the intermolecular energy E_{inter}.

A broad distribution of energies corresponds to multiple energetic states possible between the interacting partners. On one hand, Figure 3.3 shows the distributions of the intermolecular energy E_{inter} for pairs of acetone molecules after sampling (a) 10^5 or (b) 10^4 configurations with random orientations. The

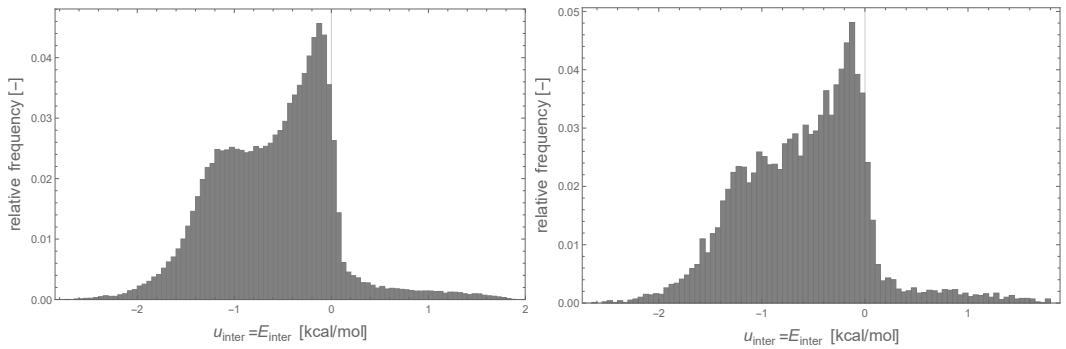

(a) (b)

Figure 3.3.: Distribution of intermolecular energy E_{inter} after pair sampling of acetone with random orientations and (a) 10^5 samples taken or (b) 10^4 samples taken using the PAC-MAC distance

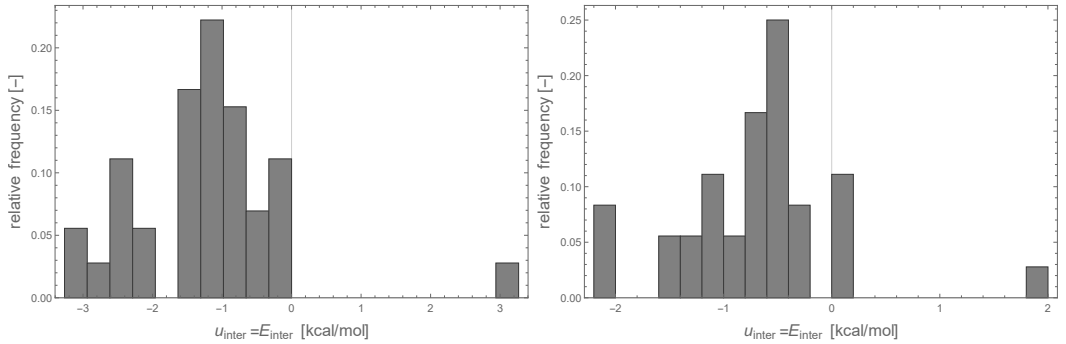

(a) (b)

Figure 3.4.: Distribution of intermolecular energy E_{inter} after pair sampling of acetone with cube-symmetry-group orientations and (a) with touching van der Waals surfaces or (b) using the PAC-MAC distance

difference in sample size is reflected in the smoothness of the histograms, both being constructed using 60 bins. Representative results of statistical sampling processes require an appropriate sample size. Furthermore, both distributions are shaped similarly, with the most probable magnitude of E_{inter} just below 0 kcal/mol. States of positive potential are less likely to occur. In addition to that, the distributions are strongly asymmetric. On the other hand, Figure 3.4 gives the distributions for cube-symmetry-group rotations, with (a) touching van der Waals surfaces or (b) the PAC-MAC distance. The differences in shape are distinct compared to Figure 3.3, while similar energetic states are attained. Predefined configurations, like those given by the symmetry group of a cube, can also be obtained by random rotations. Therefore, all the energies in Figure 3.4 are within the boundaries of the lowest and highest energy magnitudes of Figure 3.3, given that a sufficient number of configurations are sampled. However, the probabilities are scattered and only specific states are attained. This is reasonable, because a finite number of predefined configurational patterns should also yield distinct potential energies. Constraining neighboring partners to have touching van der Waals surfaces brings them together closer than with the PAC-MAC distance, resulting in a broader distribution with lower energetic minima and higher energetic maxima. Throughout this work, it has been found that the distance of touching van der Waals surfaces D_{vdW} is typically smaller than the PAC-MAC distance $D_{\text{PAC-MAC}}$.

When four molecules form a cluster, the results of sampling will essentially be similar, as long as only pairwise interactions with the central molecule are considered. In fact, a single sampling step then accounts for three pair-interactions. The energy distribution of the cluster, however, could be different. Akkermans [22] prefers bigger cluster sampling procedures over single pairs to smoothen distributions and devaluate energetic outliers. With these

applications in mind, in this work clusters of four molecules are not discussed in more detail, but could be used as enhanced pair-sampling methods, giving three pair configurations per iteration as described above.

In the following chapters, various applications of the developed molecular sampling algorithm are presented. Case studies on molecular orientations are provided along with influences of different scales for intermolecular distances as described in section 3.1. Finally, simulation results are compared to experimental data.

4. Application to Binary Systems

The molecular sampling algorithm presented in the previous section 3.3 allows for calculations of distributions of interaction energies among molecules in clusters. It is now applied to binary mixtures, using molecular pair sampling of both pure substances and the mixture itself. As will be elaborated in the following sections, the results can be used to parameterize Monte Carlo (MC) simulations, which then leads to excess properties of the liquid mixtures and comparison to experimental data.

Before MC simulation approaches are discussed, the concept of relative orientations has to be explained, as it plays an important role for the analysis of results and will be used frequently later on.

4.1. Influence of Relative Orientations

When looking at pairs of rigid molecules, intermolecular energies E_{inter} depend on the species, the intermolecular distances and the relative orientations of the partners. On one hand, different results can be expected depending on the positioning of e.g. the polar carbonyl group in acetone. On the other hand, nonpolar molecules like alkanes could be expected to show little to no

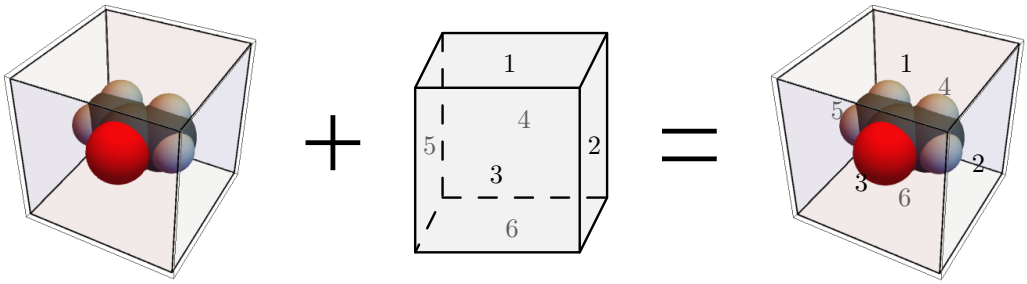

Figure 4.1.: Coupling of molecular structure for molecular sampling with six-sided die model

dependence on relative orientations. The molecular sampling algorithm shall be used to investigate these dependencies.

In order to study these effects, for given substances the molecular orientations are predefined to only provide specific configurations. For example, pairs of acetone molecules can be set up to have different positions of the carbonyl group and, thus, also the alkyl residues of the molecule. An important concept is the modeling of molecules as six-sided dice, which is accomplished by creating an imaginary box around them. Whenever a molecule is rotated, this predefined cube is rotated in an identical manner. An illustration of this concept is shown in Figure 4.1, where an acetone molecule is combined with a six-sided die with faces $1, 2, \ldots, 6$. Due to identical rotations of the molecule and the die, the internal orientation (i.e. within the die) remains the same, while external orientations (i.e. with other partners) depend on the cluster setup. It shall be noted that in the following sections the terms “cube” and “die” are often synonymous; a slight difference comes with the geometric meaning of “cube”, rather referring to the cubic box placed around molecules.

The way a molecule is placed within its respective cube can be varied through rotation prior to cube assignment. Again using the example of acetone, three extreme cases for carbonyl oxygen positions can be given: The oxygen atom

Table 4.1.: Explanation of abbreviations used for molecule rotations within their respective cubes

abbreviation for rotation	rotational details	explanation
non (only molecule name)	non (standard configuration)	chain/polar group oriented towards face of die
RotZ45	rotation of 45° around z-axis	chain/polar group oriented towards edge of die
RotZ45RotX45	rotation of 45° around z-axis and x-axis	chain/polar group oriented towards vertex of die

can point towards the face, the edge or the vertex of the cube. As the molecular structure is rigid, this also changes the positions and orientations of the alkyl residues. For convenience, abbreviations are introduced to describe these internal configurations. They are listed and explained in Table 4.1. When a molecule is oriented towards the faces of the surrounding cube, this shall be defined as "standard configuration". Using this standard configuration as starting point, rotations can be conducted to change the internal orientation of the constituent within its model die. The configuration "RotZ45" is achieved by a rotation of 45° around the z-axis, leading to the molecule pointing towards an edge of the cube. A following rotation of 45° around the x-axis creates the "RotZ45RotX45" configuration; the molecule now points towards the vertex of the cube. To summarize the terminology and give examples for different species, this procedure is illustrated for acetone, n-heptane, 1-butanol, methanol and n-dodecane in Figure 4.2. These substances and configurations will be used later on for MC simulations.

After setting up the molecules within their respective model dice, the cube-

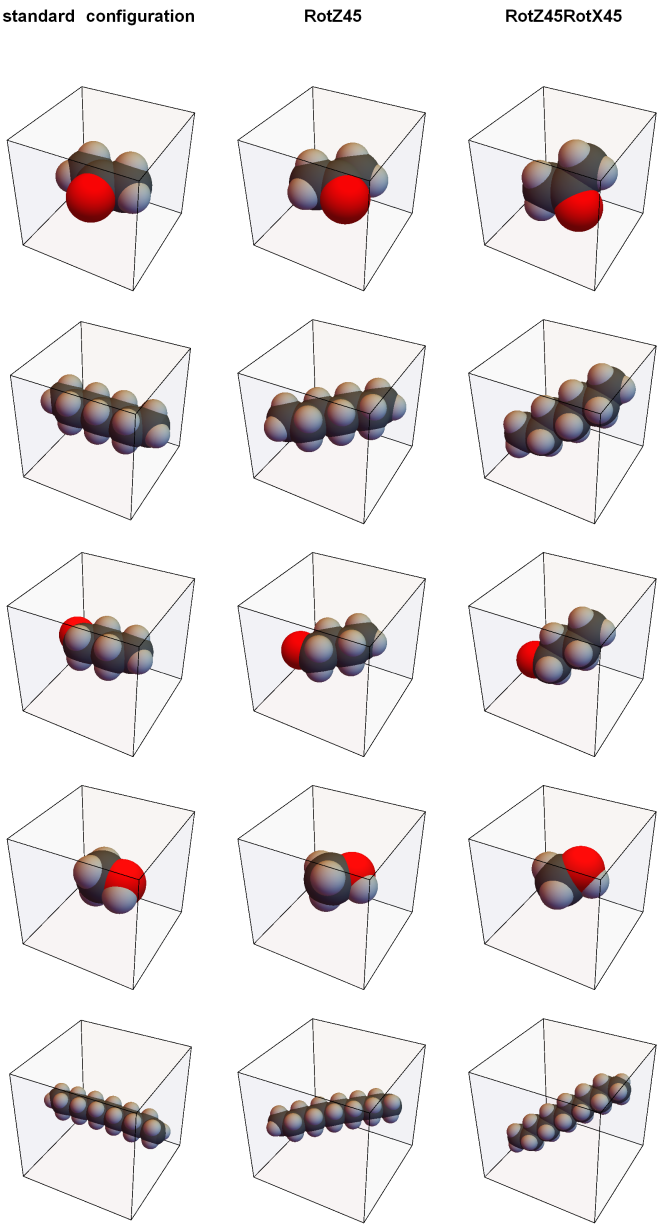

Figure 4.2.: Standard configurations, rotations of 45° around z-axis (RotZ45) and combined rotations of 45° around z-axis and x-axis (RotZ45-RotX45) for (top to bottom) acetone, n-heptane, 1-butanol, methanol and n-dodecane

symmetry-group rotations are conducted and the according intermolecular energies E_{inter} are computed during molecular pair sampling. Based on the resulting distributions of intermolecular energies E_{inter}, the influence of molecular orientations within their respective cubes can be investigated. Acetone is used as an exemplary polar molecule; n-heptane illustrates the effects on nonpolar alkanes.

Figure 4.3 shows these three cases for a pair of acetone molecules and the corresponding energy distributions. One acetone molecule of the respective pairs is always depicted next to the distribution. As can be seen, the distributions seem to vary strongly, but several common properties can be outlined. Firstly, the most probable energetic states are, independent of starting orientation, located slightly below 0 kcal/mol. Secondly, all of the distributions contain states located "relatively" far from the expected value. Positive deviations are attributed to states of the two carbonyl oxygen atoms within each others neighborhood, leading to strong Coulomb repulsion. On the other hand, significant negative deviations arise from alkyl groups at close proximity and, thereby, enhanced attraction. It is again important to say that all of the states given in Figure 4.3 can also be obtained via random sampling, as long as enough sampling steps are taken.

Outlining the differences between the setups in Figure 4.3, a very notable characteristic of different basic/starting orientations is the development of the expected values (the "centers" of the distributions). For the top case, where the carbonyl group points towards the face of the cube, a pronounced expected value at approximately -0.5 kcal/mol is developed. Adjacent energetic states are also probable, but the peak is distinct. When the carbonyl group is oriented towards an edge (middle case), this changes in favor of a less distinct, but instead broader expected-value-region. The distribution shown is bimodal, but

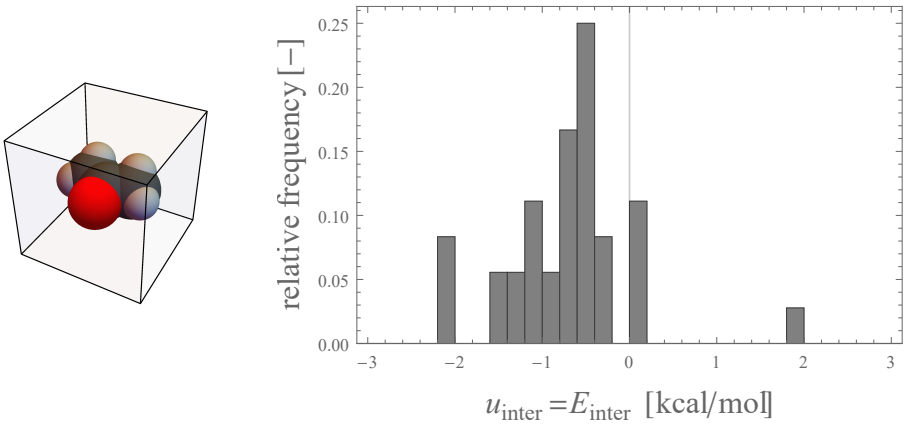

(a) Acetone - Acetone, standard configurations, PAC-MAC distance

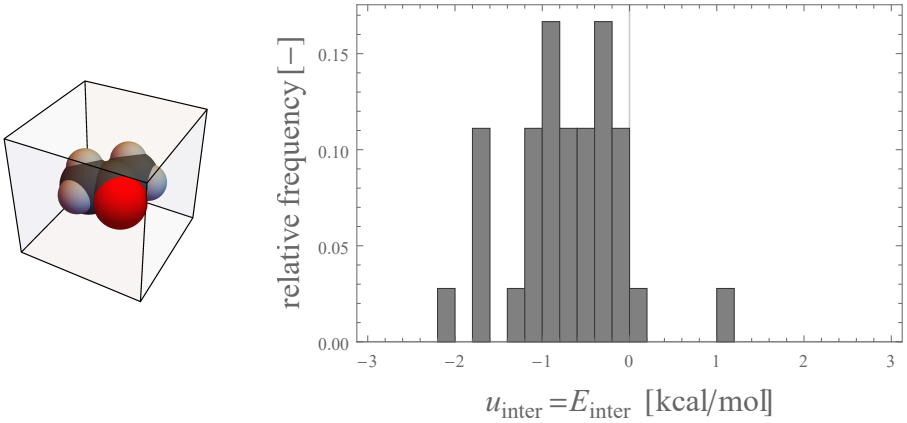

(b) Acetone(RotZ45) - Acetone(RotZ45), PAC-MAC distance

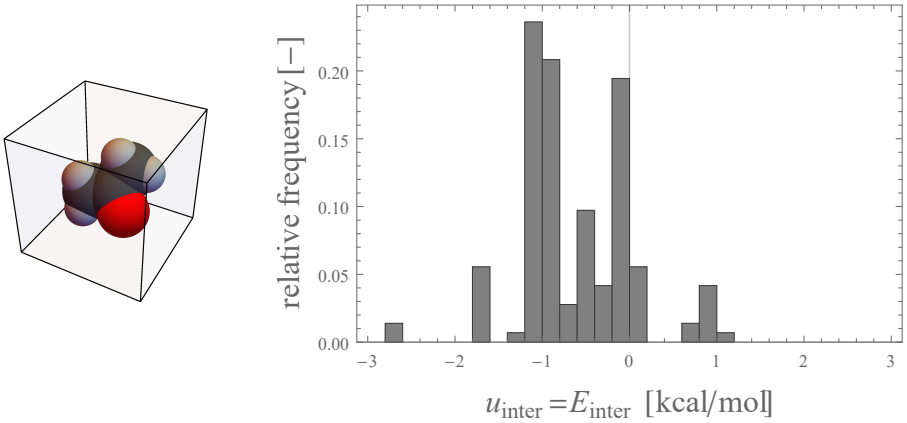

(c) Acetone(RotZ45RotX45) - Acetone(RotZ45RotX45), PAC-MAC distance

Figure 4.3.: Distribution of intermolecular energy E_{inter} after pair sampling of acetone with cube-symmetry-group orientations and PAC-MAC distances. Carbonyl group is either oriented towards (a) a face, (b) an edge or (c) a vertex of the surrounding cube.

can be interpreted as a flatter, more evenly distributed assembly of energies at the center. In contrast, the bottom case of the carbonyl group pointing towards the vertex results in a clearly bimodal distribution, with probable energetic states around 0 and -1 kcal/mol.

For comparison, the same cases can be constructed for n-heptane, which is a nonpolar alkane. Due to the absence of any polar groups, strongly repulsive states are not expected to occur. Instead, Jensen [8] reports that for alkanes the Coulomb energies E_{Coulomb} should amount to zero, while attractive van der Waals energies $E_{\text{vdW}} = E_{\text{LJ}}$ should dominate. As can be seen from Figure 4.4, there are no states of positive energies. Independent of orientation, the Coulomb terms among alkyl groups indeed cancel out, leaving the van der Waals energies to be the remaining ones. Since molecules are spaced at predefined distances (here PAC-MAC distance $D_{\text{PAC-MAC}}$, alternatively touching van der Waals surfaces D_{vdW}), the Lennard-Jones potential energy E_{LJ} is never within the positive, strongly repulsive region, leading to negative (attractive) results. In contrast to acetone and Figure 4.3, starting orientation before cube-symmetry-group sampling has a smaller influence on the expected values, but heavily determines the probability of states in the outer regions of the distributions. Having the n-heptane chain point towards the face (top case) or the edge (middle) of the cube yields very similar results, with identical span width of the distributions. In both scenarios, expected values are located just above -1 kcal/mol. However, the bottom case of the n-heptane molecule oriented towards the vertex of the cube leads to significantly decreased broadness. The expected value is still in the same region as with the other two cases, but no energetic states down to -3 kcal/mol are observed.

To further discuss this topic, the sampling algorithm of section 3.3 has to be recalled. Since cube-symmetry-group rotations are performed and both partners

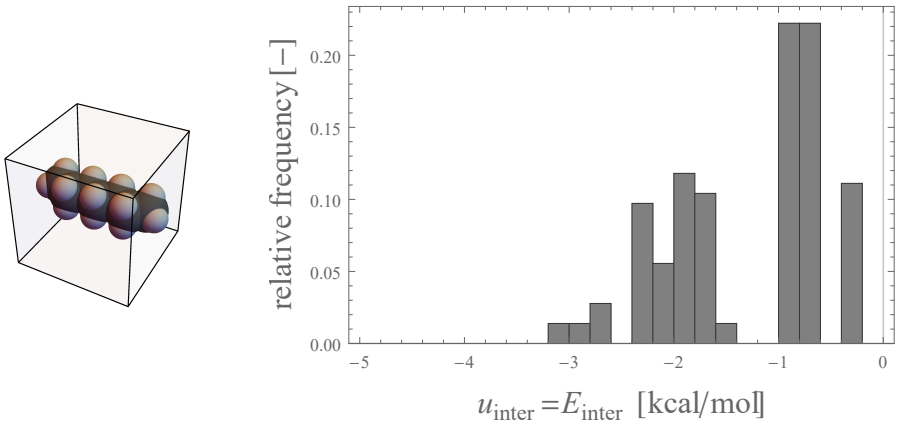

(a) n-Heptane - n-Heptane, standard configurations, PAC-MAC distance

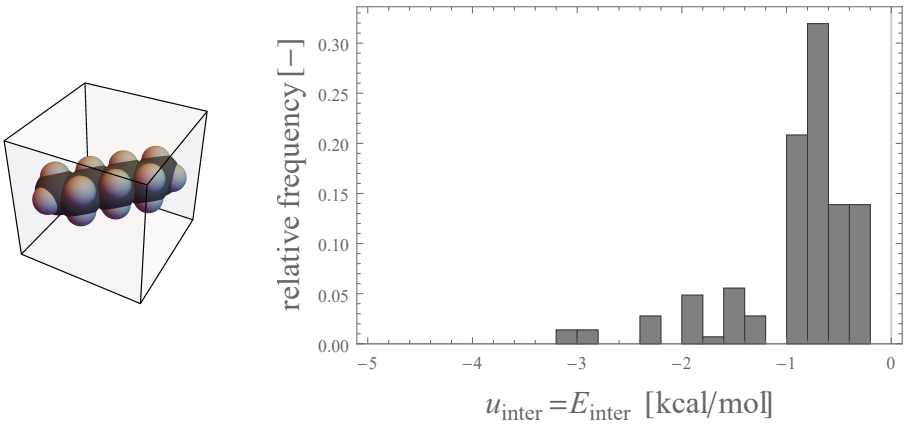

(b) n-Heptane(RotZ45) - n-Heptane(RotZ45), PAC-MAC distance

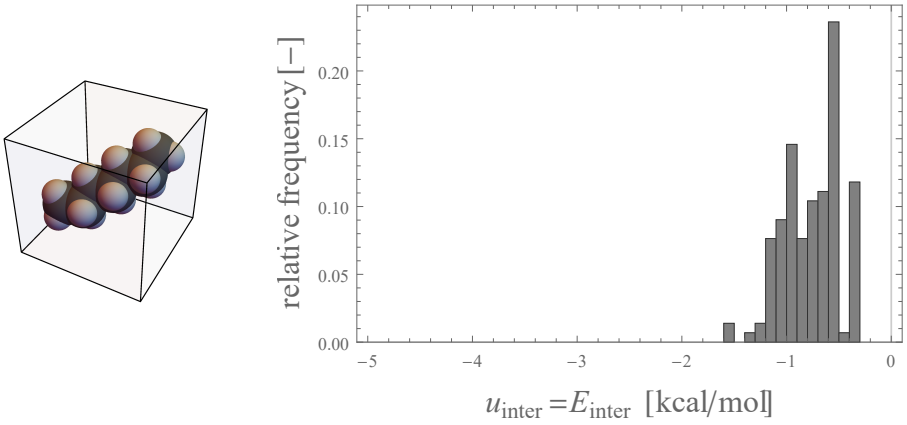

(c) n-Heptane(RotZ45RotX45) - n-Heptane(RotZ45RotX45), PAC-MAC distance

Figure 4.4.: Distribution of intermolecular energy E_{inter} after pair sampling of n-heptane with cube-symmetry-group orientations and PAC-MAC distances. Alkane chain is either oriented towards (a) a face, (b) an edge or (c) a vertex of the surrounding cube.

(here) are positioned in the exact same manner inside the cube, the starting positions heavily determine the pairs' relative orientations. For example, the top case in Figure 4.4 will create configurations where the two n-heptane molecules are parallel, thus giving short interatomic distances during the evaluation of intermolecular energies E_{inter}. Within this first case, however, also configurations of great interatomic distance are obtained, when the two molecules are in line. To summarize, the reason for the broadness of the distribution, even though alkanes do not contain any polar groups, is the chain length.

In fact, going from top to bottom in the cases of Figure 4.4 shows a transition of possible states, which is reflected in the distributions. As explained above, the top case can produce two extreme opposites, namely either all of the neighboring atoms being very close to or very far from each other. With the change of orientation towards the edge (middle), the partners are either in an angled position during sampling, or, in case of parallelism, do not cover each other completely. The negative energetic "outliers" are less probable. Finally, further adjusting the orientation of n-heptane towards the vertex leaves no possibility for mutual coverage.

Since one aim of this work is the establishment of a link between molecular sampling results and experimental data, the next section deals with the application in Monte Carlo (MC) simulations. The data obtained from such simulations can then be compared to measurements for the substances used.

4.2. Monte Carlo Simulations

Along with other procedures (like Molecular Dynamics), Monte Carlo (MC) simulations [29] are important tools in computational chemical engineering.

They use statistical processes to equilibrate a predefined system of molecules to then draw samples over a certain number of equilibrium iterations. In specific, the MC algorithm used for this work comprises molecules regarded as six-sided cubes (or dice) in a rigid, three-dimensional lattice of size 30^3. It shall be briefly explained, but is outlined more thoroughly in [30] and [31]. In addition to that, the MC algorithm is elaborated in [32, 33, 34].

At the beginning, two substances A and B are chosen for a binary system. The cubic lattice size is defined as 30^3. Prior to the actual simulation, every lattice site is randomly occupied by either a molecule of type A or a molecule of type B, with the constraint of satisfying the overall molar fraction x_A of constituent A and x_B of constituent B in the system. When the simulation is started at a given temperature T, randomly chosen pairs of A and B are permuted and/or rotated. The energy of the whole system can be calculated using the interaction energies arising from contacts of faces with certain energetic properties, which are assigned to every face of a specific cube type. If the total energy decreases, the permutation is accepted. If the energy of the system increases, the permutation is only accepted with a probability

$$\exp\left(-\frac{\Delta u}{RT}\right) \tag{4.1}$$

where Δu is the energy difference through the permutation and R is the universal gas constant. With a spherical model, every face of a specific molecule type has the same properties, leading to energies which are independent of orientation. In our case, as we use a six-sided dice model, every face can be different. When the six die-faces of molecule A are written as $i \in 1, 2, \ldots 6$ and the six faces of B are written as $j \in 7, 8, \ldots 12$, the interaction parameter ε of a face-contact can be $\varepsilon_{ii}, \varepsilon_{ij} = \varepsilon_{ji}$ and ε_{jj}, depending on the individual neighborhood within the lattice. The total internal (potential) energy $u = u^{\mathrm{mix}}$

depends on these energetic parameters and is obtained via summation of the contact energies with respect to local composition.

Whenever a mixture of certain substances is simulated, an appropriate parameterization of these ε's is needed. Since two molecule types A and B are present and each of them is represented by a six-sided die, a total of $12 \cdot 12 = 144$ values of ε are needed in order to fully specify possible interactions. As it is not important from which side contact ij is regarded and thus $\varepsilon_{ij} = \varepsilon_{ji}$, this 12x12-matrix is symmetric, giving a total of 78 independent interaction parameters ε. The intermolecular energies E_{inter} obtained via cube-symmetry-group molecular sampling shall be used to characterize the energetic, interactive behavior among the constituents.

In the following section, "ij" shall now be representative for all possibilities ii, ij, ji and jj within the context of interaction parameters ε. As ε_{ij} determines the energetic interaction between cube faces i and j of neighboring molecules, the goal is to obtain representative E_{inter} values through molecular pair sampling. Just as explained earlier, varying starting orientations are chosen for both species A and B. Summarizing the three possibilities again, they are: A standard configuration, where the molecules are aligned with the edges of the cube, a rotation of 45° around the z-axis ("RotZ45") and a rotation of 45° around the z-axis followed by a rotation of 45° around the x-axis ("RotZ45RotX45"). These setups are chosen because they provide three limiting cases of molecules "pointing" towards either a face, an edge or a vertex of their surrounding cubes. Based on these starting orientations, all the cube-symmetry-group rotations are performed for both molecules of a pair. When a mixture of A and B shall be investigated, such samples are created for pure substances (pairs A-A and B-B) and the mixture (pairs A-B). In total, $3 \cdot (24 \cdot 24) = 1728$ values for E_{inter} are thus computed.

Table 4.2.: Starting assignment of cube faces to indices $i \in 1, 2, \ldots, 6$ and $j \in 7, 8, \ldots, 12$

molecule A			molecule B		
cube face		i	cube face		j
top	...	1	top	...	7
bottom	...	6	bottom	...	12
left	...	5	left	...	11
right	...	2	right	...	8
front	...	3	front	...	9
back	...	4	back	...	10

Prior to evaluations, the cubes of molecules A and B are predefined in terms of their faces i and j. Table 4.2 summarizes the assignment of indices. For a practical example of acetone, Figure 4.1 is again referred to. When molecules are now rotated according to the cube-symmetry-group, the position of all faces are also known after every rotation. In other words, when molecules are rotated during pair sampling, the cube faces are rotated along with them, thereby giving information of the neighboring faces for every single configuration. Finally, every value of E_{inter} is assigned to the corresponding indices of the neighboring faces ij. For example, if molecules A and B are configured in a way that faces $i = 1$ and $j = 7$ are touching each other, the interaction energy E_{inter} is attributed to ε_{17}. It is worth mentioning that, due to this method, permutations of all the other, non-nearest faces are not distinguished. When two cube faces i and j are the nearest neighbors for a pair of molecules A and B, then E_{inter} is always attributed to the ij-interaction. As there are several possible configurations with i and j touching, their values for E_{inter} are averaged to give a single value for ε_{ij}. This arithmetic averaging-procedure is further elaborated on in section 4.3, during the overall discussion of results.

Regarding the number of iterations during MC simulations, a compromise between simulation time and accuracy has been found. For a chosen number, 100 equilibration loops and 100 evaluation loops are performed. In fact, this means that the number of iterations is practically increased by factor 100 due to internal and external looping. Usually, to satisfy high quality standards in terms of convergence, 10^7 iterations are necessary. This corresponds to $100 \cdot 10^7 = 10^9$ equilibration and 10^9 evaluation steps. The results presented in this work are obtained with a decreased number of 10^6 iterations (equivalently 10^8 equilibration and evaluation steps), which is sufficient to produce well-converged results of high quality while greatly reducing the simulation time required. In order to assess the error (or the uncertainty) arising from this decreased number of 10^6 iterations, a set of 108 points of different temperatures and compositions are computed using either accuracy. The interaction parameters ε_{ij} of acetone - n-heptane in standard configurations and with PAC-MAC distances are chosen. For comparison, the dimensionless internal energy

$$u' = \frac{u}{RT} \tag{4.2}$$

is calculated for every point. Figure 4.5 shows a way of analyzing the difference in results between the shorter and the longer simulation run. To assess the deviation between individual u', the relative deviation

$$\frac{u'_{10^6 \text{ iterations}} - u'_{10^7 \text{ iterations}}}{u'_{10^7 \text{ iterations}}} \cdot 100\,\% \tag{4.3}$$

can be calculated for each of the 108 data points. Figure 4.5 shows the relative deviations together with the overall minimum value of -0.050015 % and the overall maximum value 0.011324 % given by the dashed, red lines. Apart from these two values, the majority of deviations is even closer to 0. In summary,

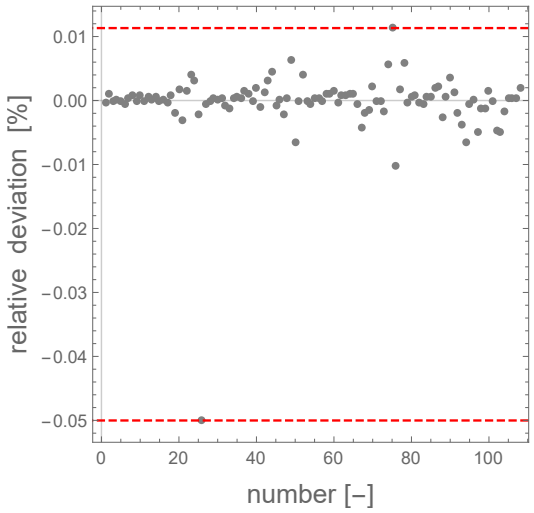

Figure 4.5.: Relative deviations of dimensionless internal energies $u' = u/(RT)$ from a shorter (10^6) and a longer (10^7 iterations) Monte Carlo simulation run

due to these small differences, the results obtained via 10^6 rather than 10^7 iterations are assumed to already be very accurate and suffice for the following discussions.

Finally, with the internal energy of the mixture $u = u^{\text{mix}}$ from Monte Carlo simulations, the excess properties of the system can be computed. The internal excess energy u^E is obtained via subtraction of the ideal mixture's contribution. With the molar fractions of component 1 (i.e. molecules of type A) being x_1, the molar fraction of component 2 (i.e. molecules of type B) being $x_2 = 1 - x_1$ and their respective (pure) internal energies u_1 and u_2 then follows

$$u^E = u^{\text{mix}} - x_1 u_1 - (1 - x_1) u_2 \ . \tag{4.4}$$

Since the product of pressure P and volume v is not defined in a rigid cubic

lattice, the enthalpy $h = u + (Pv)$ equals the internal energy u.

$$u^E = h^E \tag{4.5}$$

The excess Gibbs energy (or excess free enthalpy) g^E is calculated from the temperature dependence of g^E on h^E, using a polynomial fit according to [30].

$$\frac{\partial \frac{g^E}{T}}{\partial T} = -\frac{h^E}{T^2} \tag{4.6}$$

Eventually, the excess properties h^E and g^E can then be compared to experimental data. The focus of the following discussions shall be on the excess free enthalpy g^E, as it is our key quantity to be described for multicomponent mixtures. Four different substance systems have been chosen to give an idea of the versatility of the approach presented. Mixtures of a ketone and an alkane (acetone - n-heptane), an alkane and an alcohol (n-heptane - 1-butanol), a ketone and an alcohol (acetone - methanol) and a ketone and a long-chained alkane (acetone - n-dodecane) are presented. For convenience, only the most important results are discussed in the following sections. A collection of all computational (MC) results obtained can be found in the appendix.

Before presenting the results, it shall be mentioned that experimental data for h^E and g^E are plotted using the Redlich-Kister equation [35]

$$h^E = (x_1 - x_1^2) \cdot \sum_{l=1}^{L} C_{h^E,l}(2x_1 - 1)^{l-1} \tag{4.7}$$

$$g^E = (x_1 - x_1^2) \cdot \sum_{l=1}^{L} C_{g^E,l}(2x_1 - 1)^{l-1} \tag{4.8}$$

expanded from $l = 1$ to $l = L$.

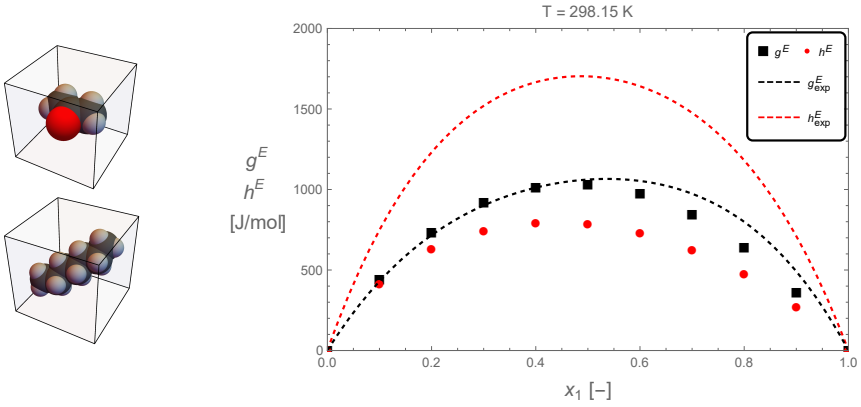

(a) Acetone - n-Heptane(RotZ45RotX45), PAC-MAC distance

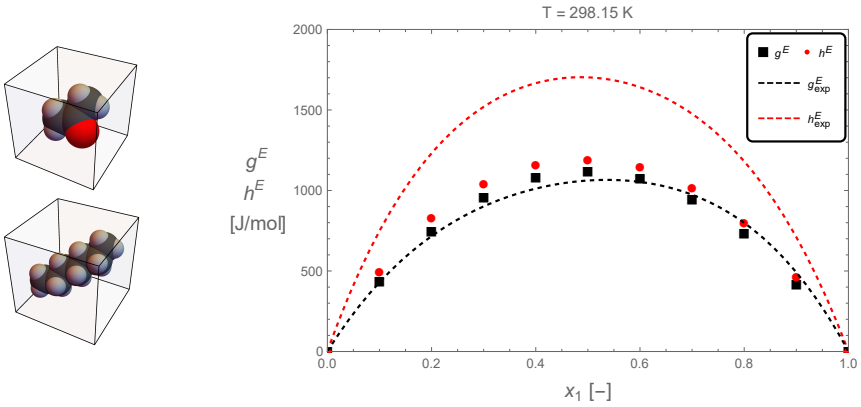

(b) Acetone(RotZ45RotX45) - n-Heptane(RotZ45RotX45), van der Waals distance

Figure 4.6.: Comparison of h^E and g^E calculated from Monte Carlo simulations with experimental data [35] for the system acetone - n-heptane

4.2.1. Acetone - n-Heptane

The binary mixture acetone - n-heptane is an example for a polar ketone interacting with a nonpolar alkane. Figure 4.6 shows computed values for h^E and g^E with acetone and n-heptane in different configurations and compares them to experimentally determined [35] data. Both data sets give good results for g^E, while h^E cannot be described properly. The rotation of n-heptane (RotZ45RotX45) is similar for both cases (a) and (b) in Figure 4.6, while acetone is (a) in standard configuration with the polar carbonyl group pointing

towards a face or (b) in RotZ45RotX45 configuration with the carboyl group oriented towards a vertex. As discussed in section 4.1, this full rotation of n-heptane leads to a narrow distribution of the intermolecular energy E_{inter}. Thus, the influence of the chain length of the alkane is decreased numerically, because the attractive potential is distributed evenly among the cube faces through the rotation. Therefore, a homogeneous set of ε_{ij} is obtained, leading to interactions which are rather insensitive to alkane orientation. In fact, this is consistent with the idea of Egner [30] to attribute a uniform interaction parameter to all faces of the alkane. However, molecular sampling yields a negative interaction parameter ε_{ij} accounting for van der Waals attraction instead of an inert value of 0.

Rotating acetone and using touching van der Waals surfaces in Figure 4.6(b) seems to provide g^E-results similar to Figure 4.6(a), where PAC-MAC distances are used. Similar to the effect observed with n-heptane, the rotation of acetone leads to a distribution of the repulsive characteristics of adjacent carbonyl groups among multiple cube faces. This is counteracted by the generally shortened distances through touching van der Waals surfaces. In total, these opposed tendencies lead to similar results for g^E.

All the h^E- and g^E-data generated via Monte Carlo simulations for acetone - n-heptane can be found in Figures B.1-B.6 of the appendix.

4.2.2. n-Heptane - 1-Butanol

Like the previous system, the binary mixture of n-heptane and 1-butanol consists of a nonpolar alkane and a polar compound. Instead of a ketone (acetone), 1-butanol is an alcohol with the polar hydroxy group at the end of the alkane

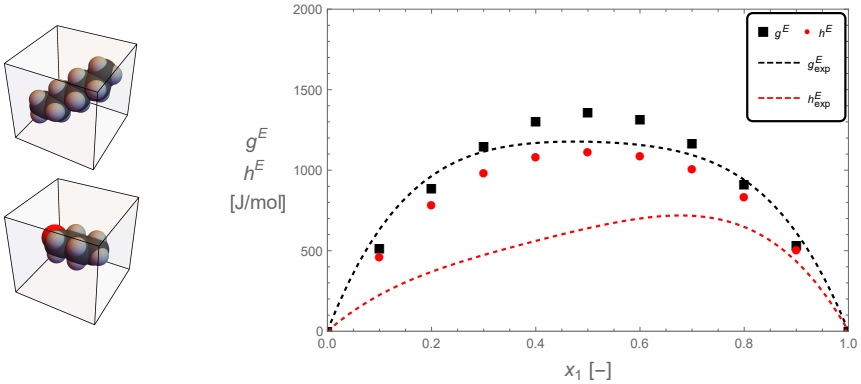

(a) n-Heptane(RotZ45RotX45) - 1-Butanol, PAC-MAC distance

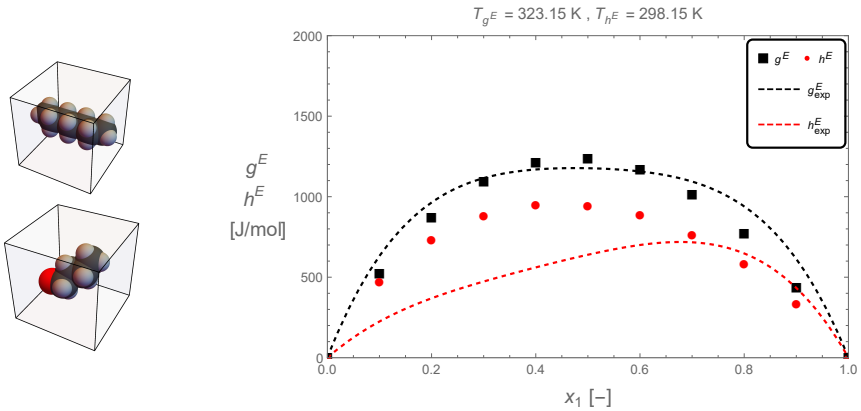

(b) n-Heptane - 1-Butanol(RotZ45RotX45), PAC-MAC distance

Figure 4.7.: Comparison of h^E and g^E calculated from Monte Carlo simulations with experimental data [36, 37] for the system n-heptane - 1-butanol

chain. Overall, the trends for g^E and h^E with molecular orientations are similar to those obtained for the system acetone - n-heptane. As can be seen in Figure 4.7(a), again a rotation of n-heptane for 45° around the z- and the x-axis (i.e. RotZ45RotX45) yields a reasonable description of g^E, when 1-butanol is in standard configuration. However, also Figure 4.7(b) gives a good description of g^E. There, 1-butanol is oriented towards the vertex of its cube, while n-heptane is in standard configuration. Seemingly, the variance in ε_{ij} through the alkane orientation (see section 4.1) can account for similar effects as the face-orientation of the hydroxy group in 1-butanol. The polar characteristics of the hydroxy group, which is oriented towards the vertex of the cube in the RotZ45RotX45-configuration, are more evenly distributed among the faces. This is coupled with possibly stronger alkane attraction through non-rotated n-heptane. Similar results can thus be obtained. In contrast to the system acetone - n-heptane, quantitative h^E trends can be described better, even though the shape of the curve cannot be represented.

It is also worth mentioning, that interatomic distances of touching van der Waals surfaces could not provide good representations of g^E with the configurations used. However, other molecular orientations of 1-butanol apart from the three given, extreme cases could probably also give reasonable g^E-results, when n-heptane is in fully rotated RotZ45RotX45 orientation.

For reasons of completeness, it shall be noted that the temperatures $T_{h^E} = 298.15\,\mathrm{K}$ of the experimental data for h^E [36] and $T_{g^E} = 323.15\,\mathrm{K}$ for g^E-data [37] are not the same. Furthermore, in [37] isothermal vapor-liquid equilibrium data are given. The excess free enthalpy g^E is calculated using the simplified equilibrium relation for every component k

$$x_k \gamma_k P_k^S = y_k P \tag{4.9}$$

with the liquid molar fraction x_k, activity coefficient γ_k, pure component vapor pressure P_k^S, vapor molar fraction y_k and system pressure P. The activity coefficients γ_k can be summed up to yield g^E.

$$g^E = RT \sum_k^{1,2} x_k \ln \gamma_k \tag{4.10}$$

All the h^E- and g^E-data generated via Monte Carlo simulations for n-heptane - 1-butanol can be found in Figures B.7-B.12 of the appendix.

4.2.3. Acetone - Methanol

The mixture acetone - methanol, consisting of a ketone and an alcohol, comprises two substances with polar groups. In contrast to 1-butanol, methanol only consists of a hydroxy group and a methyl residue, resulting in a nearly negligible influence of alkane chain length. Figure 4.8 shows configurations where the hydroxy group is oriented towards the edge of the cube and acetone adopts all the three considered orientations. A weaker dependence on acetone-orientation is observed, with all three possibilities yielding good representations of g^E using PAC-MAC distances. For this mixture, this general trend of methanol-orientation having a stronger influence can be observed for all data generated in Figures B.13-B.18 of the appendix.

On the other hand, Figure 4.9 gives an excellent prediction for g^E using touching van der Waals surfaces. Furthermore, even though g^E-predictions are the focus of this work, h^E-data can be described properly by several configurations given in Figures B.13-B.18, especially when van der Waals distances are used.

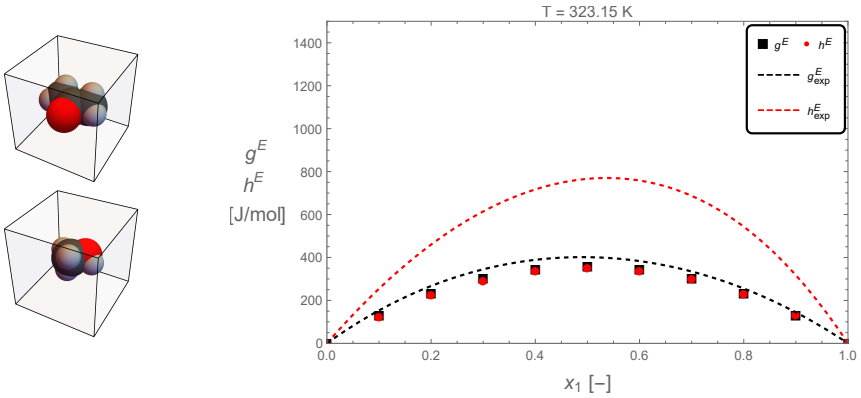

(a) Acetone - Methanol(RotZ45), PAC-MAC distance

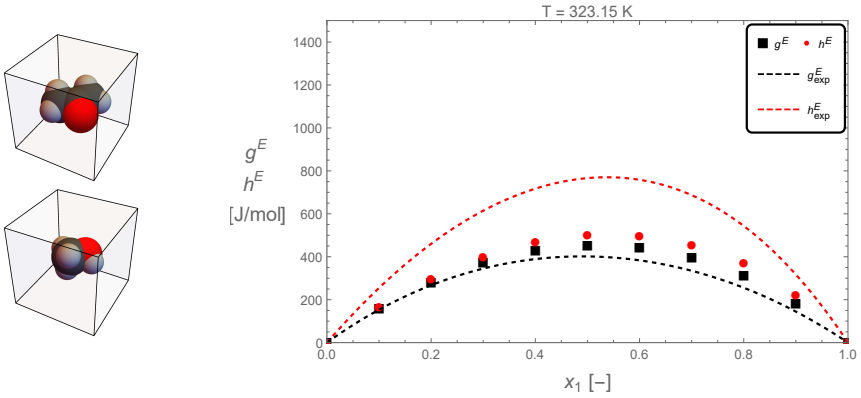

(b) Acetone(RotZ45) - Methanol(RotZ45), PAC-MAC distance

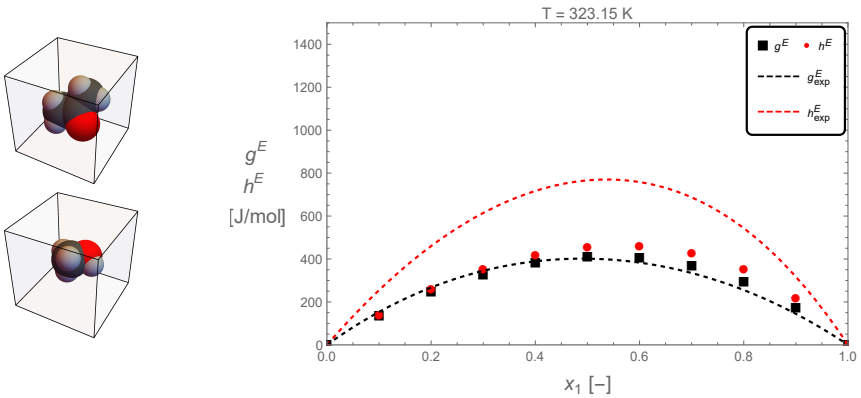

(c) Acetone(RotZ45RotX45) - Methanol(RotZ45), PAC-MAC distance

Figure 4.8.: Comparison of h^E and g^E calculated from Monte Carlo simulations with experimental data [38, 39] for the system acetone - methanol

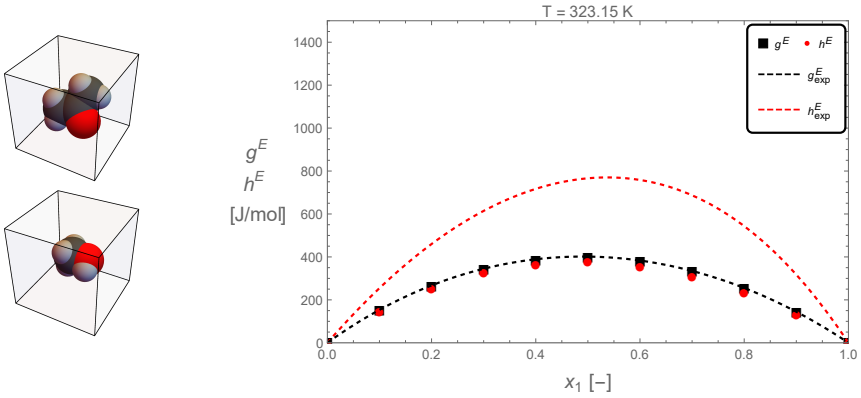

Figure 4.9.: Comparison of h^E and g^E calculated from Monte Carlo simulations with experimental data [38, 39] for the system acetone(RotZ45RotX45) - methanol using van der Waals distances

Also for this system vapor-liquid equilibrium data [39] are used to compute g^E with equations (4.9) and (4.10).

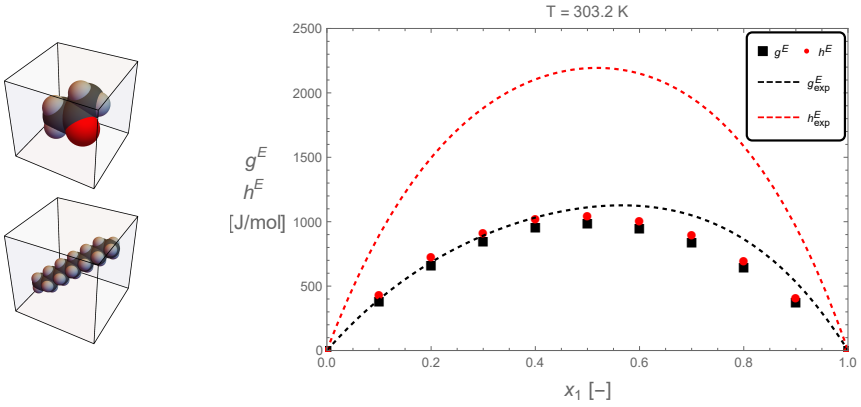

(a) Acetone(RotZ45RotX45) - n-Dodecane(RotZ45RotX45), PAC-MAC distance

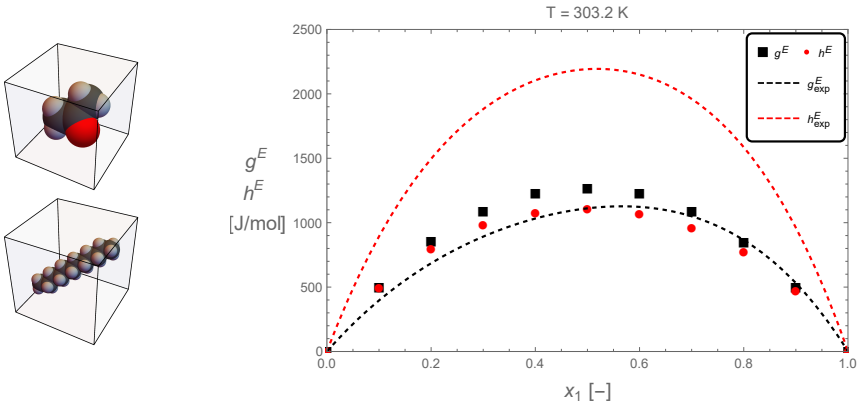

(b) Acetone(RotZ45RotX45) - n-Dodecane(RotZ45RotX45), van der Waals distance

Figure 4.10.: Comparison of h^E and g^E calculated from Monte Carlo simulations with experimental data [35] for the system acetone - n-dodecane

4.2.4. Acetone - n-Dodecane

The system acetone - n-dodecane is chemically similar to the previously presented binary mixture of acetone and n-heptane. However, the increase in alkane chain length from C_7 to C_{12} comes with stronger attraction in the Lennard-Jones potential energy terms of the intermolecular energy E_{inter}. Longer chains are also expected to be described less accurately by a cube/die model. The results in Figure 4.10 show that for two similar configurations the PAC-

MAC distance underestimates g^E, while the van der Waals distance, which typically brings the molecules closer together during molecular sampling, overestimates g^E. It is thus expected, that the truth lies somewhere between those two cases. Again, it is worth mentioning that only the full rotation of n-dodecane (i.e. RotZ45RotX45) gives a reasonable description of g^E. Other orientations of the alkane within its cube lead to great variance of ε_{ij} and correspondingly, very inhomogeneous contact properties of the alkane. Due to the chain length, this effect is even more pronounced for n-dodecane than for n-heptane. Furthermore, the full set of results in Figures B.19-B.22 of the appendix shows simulation artifacts for h^E. Especially for $x_1 = 0.4$, the h^E-curve is not smooth. The reason is the development of energetically preferable structures within the domain due to this great variance of ε_{ij} for certain configurations. Refinements need to be adopted in the polynomial fitting procedure of h^E.

4.3. Discussion

With this vast number of results provided, several statements regarding the suitability of the molecular sampling algorithm to give physically reasonable results can be made. First of all, there is always at least one configuration for the four tested systems which is capable of describing the excess free enthalpy g^E. For nonpolar alkanes, the fully rotated RotZ45RotX45 configuration has proven successful, as it limits the effects of chain length in intermolecular energy E_{inter} calculations. More polar molecules can provide reasonable results in standard or rotated setups. The results for the systems acetone - n-heptane and acetone - n-dodecane support these findings, as well as one configuration for n-heptane - 1-butanol. However, the increased chain length of n-dodecane

limits the applicability of the six-sided dice model. Long-chained molecules are not expected to be suitable for simple single-die systems.

Two polar molecule types are present in the system acetone - methanol. Several configurations are viable to properly describe g^E, which can be attributed to the absence of long alkane chains. The functional carbonyl and hydroxy groups mainly govern the energetic behavior, allowing for a greater configurational margin. On top of that, h^E and g^E both show a stronger dependence on methanol orientation rather than on acetone orientation. Methanol only carries a single methyl group, acetone carries two. Furthermore, the oxygen and hydrogen atoms of alcohol groups carry higher charges for the Coulomb potential energy than carbonyl carbon and oxygen. Therefore, the hydroxy group and its positioning have an increased impact on intermolecular energies E_{inter}. Energetically, the capability of methanol hydrogen-bonding has to be mentioned. The orientation of methanol molecules thus plays a dominating role.

The difference between PAC-MAC distances $D_{\text{PAC-MAC}}$ and distances of touching van der Waals surfaces D_{vdW} (here often called van der Waals distance) lies in the spacing of partners of molecules during molecular pair sampling. Typically, D_{vdW} yields significantly shorter distances between atoms. The distributions of intermolecular energies E_{inter} are usually broadened and slightly shifted towards repulsion. Practically, a common feature found is that D_{vdW} further "enhances" the trends in g^E and h^E given by $D_{\text{PAC-MAC}}$. This means, that oftentimes gaps between g^E and h^E with $D_{\text{PAC-MAC}}$ are broadened when using D_{vdW}. However, this is not universally true and depends on relative molecular orientations, as sometimes entirely different results are obtained with D_{vdW}.

As mentioned in section 4.2, the arithmetic averaging-procedure of a multitude of E_{inter}-values to a single ε_{ij}-value has to be brought up as a major loss of information when transitioning from molecular sampling results to MC simulations. The pair sampling procedure yields a variety of intermolecular energies E_{inter} assigned to a certain face-contact ij. In order to condense these energies to a single value, an arithmetic mean of all E_{inter} values for this contact ij is computed and used as ε_{ij}. However, these values for E_{inter} can differ significantly because the positions of atoms which are not in the immediate neighborhood still make an energetic difference. Just because face i and face j of two neighboring molecule-dice form a contact ij does not mean that intermolecular energies E_{inter} might not deviate strongly from each other. The ten remaining faces of both dice might come in varying configurations.

An example for molecular pair sampling of acetone - acetone in standard configurations with PAC-MAC distances is provided. The assignment of face-indices can be seen in Figure 4.1. Following the numbering given in this figure, contacts $ij = ii = 33$ are configurations of neighboring acetone molecules with touching carbonyl-oxygen-faces. Strong repulsion is expected for these orientations. Figure 4.11(a) shows that for 33-contacts the intermolecular energies E_{inter} are basically independent of the orientation of the rest of the die-faces. The strong repulsion induced by carbonyl-group-proximity fully governs the energetic magnitude of the interaction. A minimum value of 954.82 K, a maximum value of 955.22 K and mean value $\varepsilon_{33}/R = 955.02\,\text{K}$ are obtained. On the other hand, when all contacts of $ij = ii = 22$ are chosen, the situation is different. In Figure 4.11(b) the values of E_{inter}/R and the corresponding mean value ε_{22}/R are given. Acetone-die-face $i = 2$ partially covers a methyl group. The positioning of the carbonyl group (face $i = 3$) can vary; for neighboring acetone molecules with 22-contacts, the carbonyl groups might be on the

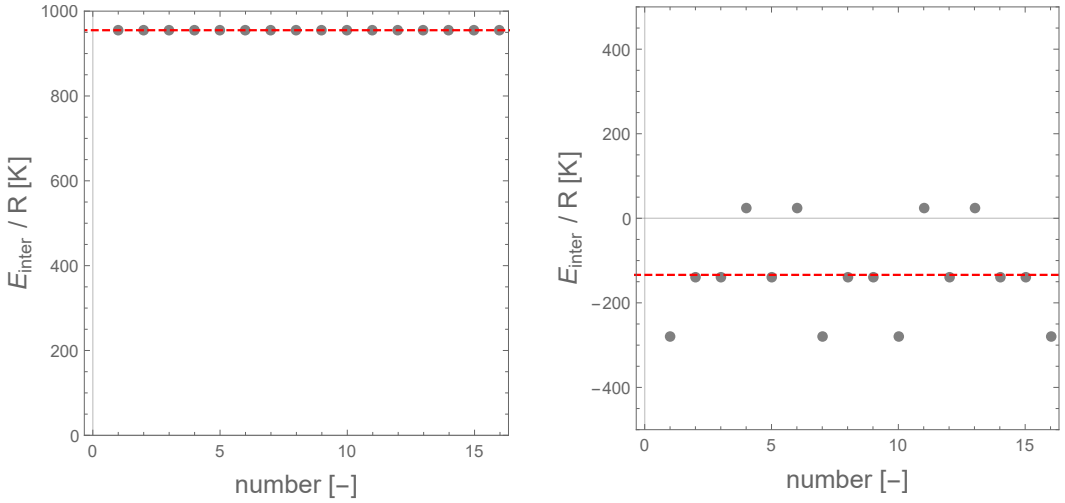

(a) Determination of ε_{33}

(b) Determination of ε_{22}

Figure 4.11.: Examples for determination of ε_{33} and ε_{22} from pair sampling of acetone - acetone in standard configurations with PAC-MAC distances; points are values of E_{inter}/R for respective contacts, dashed lines are their mean values ε

contact, on opposing sides or in perpendicular positions. Therefore, three distinct energy levels are established for E_{inter}. A minimum value of $-277.98\,\text{K}$, a maximum value of $22.87\,\text{K}$ and mean value $\varepsilon_{22}/R = -133.84\,\text{K}$ are obtained. Noticeably, the arithmetic mean ε_{22}/R cannot describe all three states.

Even though good representations for g^E could be found, h^E-predictions are often poor. On top of that, the simultaneous description of h^E and g^E has proven to be difficult and could, at best, only be achieved qualitatively. With this in mind, there is still plenty of room for improvements regarding the sampling strategies, the relative orientations and the transitions from sampling to MC simulations.

5. Summary and Outlook

Various aspects of molecular sampling, a statistical procedure of creating molecular clusters of small size and subsequent calculation of potential energies using a force field, are addressed and explained throughout this work. The force field chosen is OPLS-AA [6], a well-known and broadly accepted set of equations for potential energy in the liquid phase. For interatomic and intermolecular distances either the PAC-MAC distance $D_{\text{PAC-MAC}}$ [23] or the distance of touching van der Waals surfaces D_{vdW} can be used. Pair sampling has proven to be an effective and computationally cheap method to obtain interaction energies. On top of that, only the intermolecular energy E_{inter} of the OPLS-AA force field is used to energetically characterize pair interactions, omitting the intramolecular part E_{intra}.

Variations of molecular orientations during the sampling procedure are achieved either through random rotations or via cube-symmetry-group rotations. The latter are an assembly of 24 possible rotations of a cube in three-dimensional space which change the orientation of its sides without changing the cube as a whole. This is particularly useful when molecules are regarded as six-sided dice, as all possible permutations can be obtained while keeping the molecular structure coupled to its surrounding, artificial cubic box.

When placing a molecule within its model die, the internal orientation of the constituent strongly impacts the distribution of intermolecular energy E_{inter} which is obtained from molecular sampling with cube-symmetry-group rotations. Having acetone serve as an example for polar molecules, the broadness and the expected value of the distribution of E_{inter} show a distinct dependence on these internal orientations. For nonpolar alkanes, with n-heptane as a representative example, the shape of the distribution is governed by attractive van der Waals forces and influenced by chain length, both of which can be tuned through internal orientations within the cube.

Monte Carlo (MC) simulations of binary mixtures are performed to validate the molecular sampling results. The excess properties g^E and h^E are computed with input parameters generated through pair sampling. This is achieved via coupling of molecular orientations with a six-sided dice model and assignment of E_{inter}-values as contact interaction parameters ε_{ij} for MC runs. Since several permutations with identical contacting die-faces but different positions of the other, non-contacting faces are obtained, the arithmetic mean of E_{inter} for every contact ij is used to approximate ε_{ij}. This inherent loss of information is discussed in detail and identified as a major potential for further improvements in future research.

The g^E- and h^E-data computed via MC simulations are presented for the binary mixtures acetone - n-heptane, n-heptane - 1-butanol, acetone - methanol and acetone - n-dodecane for a variety of starting configurations. For every substance system at least one configuration could predict the experimental g^E-data very well, which was the main focus of evaluation. Excess enthalpies h^E are not predicted as efficiently, and simultaneous description of g^E and h^E has proven to be intricate. Common trends for good results are full rotations towards the vertex of the surrounding model die for n-alkanes to avoid overes-

timation of attraction; polar molecules like acetone, 1-butanol and methanol can give reasonable predictions in any of the given configurations and are influenced by the nature of their partner molecule (alkane chain length, polarity, orientation) and the length of their own alkyl residues next to their polar functional groups. Longer-chained alkanes, with n-dodecane as an example, are expected to be less suitable for this approach, due to the constraint of packing a threadlike molecule into an equilateral cuboid.

Molecular orientation in general has shown to be a key factor. Future work within this field should aim at enhanced studies of orientational effects. Other rotations apart from the three extreme cases used in this work could yield promising results and possibly provide orientation thresholds for certain substance groups. Furthermore, the application of the molecular sampling algorithm in the context of input data generation for the recently developed thermodynamic model in [5] can be looked forward to.

Bibliography

[1] M. Levitt. "Protein Conformation, Dynamics, and Folding by Computer Simulation". In: *Annual Review of Biophysics and Bioengineering* 11 (1982), pp. 251–271.

[2] C.F. Fan, B.D. Olafson, and M. Blanco. "Applications of Molecular Simulation To Derive Phase Diagrams of Binary Mixtures". In: *Macromolecules* 25 (1992), pp. 3667–3676.

[3] D. Frenkel and B. Smit. *Understanding Molecular Simulations. From Algorithms to Applications*. Academic Press, 1996. ISBN: 0-12-267351-4.

[4] K. Vanommeslaeghe, O. Guvench, and A.D. MacKerell Jr. "Molecular Mechanics". In: *Current pharmaceutical design* 20(20) (2013), pp. 3281–3292.

[5] T. Wallek, C. Mayer, and A. Pfennig. "Discrete Modeling Approach as a Basis of Excess Gibbs-Energy Models for Chemical Engineering Applications". In: *Journal of Industrial and Engineering Chemistry* 57(4) (2018), pp. 1294–1306.

[6] W.L. Jorgensen, D.S. Mawell, and J. Tirado-Rives. "Development and Testing of the OPLS All-Atom Force Field on Conformational Energetics and Properties of Organic Liquids". In: *Journal of the American Chemical Society* 118 (1996), pp. 11225–11236.

[7] M. Binneweis, M. Finze, M. Jäckel, P. Schmidt, H. Willner, and G. Rayner-Canham. *Allgemeine und Anorganische Chemie*. 3rd ed. Springer Spektrum, 2016, pp. 59, 949. ISBN: 9783662450666.

[8] F. Jensen. *Introduction to Computational Chemistry*. John Wiley & Sons, 2001. ISBN: 0-471-98085-4.

[9] S.J. Weiner, P.A. Kollman, D.A. Case, U.C. Singh, C. Ghio, G. Alagona, S. Profeta Jr., and P. Weiner. "A New Force Field for Molecular Mechanical Simulation of Nucleic Acids and Proteins". In: *Journal of the American Chemical Society* 106 (1984), pp. 765–784.

[10] S.J. Weiner, P.A. Kollman, D.T. Nguyen, and D.A. Case. "An All Atom Force Field for Simulation of Nucleic Acids and Proteins". In: *Journal of Computational Chemistry* 7(2) (1986), pp. 230–252.

[11] B.R. Brooks, R.E. Bruccoleri, B.D. Olafson, D.J. States, S. Swaminathan, and M. Karplus. "CHARMM: A program for macromolecular energy, minimization, and dynamics calculations". In: *Journal of Computational Chemistry* 4(2) (1983), pp. 187–217.

[12] C. Oostenbrink, A. Villa, A.E. Mark, and W.F. van Gunsteren. "A biomolecular force field based on the free enthalpy of hydration and solvation: The GROMOS force-field parameter sets 53A5 and 53A6: The GROMOS force-field parameter sets 53A5 and 53A6". In: *Journal of Computational Chemistry* 25(13) (2004), pp. 1656–1676.

[13] W.L. Jorgensen, J.D. Madura, and C.J. Swenson. "Optimized Intermolecular Potential Functions for Liquid Hydrocarbons". In: *Journal of the American Chemical Society* 106(22) (1984), pp. 6638–6646.

[14] W.L. Jorgensen. “Optimized Intermolecular Potential Functions for Liquid Alcohols”. In: *Journal of Computational Chemistry* 90(7) (1986), pp. 1276–1284.

[15] W.L. Jorgensen and J. Tirado-Rives. “The OPLS Potential Functions for Proteins. Energy Minimizations for Crystals of Cyclic Peptides and Crambin”. In: *Journal of the American Chemical Society* 110(6) (1988), pp. 1657–1666.

[16] B. Chen, M.G. Martin, and J.I. Siepmann. “Thermodynamic Properties of the Williams, OPLS-AA, and MMFF94 All-Atom Force Fields for Normal Alkanes”. In: *Journal of Physical Chemistry B* 102 (1998), pp. 2578–2586.

[17] G.A. Kaminski, E.M. Duffy, T. Matsui, and W.L. Jorgensen. “Free Energies of Hydration and Pure Liquid Properties of Hydrocarbons from the OPLS All-Atom Model”. In: *Journal of Physical Chemistry B* 98 (1994), pp. 13077–13082.

[18] G.A. Kaminski, R.A. Friesner, J. Tirado-Rives, and W.L. Jorgensen. “Evaluation and Reparametrization of the OPLS-AA Force Field for Proteins via Comparison with Accurate Quantum Chemical Calculations on Peptides”. In: *Journal of Physical Chemistry B* 105 (2001), pp. 64174–6487.

[19] A.J.M. Sweere and J.G.E.M. Fraaije. “Accuracy Test of the OPLS-AA Force Field for Calculating Free Energies of Mixing and Comparison with PAC-MAC”. In: *Journal of Chemical Theory and Computation* 13 (2017), pp. 1911–1923.

[20] M.L.P. Price, D. Ostrovsky, and W.L. Jorgensen. “Gas-Phase and Liquid-State Properties of Esters, Nitriles, and Nitro Compounds with the

OPLS-AA Force Field". In: *Journal of Computational Chemistry* 22(13) (2001), pp. 1340–1352.

[21] K. Kahn and T.C. Bruice. "Parameterization of OPLS–AA Force Field for the Conformational Analysis of Macrocyclic Polyketides". In: *Journal of Computational Chemistry* 23 (2002), pp. 977–996.

[22] R.L.C. Akkermans. "Mesoscale model parameters from molecular cluster calculations". In: *Journal of Chemical Physics* 128 (2008).

[23] A.J.M. Sweere and J.G.E.M. Fraaije. "Force-Field Based Quasi-Chemical Method for Rapid Evaluation of Binary Phase Diagrams". In: *Journal of Physical Chemistry B* 119 (2015), pp. 14201–14200.

[24] A.J.M. Sweere, R.S. Gracia, and J.G.E.M. Fraaije. "Extensive Accuracy Test of the Force-Field-Based Quasichemical Method PAC-MAC". In: *Journal of Chemical And Engineering Data* 61(12) (2016), pp. 3989–3997.

[25] A. Bondi. "Van der Waals Volumes and Radii". In: *Journal of Physical Chemistry* 68(3) (1964), pp. 441–451.

[26] M. Blanco. "Molecular Silverware. I. General Solutions to Excluded Volume Constrained Problems". In: *Journal of Computational Chemistry* 12 (1991), pp. 237–247.

[27] M.J. Abraham, T. Murtola, R. Schulz, S. Páll, J.C. Smith, B. Hess, and E. Lindahl. "GROMACS: High performance molecular simulations through multi-level parallelism from laptops to supercomputers". In: *SoftwareX* 1-2 (2015), pp. 19–25.

[28] M.A. Armstrong. *Groups and Symmetry. With 54 Illustrations*. Springer, 1988, p. 37. ISBN: 0387966757.

[29] M.P. Allen and D.J. Tildesley. *Computer Simulation of Liquids*. Oxford University Press, 1987. ISBN: 0-19-855375-7.

[30] K. Egner. "Ein neues Modell zur Berechnung der Exzeßgrößen stark nichtidealer Mischungen und Messungen ternärer Exzessenthalpien". PhD thesis. Technische Universität Darmstadt, 1998.

[31] K. Egner, J. Gaube, and A. Pfennig. "GEQUAC, an Excess Gibbs Energy Model for Simultaneous Description of Associating and Non-Associating Liquid Mixtures". In: *Berichte der Bunsengesellschaft für physikalische Chemie* (1996), pp. 209–218.

[32] L.M. König. "Auswertung von Monte Carlo-Simulationen zur Validierung thermodynamischer Modelle". BSc thesis. Technische Universität Graz, 2013.

[33] A. Thaller. "Monte Carlo Simulationen von Mischungen aus Polymeren". BSc thesis. Technische Universität Graz, 2015.

[34] T. Grubinger. "Thermodynamische Evaluierung von Monte-Carlo Simulationen". BSc thesis. Technische Universität Graz, 2016.

[35] L. Krenzer. "Untersuchungen zur Beeinflussung der Exzessenthalpie, der freien Exzessenthalpie und der Exzessentropie von binären Mischungen mit polaren Komponenten durch die Moleküleigenschaften". PhD thesis. Technische Hochschule Darmstadt, 1985.

[36] E.N. Rezanova, K. Kammerer, and R.N. Lichtenthaler. "Excess Enthalpies and Volumes of Ternary Mixtures Containing 1-Propanol or 1-Butanol, an Ether (Diisopropyl Ether or Dibutyl Ether), and Heptane". In: *Journal of Chemical and Engineering Data* 45 (2000), pp. 124–130.

[37] C.P. Smyth and E.W. Engel. "Molecular Orientation and the Partial Vapor Pressure of Binary Mixtures". In: *Journal of the American Chemical Society* 51 (1929), pp. 2646–2670.

[38] C. Christensen, J. Gmehling, P. Rasmussen, and U. Weidlich. *Heats of Mixing Data Collection. Binary Systems*. Dechema Chemistry Data Series, Vol. III, Part 1, 1984.

[39] J. Gmehling and U. Onken. *Vapor-Liquid Equilibrium Data Collection. Alcohols: Methanol Supplement 5*. Dechema Chemistry Data Series, Vol. I, Part 2g, 2005.

Appendix

Appendix A.

Lists of Symbols and Indices

Symbol	Units	Explanation
α	rad	angle
Δ	-	operator for difference
Δh^{V}	J/mol	enthalpy of vaporization
ϵ	kcal/mol	Lennard-Jones potential well-depth
ε	J/mol	cube-face interaction parameter
γ	-	activity coefficient
ρ	kg/m^3 or kg/mol^3	density
ϕ	rad	dihedral angle
σ	Å	Lennard-Jones distance of 0-potential
C	J/mol	model constant
D	Å	distance
e^2	$\frac{\text{kcal Å}}{(\text{e}^-)^2\ \text{mol}}$	pre- and conversion factor in Coulomb energy

Continued

Continued

Symbol	Units	Explanation
E	kcal/mol	(potential) energy
f	rad	torsional phase angle
F	N	force
g	J/mol	molar free enthalpy
h	J/mol	molar enthalpy
K	kcal/mol	coefficient in intramolecular energies
L	-	order of expansion in Redlich-Kister equation
$\vec{n}$	-	(unit) direction vector
$\vec{n}$	-	normal vector
P	Pa	pressure
q	e^-	charge
r	Å	(interatomic) distance
r	Å	radius
R	J/(mol K)	universal gas constant
S	$Å^2$	surface area
T	K	temperature
u	kcal/mol	internal (potential) energy
u	J/mol	molar internal energy
v	m^3/mol	molar volume
V	kcal/mol	coefficients in torsional energies
x	-	liquid mole fraction
$\vec{x}$	Å	position vector
y	-	vapor mole fraction

Index Subscript Superscript	Explanation
θ	angular
AB	between partners A and B
angle	concerning intramolecular angles
A	atom, molecule
bond	concerning intramolecular bonds
B	atom, molecule
C	atom, molecule
Coulomb	concerning Coulomb (potential) energy
D	atom, molecule
E	excess
eq	equilibrium
exp	experimental data
g^E	concerning excess free enthalpy
gen	general
h^E	concerning excess enthalpy
i	atom/molecule index
ii	pure species i
inter	intermolecular
intra	intramolecular
j	atom/molecule index
jj	pure species j

Continued

Continued

Index Subscript Superscript	Explanation
k	component
l	index for Redlich-Kister equation
mix	mixture
OPLS-AA	Optimized Potential for Liquid Simulations - All Atom
PAC-MAC	Pair Configuration to Molecular Activity Coefficient
r	concerning distance (i.e. bonds)
torsion	concerning intramolecular dihedrals
S	saturation
vdW	van der Waals
$+$	the positive square root
$\pm$	the positive and the negative square root
$'$	dimensionless quantity

Appendix B.

Collection of Monte Carlo Simulation Results

This section contains all the h^E- and g^E-data generated through Monte Carlo simulations for the systems

- Acetone - n-Heptane,
- n-Heptane - 1-Butanol,
- Acetone - Methanol and
- Acetone - n-Dodecane.

They are compared to experimental data given in [35]-[39].

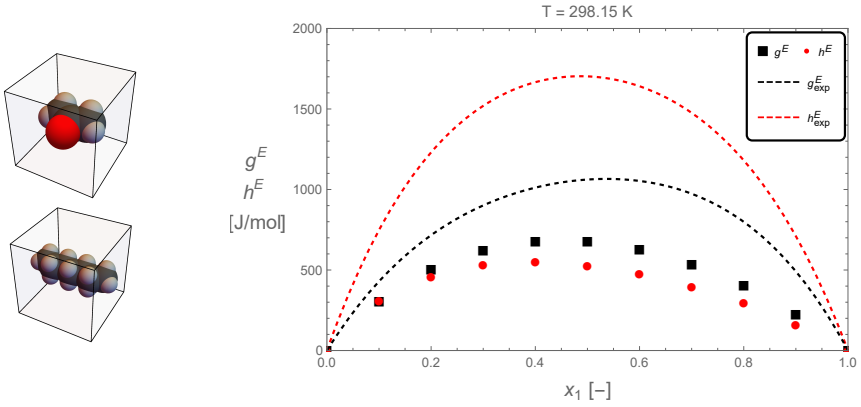

(a) Acetone - n-Heptane, standard configurations

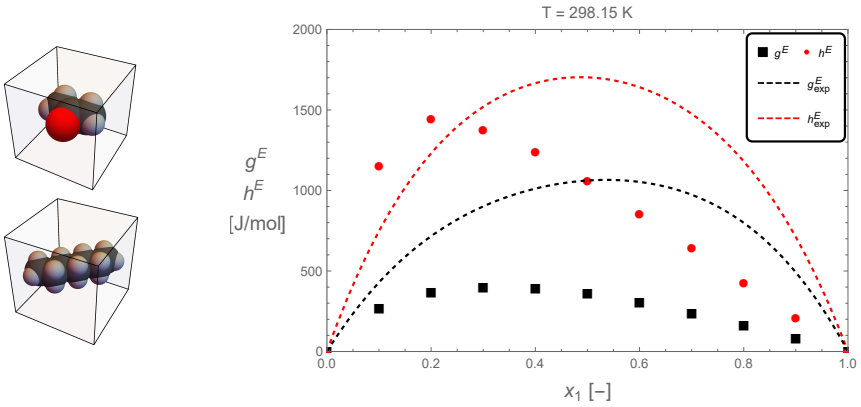

(b) Acetone - n-Heptane(RotZ45)

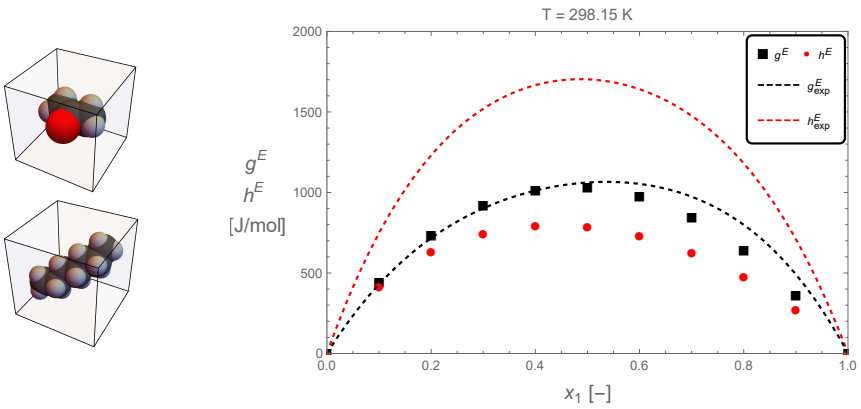

(c) Acetone - n-Heptane(RotZ45RotX45)

Figure B.1.: Comparison of h^E and g^E data obtained via MC simulations with experimental data [35] for the mixture acetone - n-heptane with acetone in standard configuration and n-heptane (a) in standard configuration, (b) rotated for 45° around z-axis, (c) rotated for 45° around z-axis and x-axis; PAC-MAC distances used

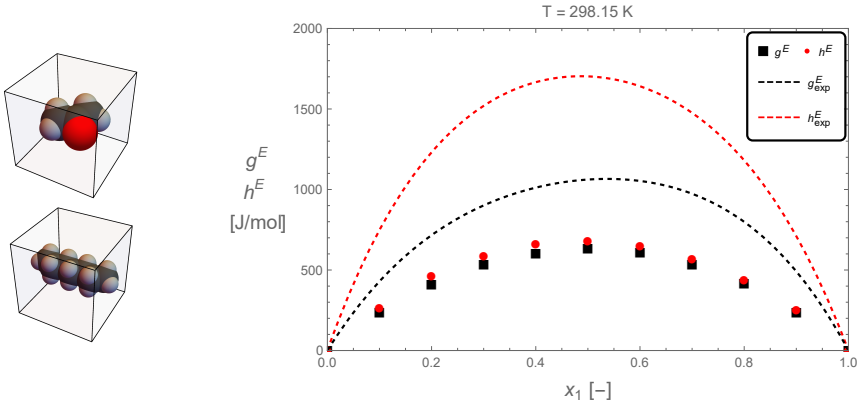

(a) Acetone(RotZ45) - n-Heptane

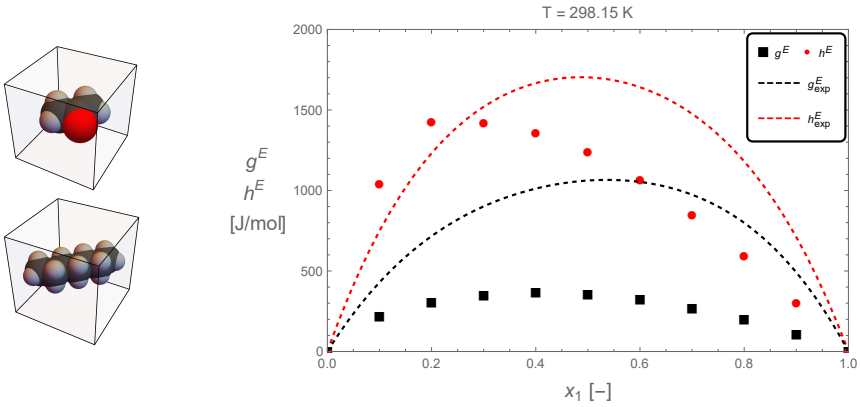

(b) Acetone(RotZ45) - n-Heptane(RotZ45)

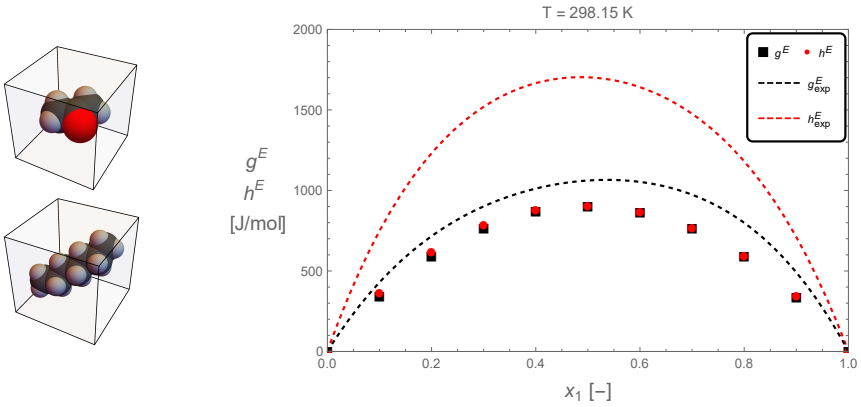

(c) Acetone(RotZ45) - n-Heptane(RotZ45RotX45)

Figure B.2.: Comparison of h^E and g^E data obtained via MC simulations with experimental data [35] for the mixture acetone - n-heptane with acetone rotated for 45° around z-axis and n-heptane (a) in standard configuration, (b) rotated for 45° around z-axis, (c) rotated for 45° around z-axis and x-axis; PAC-MAC distances used

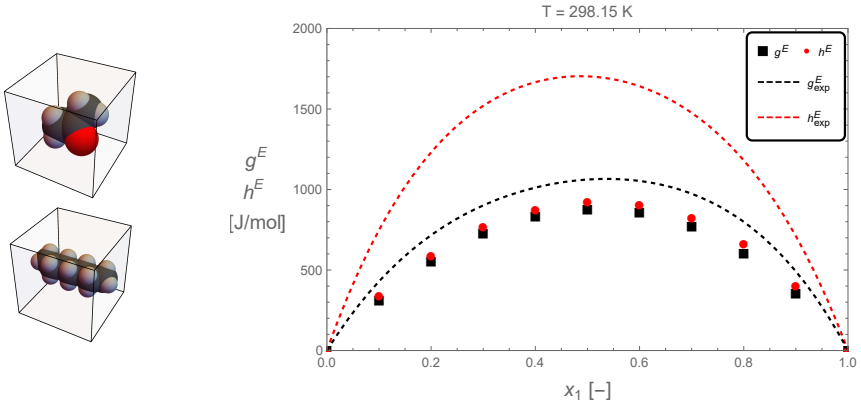

(a) Acetone(RotZ45RotX45) - n-Heptane

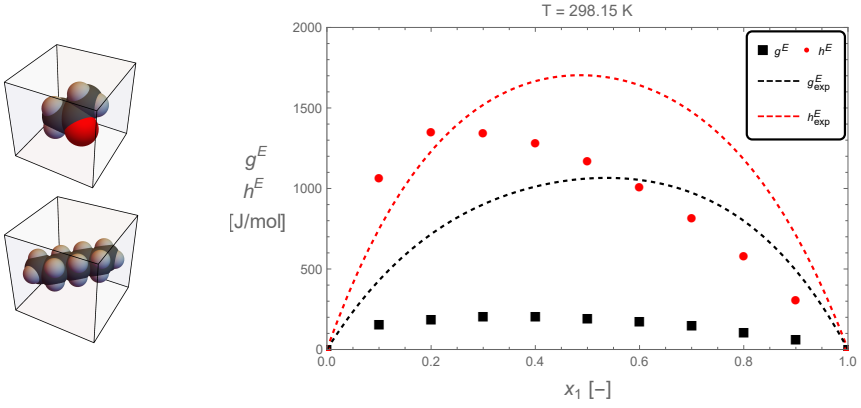

(b) Acetone(RotZ45RotX45) - n-Heptane(RotZ45)

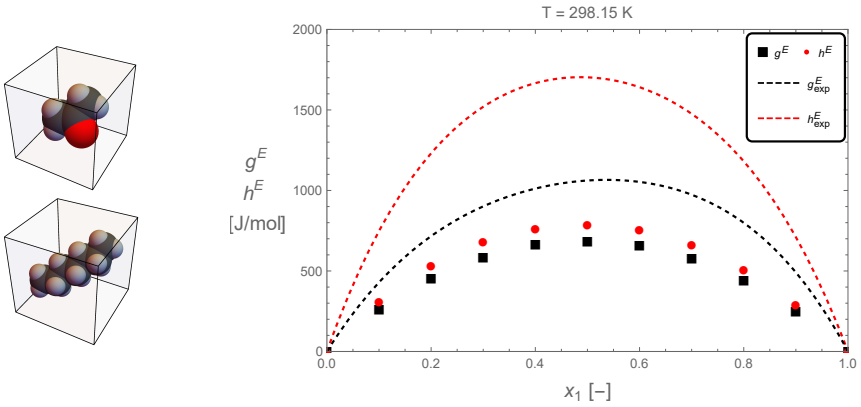

(c) Acetone(RotZ45RotX45) - n-Heptane(RotZ45RotX45)

Figure B.3.: Comparison of h^E and g^E data obtained via MC simulations with experimental data [35] for the mixture acetone - n-heptane with acetone rotated for 45° around z-axis and $x-$axis and n-heptane (a) in standard configuration, (b) rotated for 45° around z-axis, (c) rotated for 45° around z-axis and x-axis; PAC-MAC distances used

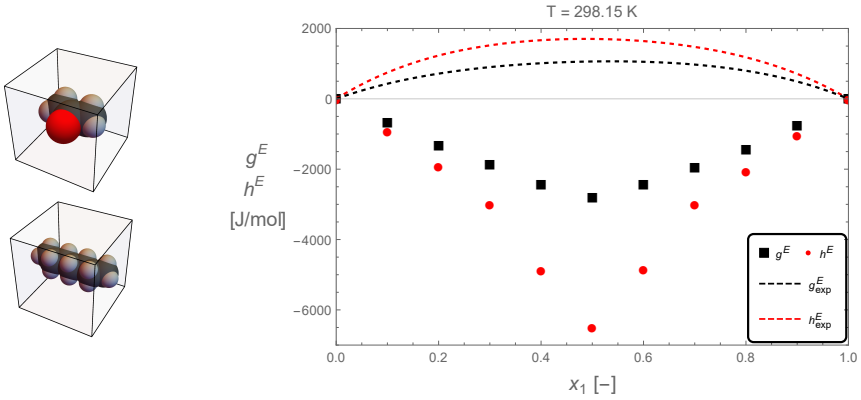

(a) Acetone - n-Heptane

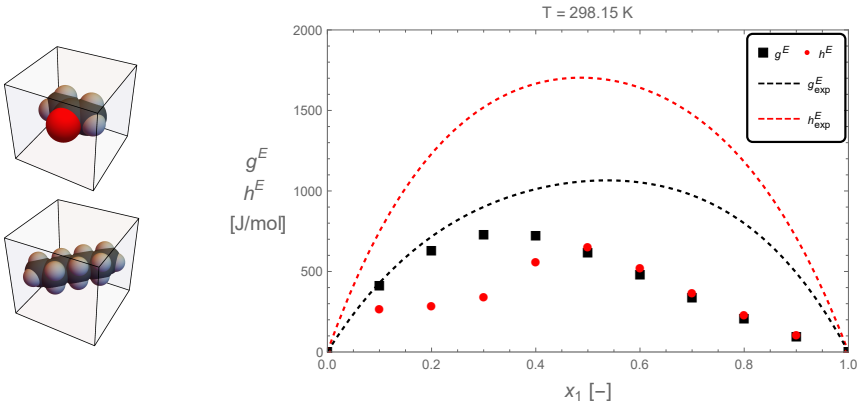

(b) Acetone - n-Heptane(RotZ45)

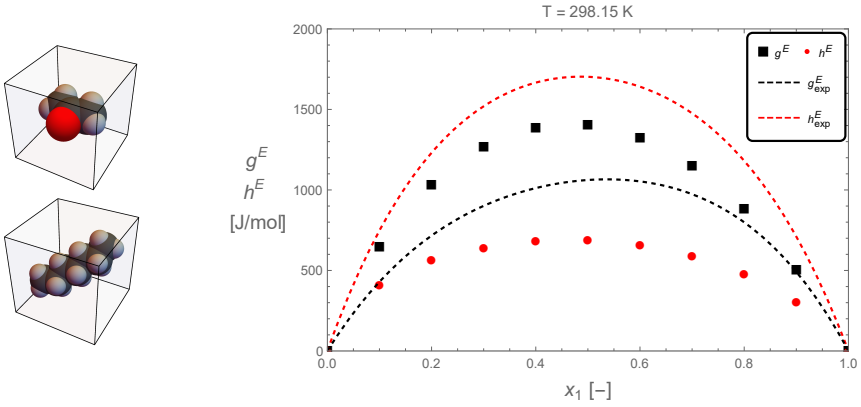

(c) Acetone - n-Heptane(RotZ45RotX45)

Figure B.4.: Comparison of h^E and g^E data obtained via MC simulations with experimental data [35] for the mixture acetone - n-heptane with acetone in standard configuration and n-heptane (a) in standard configuration, (b) rotated for 45° around z-axis, (c) rotated for 45° around z-axis and x-axis; van der Waals distances used

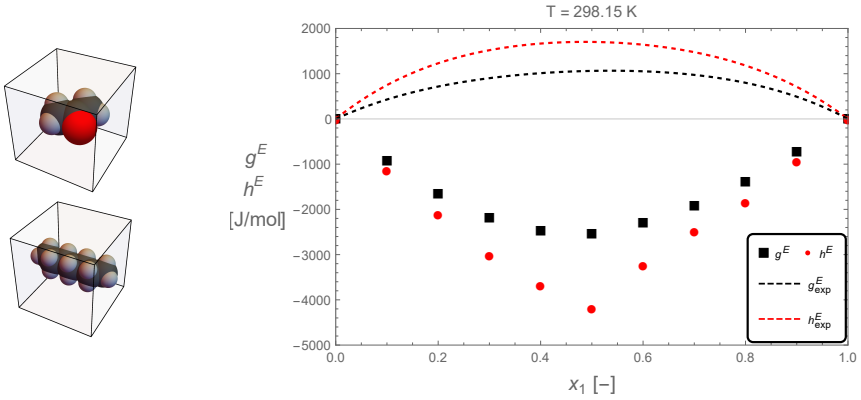

(a) Acetone(RotZ45) - n-Heptane

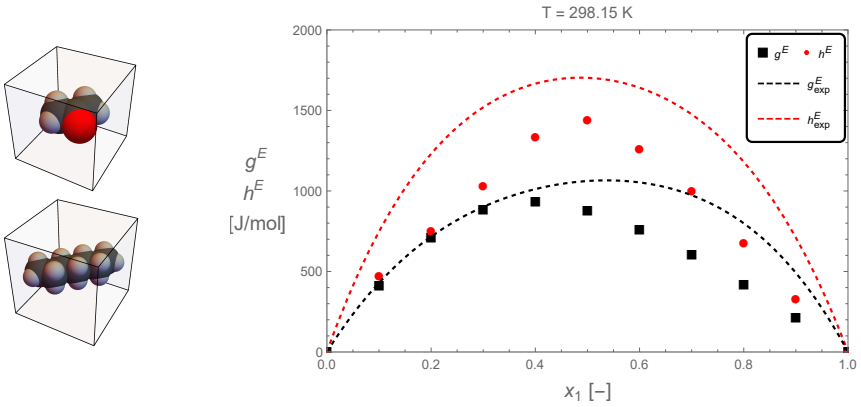

(b) Acetone(RotZ45) - n-Heptane(RotZ45)

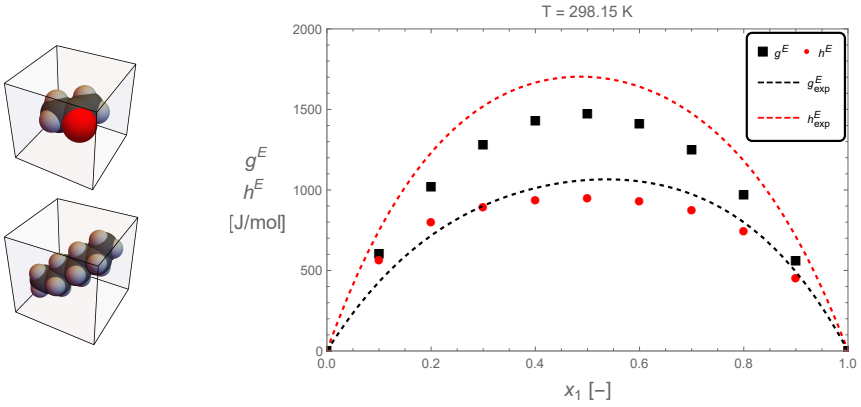

(c) Acetone(RotZ45) - n-Heptane(RotZ45RotX45)

Figure B.5.: Comparison of h^E and g^E data obtained via MC simulations with experimental data [35] for the mixture acetone - n-heptane with acetone rotated for 45° around z-axis and n-heptane (a) in standard configuration, (b) rotated for 45° around z-axis, (c) rotated for 45° around z-axis and x-axis; van der Waals distances used

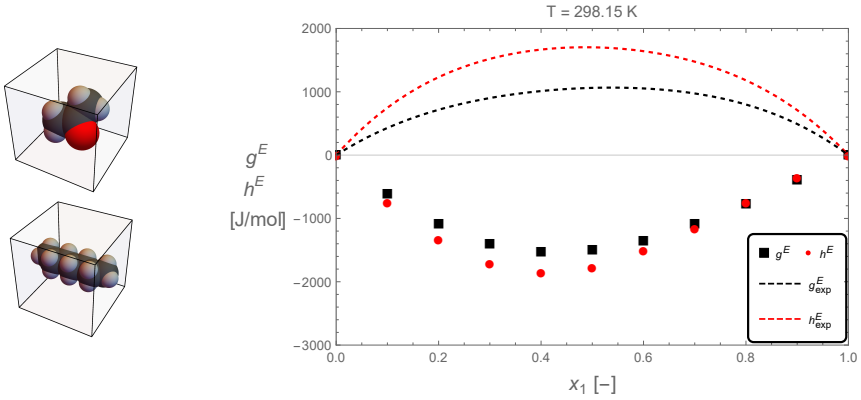

(a) Acetone(RotZ45RotX45) - n-Heptane

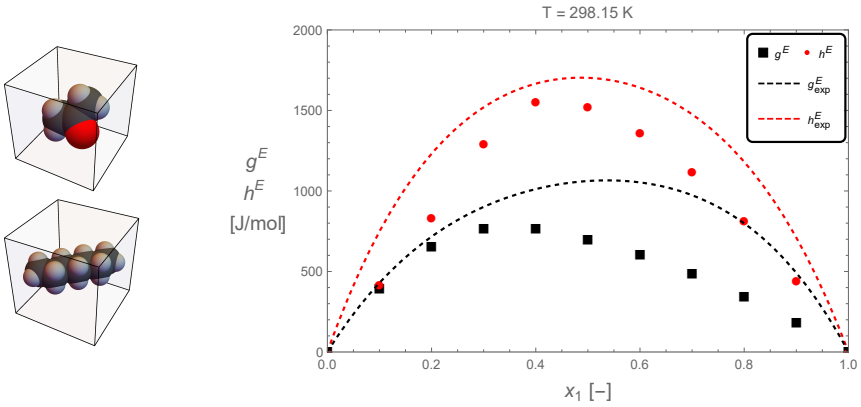

(b) Acetone(RotZ45RotX45) - n-Heptane(RotZ45)

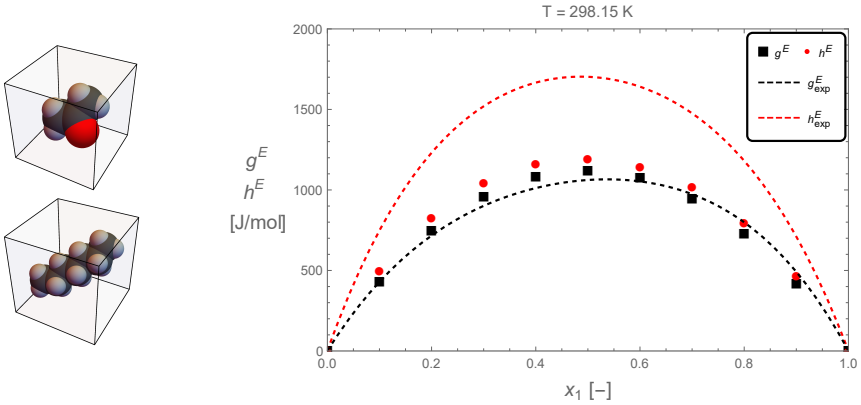

(c) Acetone(RotZ45RotX45) - n-Heptane(RotZ45RotX45)

Figure B.6.: Comparison of h^E and g^E data obtained via MC simulations with experimental data [35] for the mixture acetone - n-heptane with acetone rotated for 45° around z-axis and $x-$axis and n-heptane (a) in standard configuration, (b) rotated for 45° around z-axis, (c) rotated for 45° around z-axis and x-axis; van der Waals distances used

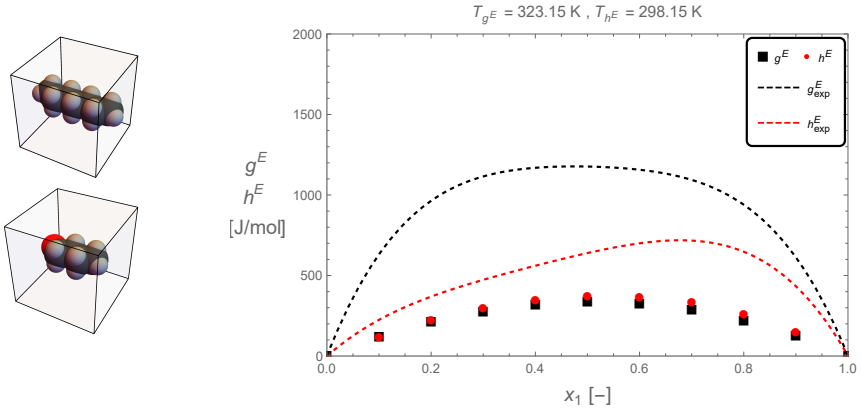

(a) n-Heptane - 1-Butanol, standard configurations

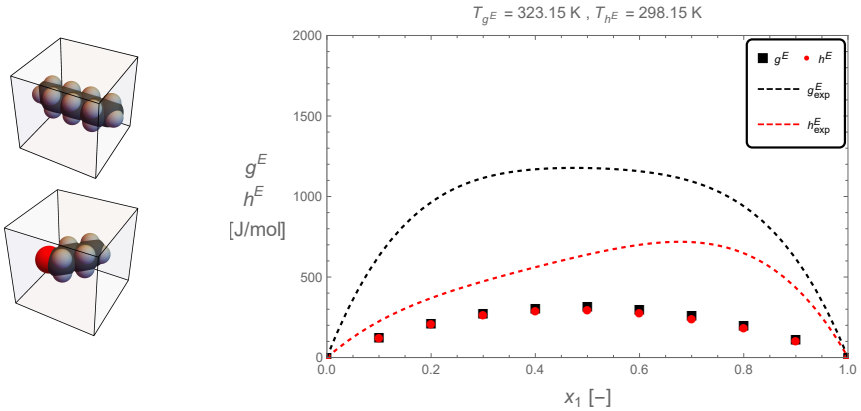

(b) n-Heptane - 1-Butanol(RotZ45)

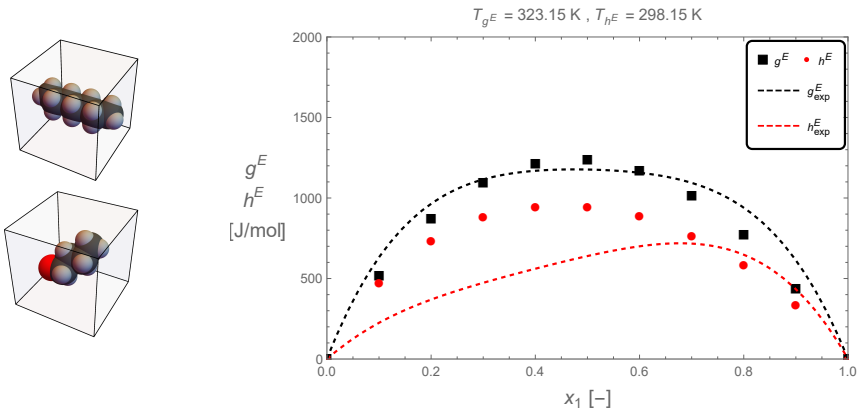

(c) n-Heptane - 1-Butanol(RotZ45RotX45)

Figure B.7.: Comparison of h^E and g^E data obtained via MC simulations with experimental data [36, 37] for the mixture n-heptane - 1-butanol with n-heptane in standard configuration and 1-butanol (a) in standard configuration, (b) rotated for 45° around z-axis, (c) rotated for 45° around z-axis and x-axis; PAC-MAC distances used

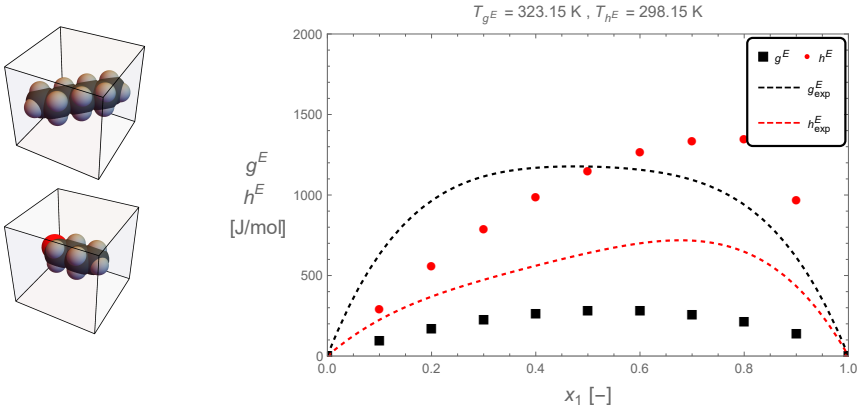

(a) n-Heptane(RotZ45) - 1-Butanol

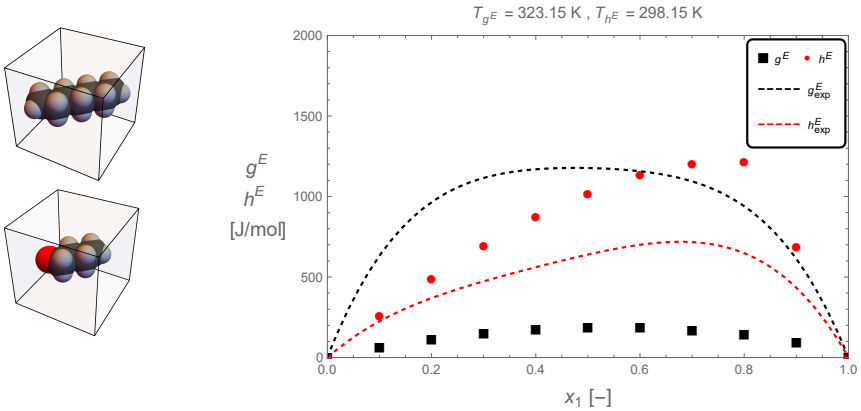

(b) n-Heptane(RotZ45) - 1-Butanol(RotZ45)

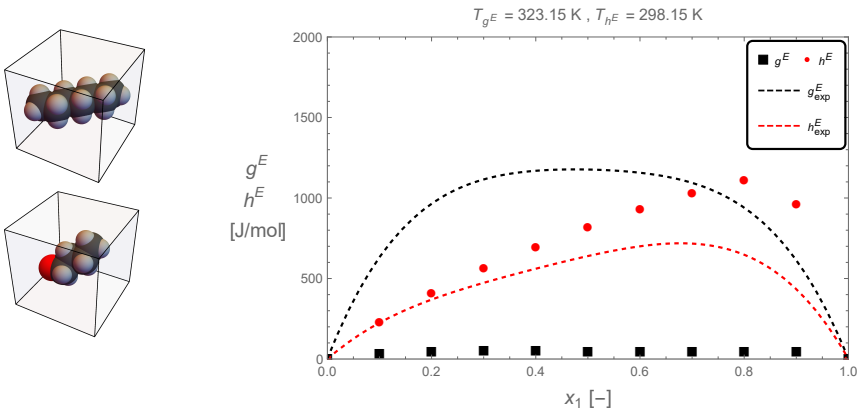

(c) n-Heptane(RotZ45) - 1-Butanol(RotZ45RotX45)

Figure B.8.: Comparison of h^E and g^E data obtained via MC simulations with experimental data [36, 37] for the mixture n-heptane - 1-butanol with n-heptane rotated for 45° around z-axis and 1-butanol (a) in standard configuration, (b) rotated for 45° around z-axis, (c) rotated for 45° around z-axis and x-axis; PAC-MAC distances used

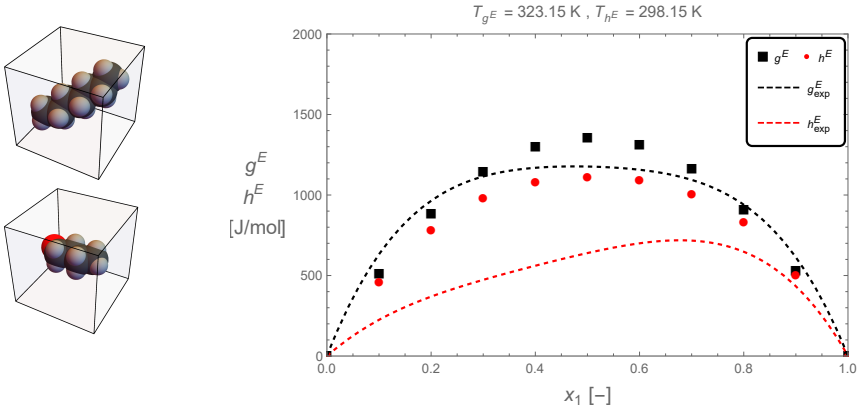

(a) n-Heptane(RotZ45RotX45) - 1-Butanol

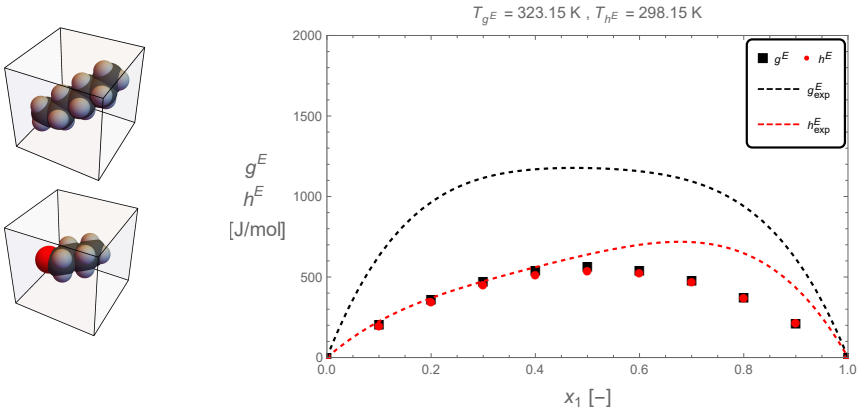

(b) n-Heptane(RotZ45RotX45) - 1-Butanol(RotZ45)

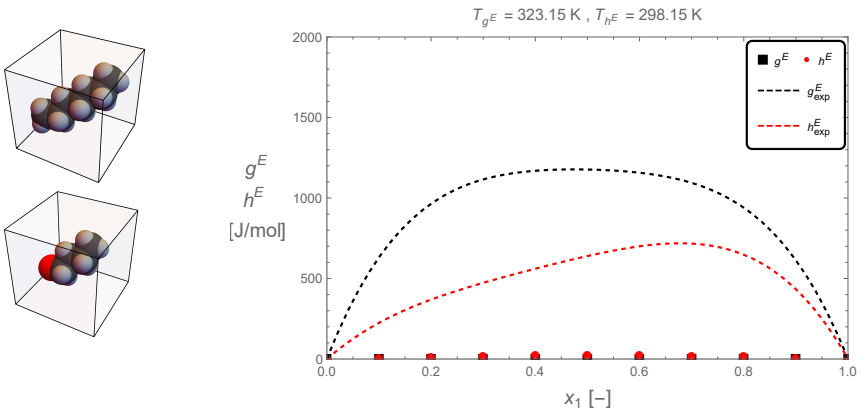

(c) n-Heptane(RotZ45RotX45) - 1-Butanol(RotZ45RotX45)

Figure B.9.: Comparison of h^E and g^E data obtained via MC simulations with experimental data [36, 37] for the mixture n-heptane - 1-butanol with n-heptane rotated for 45° around z-axis and x-axis and 1-butanol (a) in standard configuration, (b) rotated for 45° around z-axis, (c) rotated for 45° around z-axis and x-axis; PAC-MAC distances used

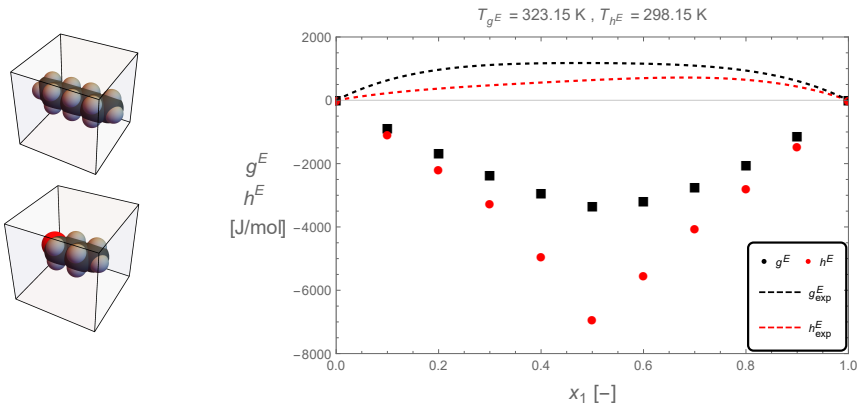

(a) n-Heptane - 1-Butanol

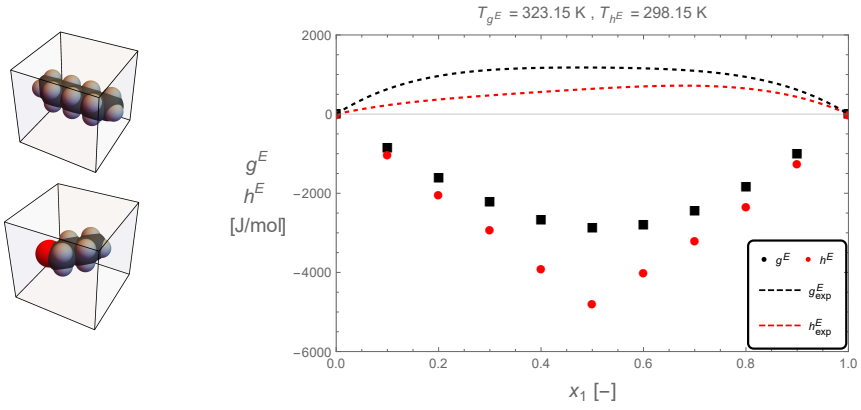

(b) n-Heptane - 1-Butanol(RotZ45)

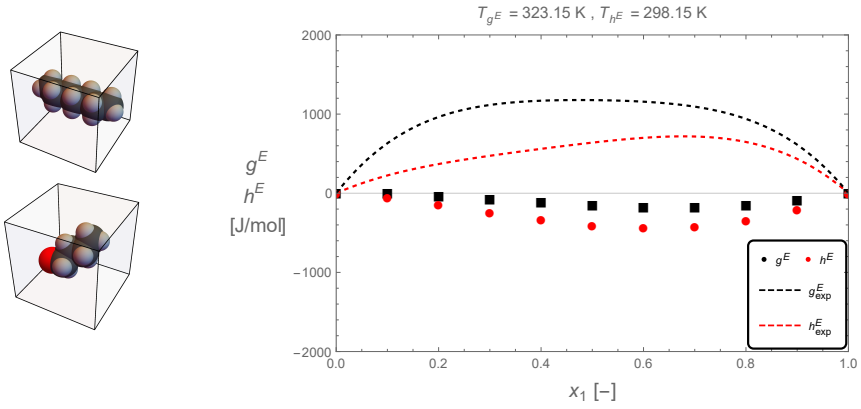

(c) n-Heptane - 1-Butanol(RotZ45RotX45)

Figure B.10.: Comparison of h^E and g^E data obtained via MC simulations with experimental data [36, 37] for the mixture n-heptane - 1-butanol with n-heptane in standard configuration and 1-butanol (a) in standard configuration, (b) rotated for 45° around z-axis, (c) rotated for 45° around z-axis and x-axis; van der Waals distances used

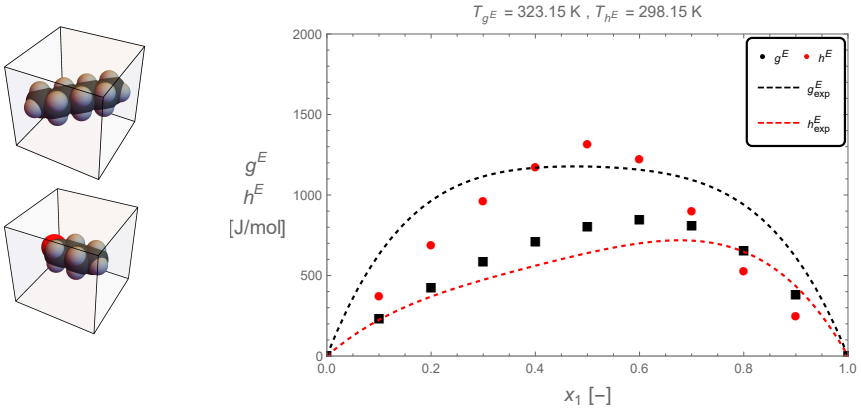

(a) n-Heptane(RotZ45) - 1-Butanol

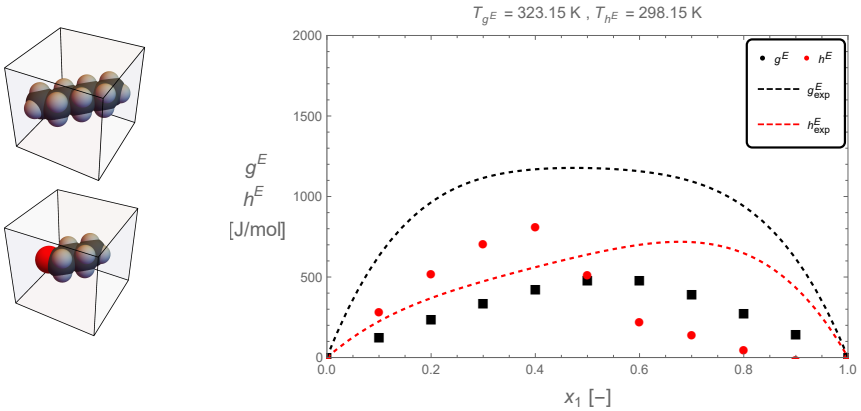

(b) n-Heptane(RotZ45) - 1-Butanol(RotZ45)

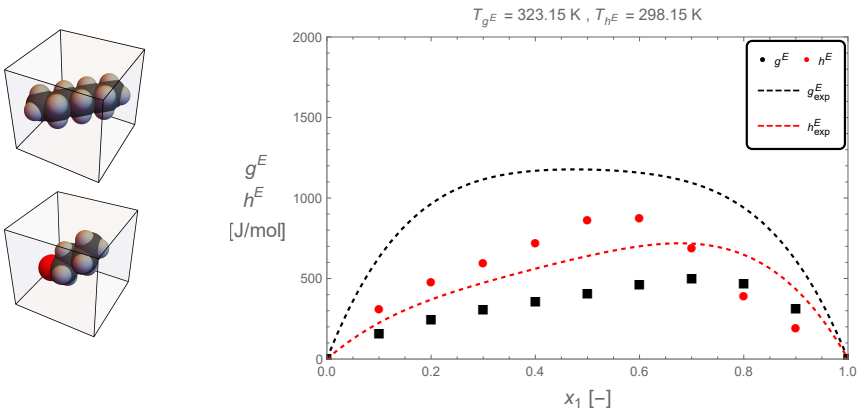

(c) n-Heptane(RotZ45) - 1-Butanol(RotZ45RotX45)

Figure B.11.: Comparison of h^E and g^E data obtained via MC simulations with experimental data [36, 37] for the mixture n-heptane - 1-butanol with n-heptane rotated for 45° around z-axis and 1-butanol (a) in standard configuration, (b) rotated for 45° around z-axis, (c) rotated for 45° around z-axis and x-axis; van der Waals distances used

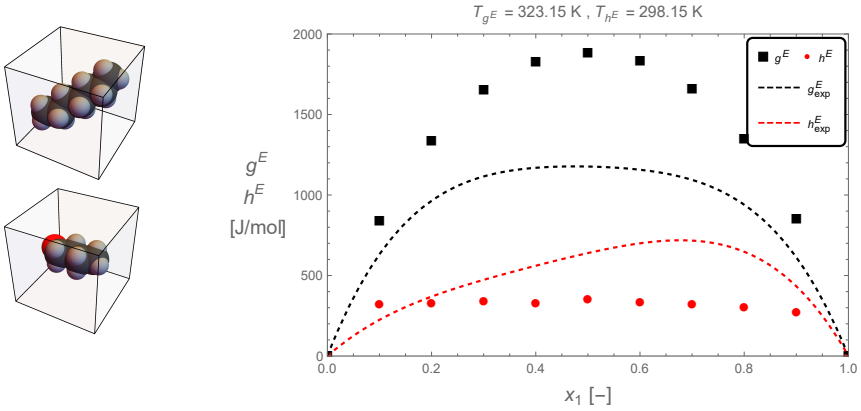

(a) n-Heptane(RotZ45RotX45) - 1-Butanol

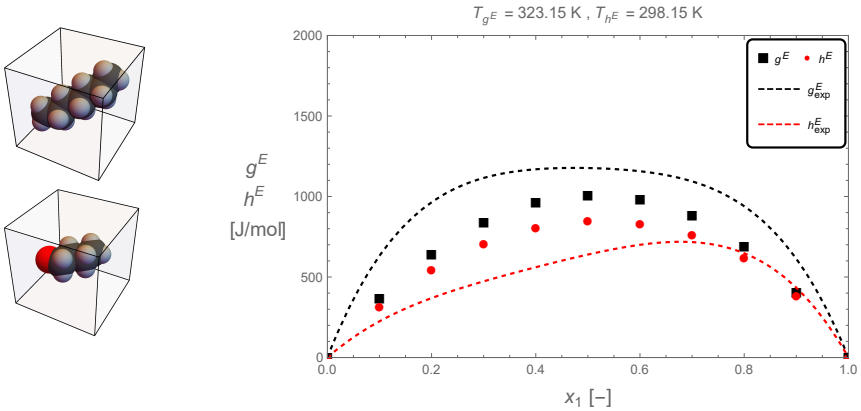

(b) n-Heptane(RotZ45RotX45) - 1-Butanol(RotZ45)

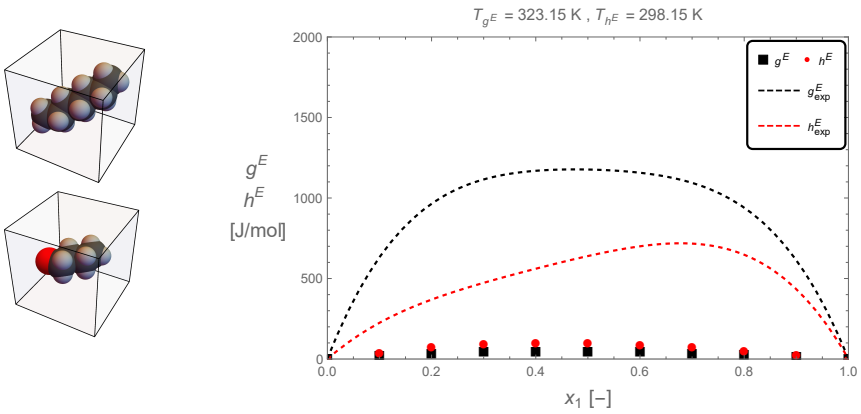

(c) n-Heptane(RotZ45RotX45) - 1-Butanol(RotZ45RotX45)

Figure B.12.: Comparison of h^E and g^E data obtained via MC simulations with experimental data [36, 37] for the mixture n-heptane - 1-butanol with n-heptane rotated for 45° around z-axis and x-axis and 1-butanol (a) in standard configuration, (b) rotated for 45° around z-axis, (c) rotated for 45° around z-axis and x-axis; van der Waals distances used

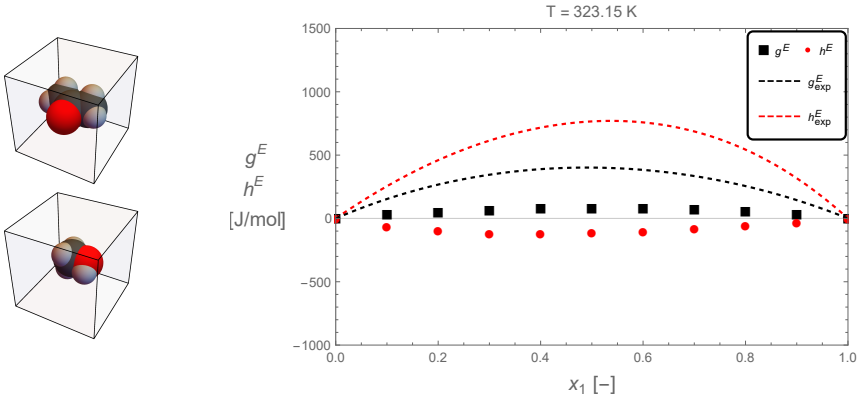

(a) Acetone - Methanol, standard configurations

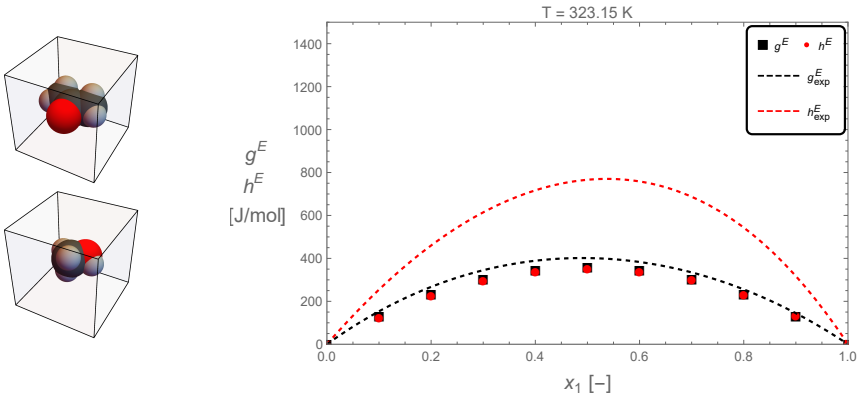

(b) Acetone - Methanol(RotZ45)

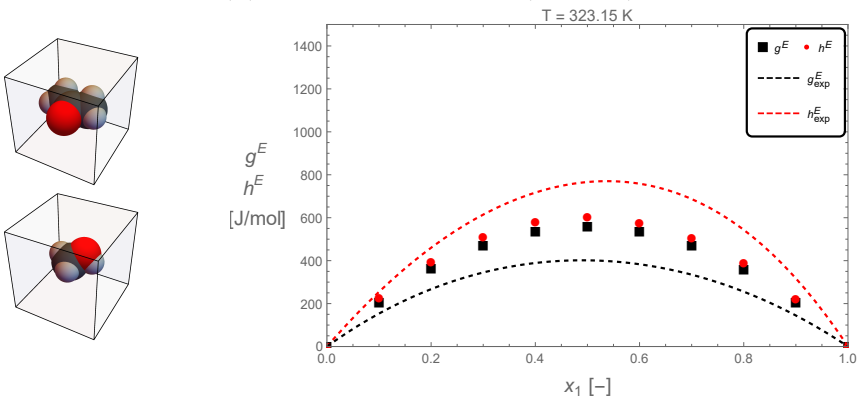

(c) Acetone - Methanol(RotZ45RotX45)

Figure B.13.: Comparison of h^E and g^E data obtained via MC simulations with experimental data [38, 39] for the mixture acetone - methanol with acetone in standard configuration and methanol (a) in standard configuration, (b) rotated for 45° around z-axis, (c) rotated for 45° around z-axis and x-axis; PAC-MAC distances used

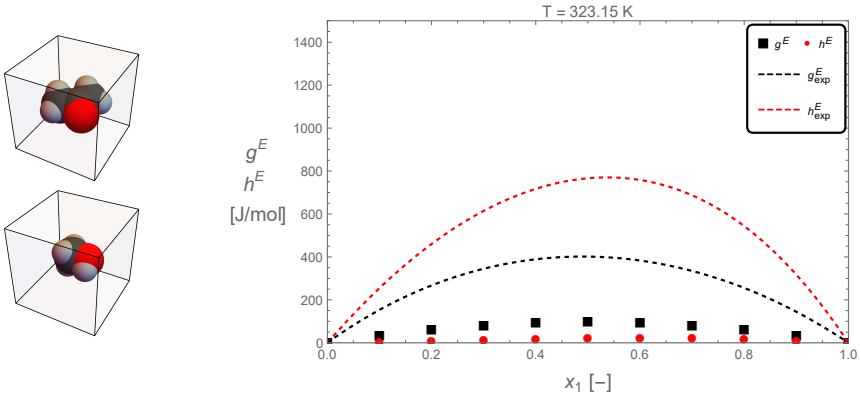

(a) Acetone(RotZ45) - Methanol

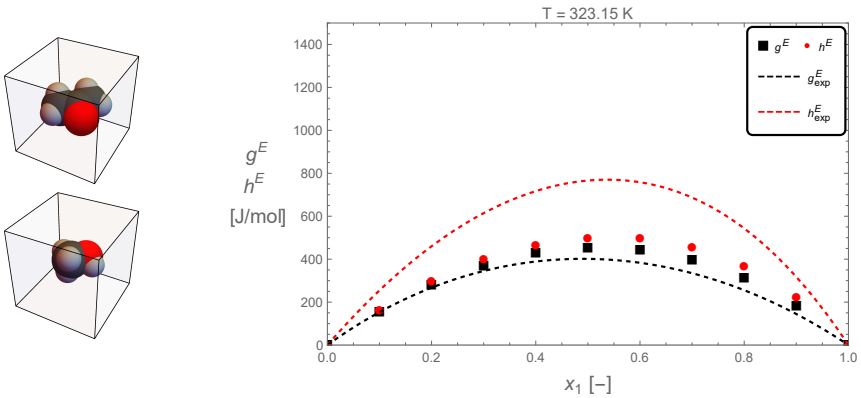

(b) Acetone(RotZ45) - Methanol(RotZ45)

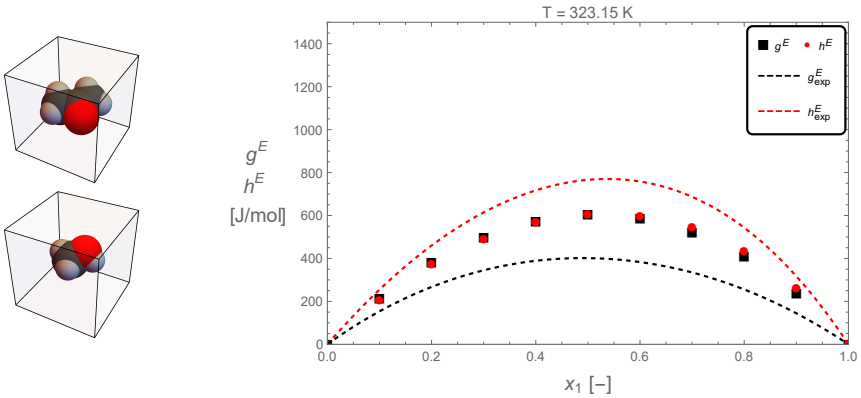

(c) Acetone(RotZ45) - Methanol(RotZ45RotX45)

Figure B.14.: Comparison of h^E and g^E data obtained via MC simulations with experimental data [38, 39] for the mixture acetone - methanol with acetone rotated for 45° around z-axis and methanol (a) in standard configuration, (b) rotated for 45° around z-axis, (c) rotated for 45° around z-axis and x-axis; PAC-MAC distances used

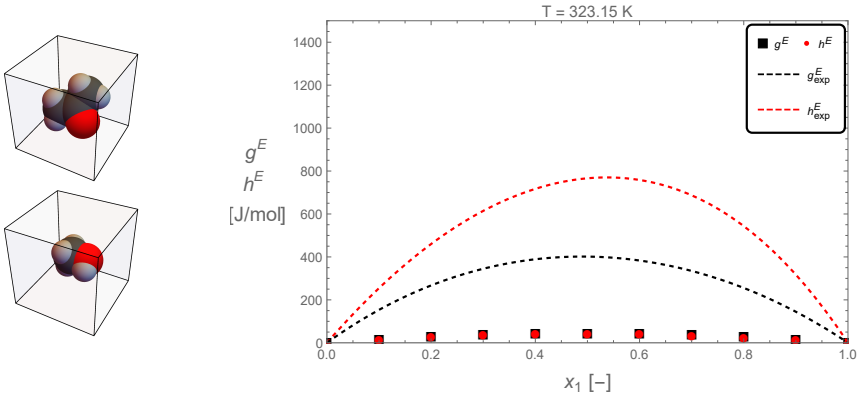

(a) AcetoneRotZ45RotX45 - Methanol

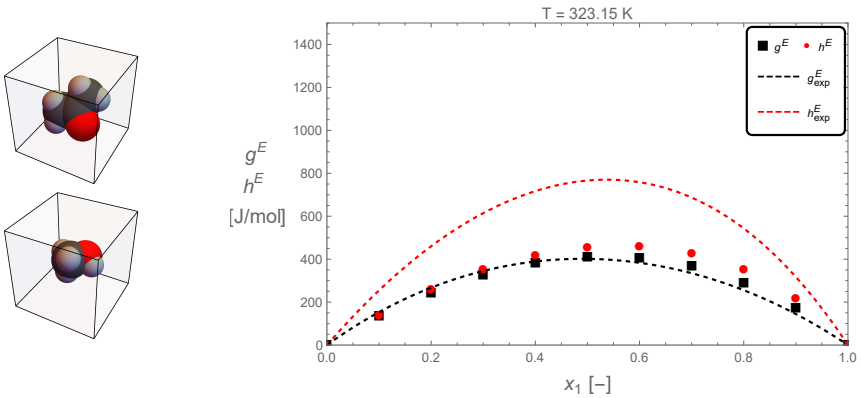

(b) AcetoneRotZ45RotX45 - Methanol(RotZ45)

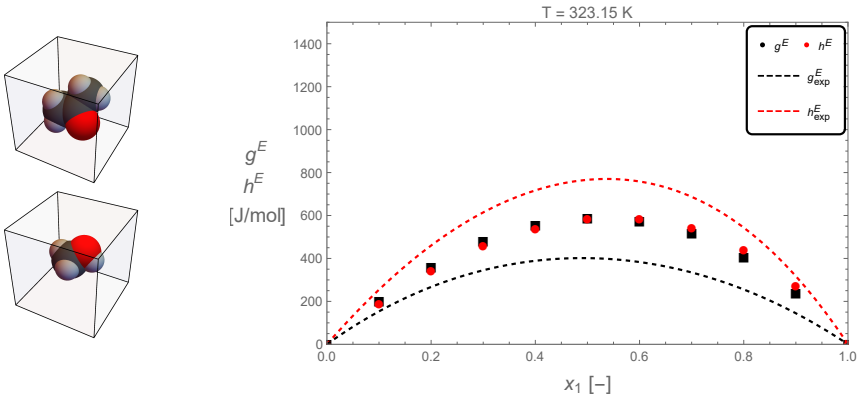

(c) AcetoneRotZ45RotX45 - Methanol(RotZ45RotX45)

Figure B.15.: Comparison of h^E and g^E data obtained via MC simulations with experimental data [38, 39] for the mixture acetone - methanol with acetone rotated for 45° around z-axis and $x-$axis and methanol (a) in standard configuration, (b) rotated for 45° around z-axis, (c) rotated for 45° around z-axis and x-axis; PACMAC distances used

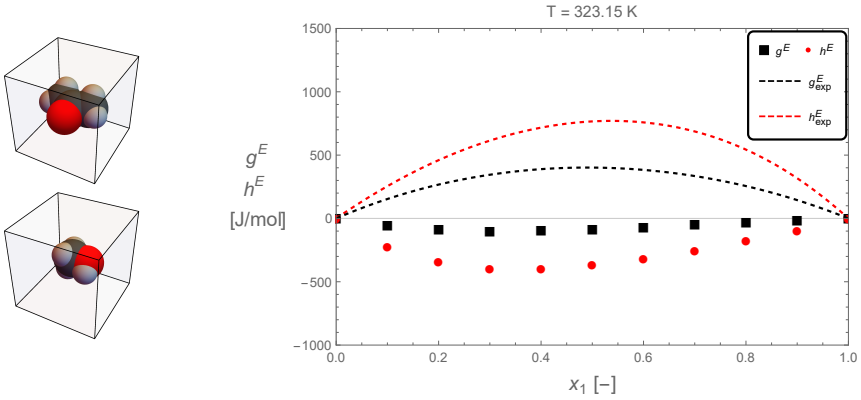

(a) Acetone - Methanol, standard configurations

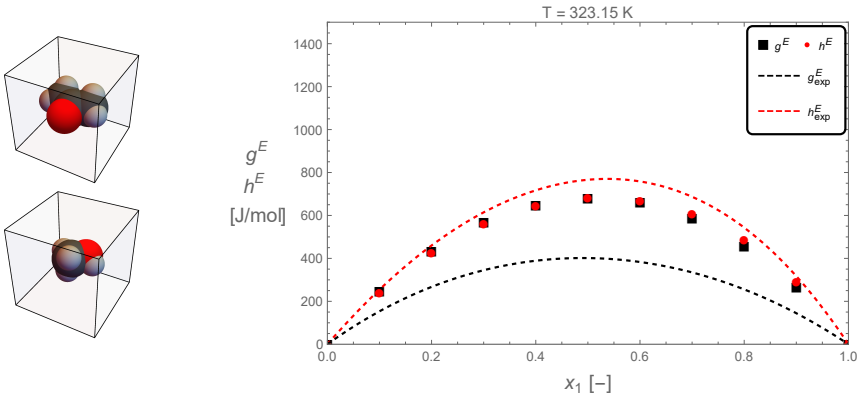

(b) Acetone - Methanol(RotZ45)

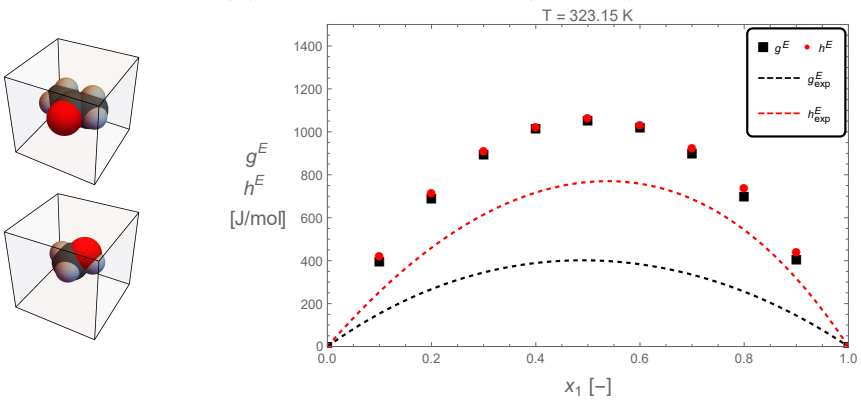

(c) Acetone - Methanol(RotZ45RotX45)

Figure B.16.: Comparison of h^E and g^E data obtained via MC simulations with experimental data [38, 39] for the mixture acetone - methanol with acetone in standard configuration and methanol (a) in standard configuration, (b) rotated for 45° around z-axis, (c) rotated for 45° around z-axis and x-axis; van der Waals distances used

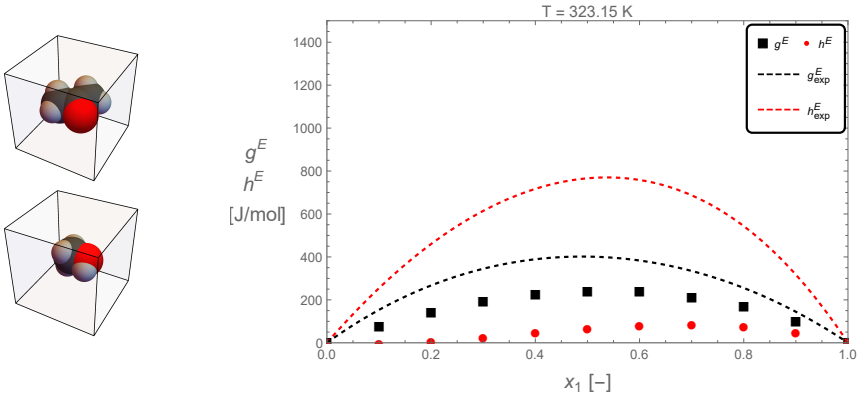

(a) Acetone(RotZ45) - Methanol

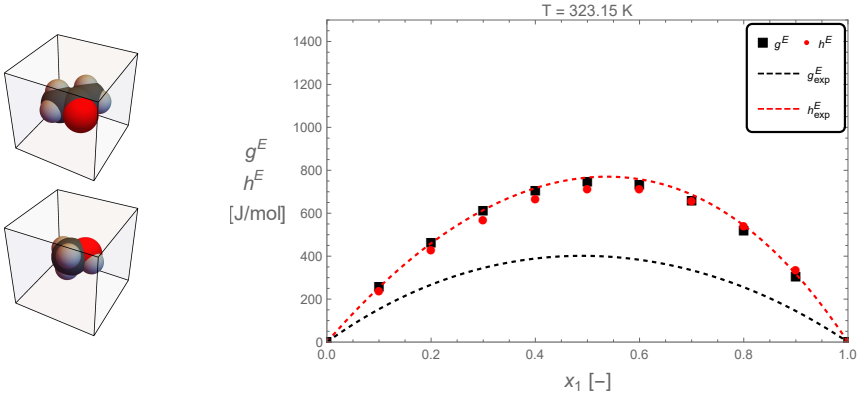

(b) Acetone(RotZ45) - Methanol(RotZ45)

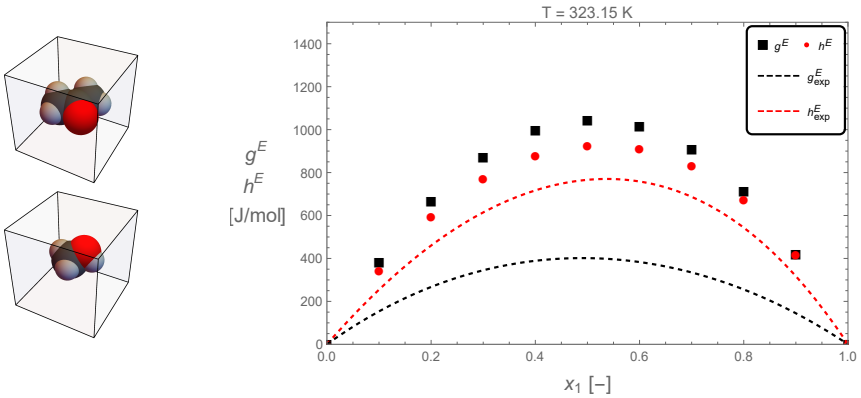

(c) Acetone(RotZ45) - Methanol(RotZ45RotX45)

Figure B.17.: Comparison of h^E and g^E data obtained via MC simulations with experimental data [38, 39] for the mixture acetone - methanol with acetone rotated for 45° around z-axis and methanol (a) in standard configuration, (b) rotated for 45° around z-axis, (c) rotated for 45° around z-axis and x-axis; van der Waals distances used

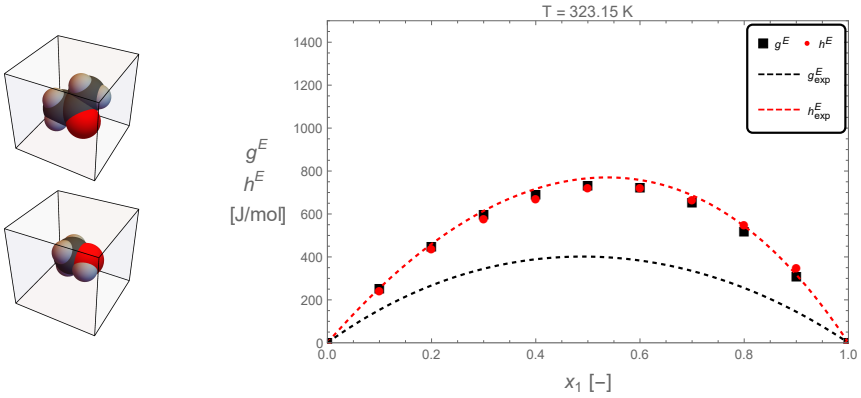

(a) Acetone(RotZ45RotX45) - Methanol

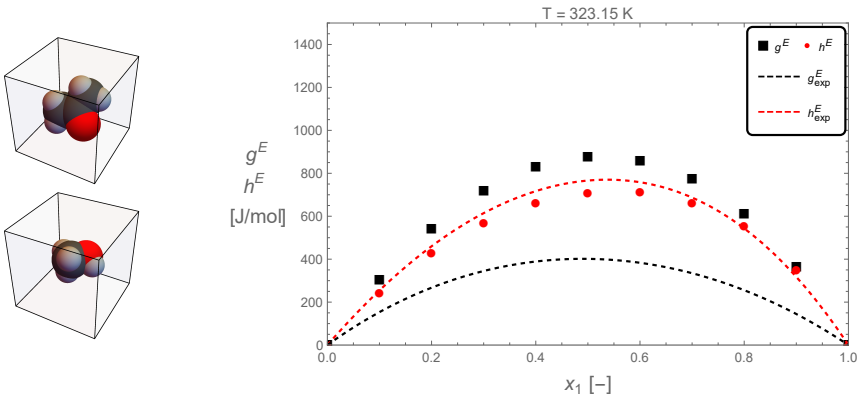

(b) Acetone(RotZ45RotX45) - Methanol(RotZ45)

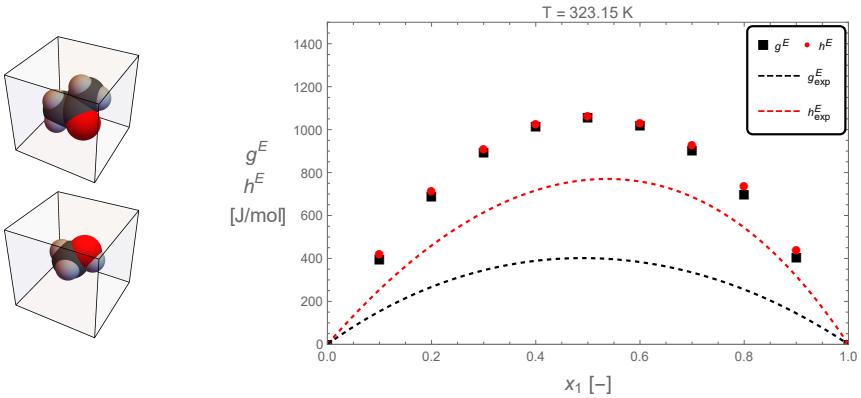

(c) Acetone(RotZ45RotX45) - Methanol(RotZ45RotX45)

Figure B.18.: Comparison of h^E and g^E data obtained via MC simulations with experimental data [38, 39] for the mixture acetone - methanol with acetone rotated for 45° around z-axis and $x-$axis and methanol (a) in standard configuration, (b) rotated for 45° around z-axis, (c) rotated for 45° around z-axis and x-axis; van der Waals distances used

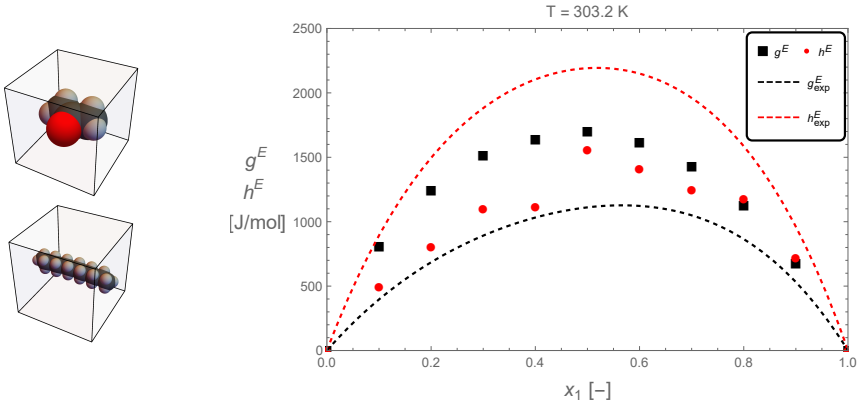

(a) Acetone - n-Dodecane, standard configurations

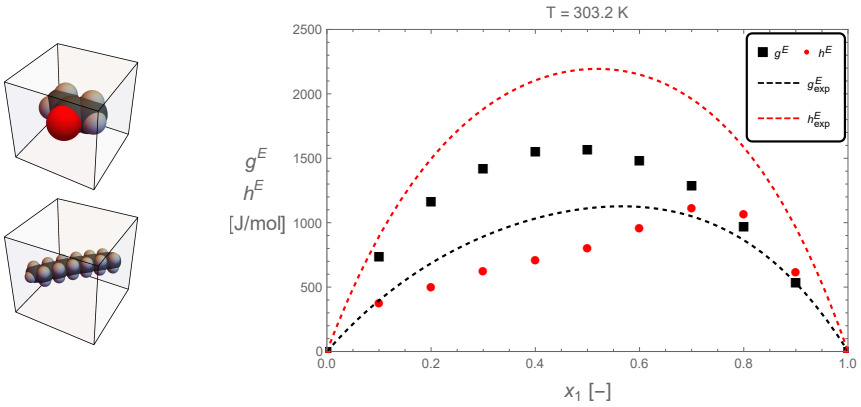

(b) Acetone - n-Dodecane(RotZ45)

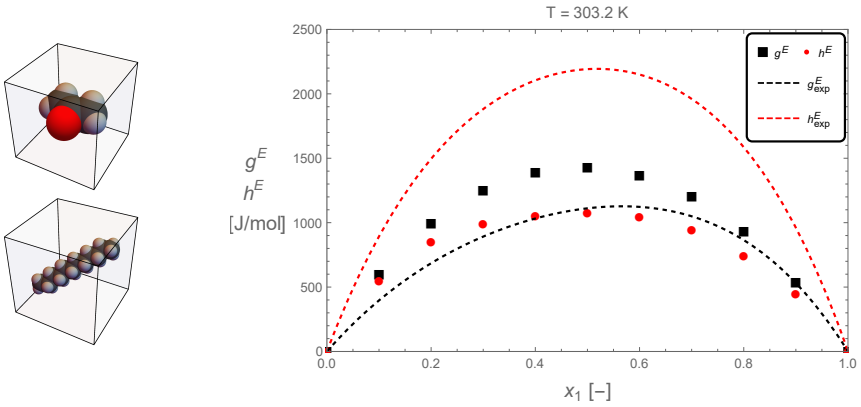

(c) Acetone - n-Dodecane(RotZ45RotX45)

Figure B.19.: Comparison of h^E and g^E data obtained via MC simulations with experimental data [35] for the mixture acetone - n-dodecane with acetone in standard configuration and n-dodecane (a) in standard configuration, (b) rotated for 45° around z-axis, (c) rotated for 45° around z-axis and x-axis; PAC-MAC distances used

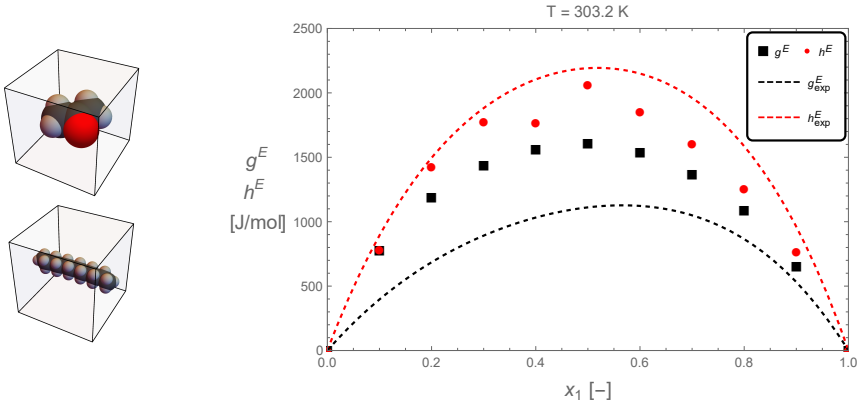

(a) Acetone(RotZ45) - n-Dodecane

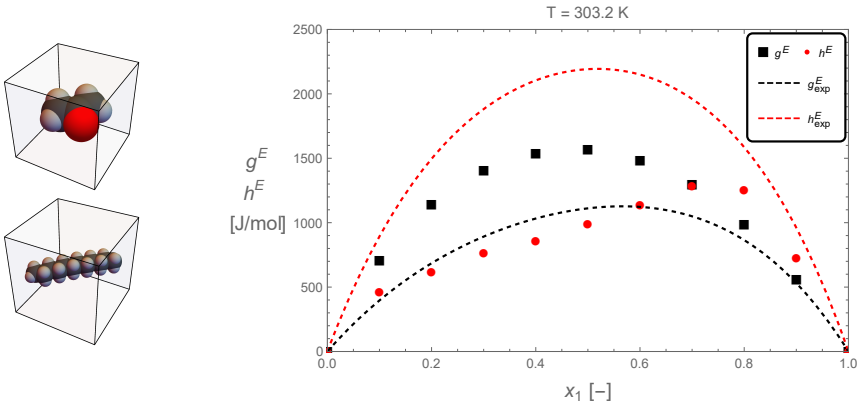

(b) Acetone(RotZ45) - n-Dodecane(RotZ45)

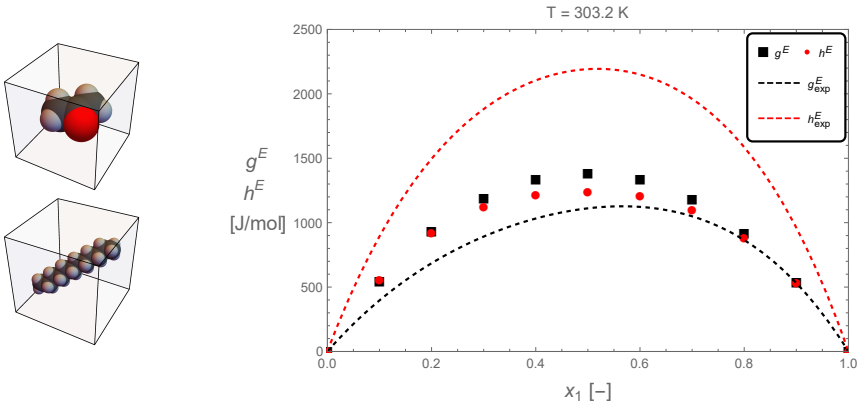

(c) Acetone(RotZ45) - n-Dodecane(RotZ45RotX45)

Figure B.20.: Comparison of h^E and g^E data obtained via MC simulations with experimental data [35] for the mixture acetone - n-dodecane with acetone rotated for 45° around z-axis and n-dodecane (a) in standard configuration, (b) rotated for 45° around z-axis, (c) rotated for 45° around z-axis and x-axis; PAC-MAC distances used

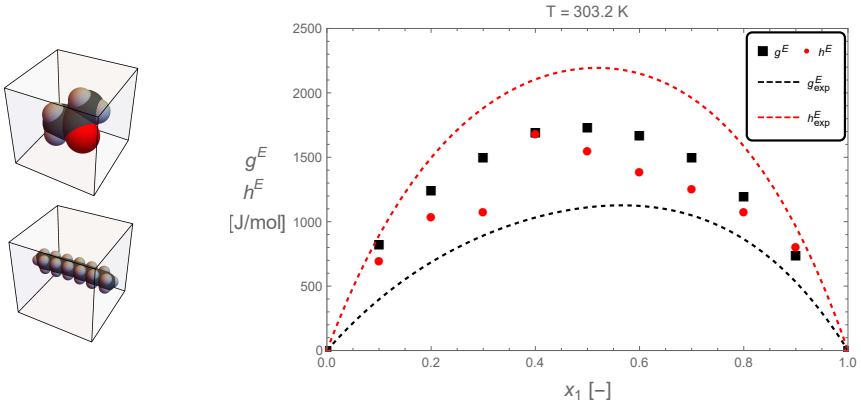

(a) AcetoneRotZ45RotX45 - n-Dodecane

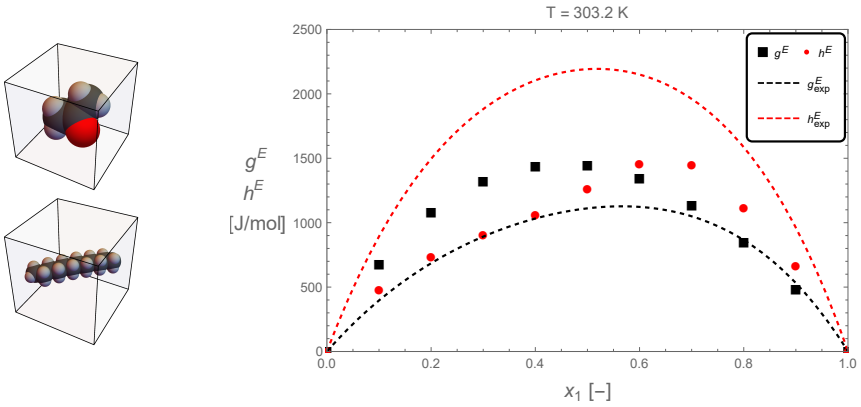

(b) AcetoneRotZ45RotX45 - n-Dodecane(RotZ45)

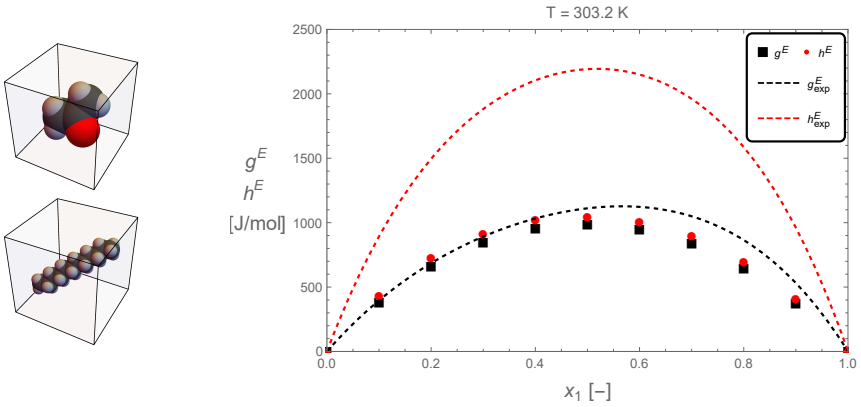

(c) AcetoneRotZ45RotX45 - n-Dodecane(RotZ45RotX45)

Figure B.21.: Comparison of h^E and g^E data obtained via MC simulations with experimental data [35] for the mixture acetone - n-dodecane with acetone rotated for 45° around z-axis and $x-$axis and n-dodecane (a) in standard configuration, (b) rotated for 45° around z-axis, (c) rotated for 45° around z-axis and x-axis; PAC-MAC distances used

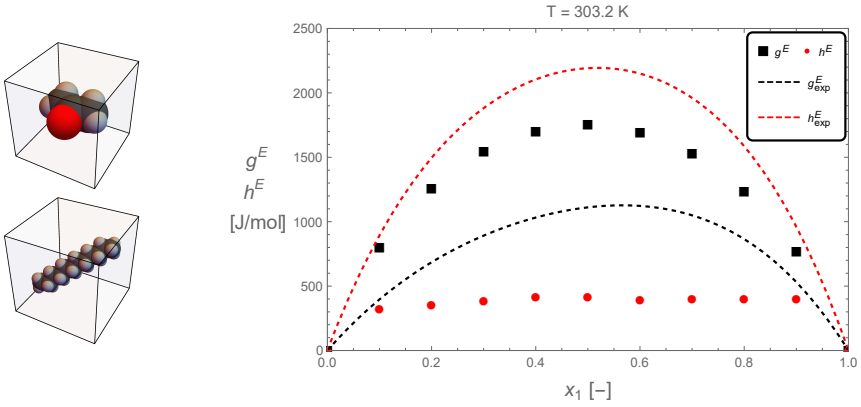

(a) Acetone - n-Dodecane(RotZ45RotX45)

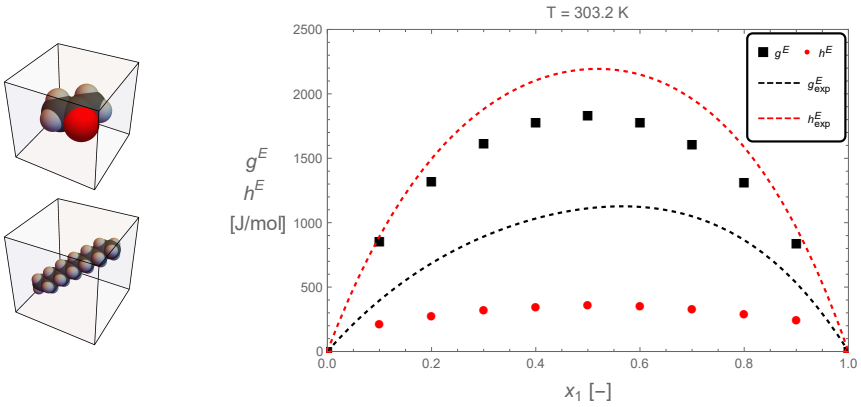

(b) Acetone(RotZ45) - n-Dodecane(RotZ45RotX45)

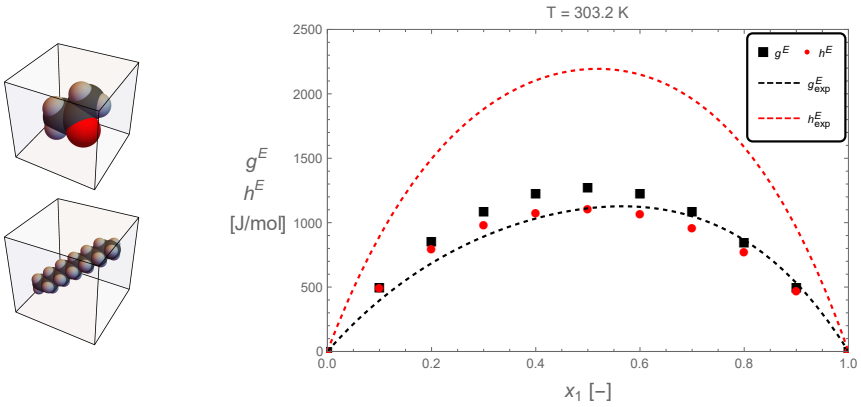

(c) Acetone(RotZ45RotX45) - n-Dodecane(RotZ45RotX45)

Figure B.22.: Comparison of h^E and g^E data obtained via MC simulations with experimental data [35] for the mixture acetone - n-dodecane with n-dodecane rotated for 45° around z-axis and $x-$axis and acetone (a) in standard configuration, (b) rotated for 45° around z-axis, (c) rotated for 45° around z-axis and x-axis; van der Waals distances used